Dynamic Characterization and Active Control of Unstarts in a Near-Isentropic Supersonic Inlet

by

Umair Ahsun

B.Sc. Electrical Engineering, University of Engineering & Technology, Lahore Pakistan (1996).

Submitted to the Department of Aeronautics and Astronautics in partial fulfillment of the requirements for the degree of

MASTER OF SCIENCE in AERONAUTICS & ASTRONAUTICS

at the

MASSACHUSETTS INSTITUTE OF TECHNOLOGY

February 2004

Author_____
Department of Aeronautics and Astronautics
27th January, 2004

Certified by_____
Dr. James D. Paduano
Principle Research Engineer, Department of Aeronautics and Astronautics
Thesis Supervisor

Accepted by_____
Edward M. Greitzer
H.N. Slater Professor of Aeronautics and Astronautics
Chair, Committee on Graduate Students

Dynamic Characterization and Active Control of Unstarts in a Near-Isentropic Supersonic Inlet

by

Umair Ahsun

B.Sc. Electrical Engineering, University of Engineering & Technology, Lahore Pakistan (1996).

Submitted to the Department of Aeronautics and Astronautics
February 2004
in partial fulfillment of the requirements for the degree of
MASTER OF SCIENCE in AERONAUTICS AND ASTRONAUTICS

Abstract

A near-isentropic supersonic inlet, at Mach 2.2, has been designed to give enhanced recovery and thus increased range for a supersonic transport aircraft. In such a design a mixed compression inlet design is typically used. Enhanced recovery of 97% in total pressure is achieved by reducing the unstart-tolerance of the inlet and by an efficient boundary layer control mechanism. Thus the resulting inlet design has reduced stability to unstart in the face of atmospheric and engine-born disturbances, necessitating active control. An active stabilization bleed system is introduced that recovers the disturbance-rejection capabilities required of modern inlets. The bleed system requires 4% steady state bleed and up to 6% additional unsteady bleed for active stabilization. Two separate physical mechanisms for unstart are identified, and active control algorithms to prevent these forms of unstart are designed and demonstrated using quasi-1-D and 2-D unsteady Euler simulations. The CFD codes used have been optimized for accurate propagation of disturbances, to insure that physical mechanisms are correctly captured. The resulting actively stabilized inlet can withstand worst-case empirically determined (by NASA) atmospheric disturbances such as flight velocity, temperature, and angle of attack perturbations consistent with atmospheric flight.

Thesis Supervisor: Dr. James D. Paduano
Title: Principle Research Engineer, Department of Aeronautics and Astronautics

Acknowledgements

The purpose of research is to learn new ideas and explore new frontiers. During my research at Gas Turbine Lab I have learnt a great deal but in reality I have just started on the road to explore new ideas. I want to acknowledge and thank my advisor Dr. James D. Paduano for giving me the opportunity to work on this project and guiding me throughout with patience and understanding. I would also like to thank him for reading my thesis meticulously and making it more readable.

I would also like to thank Dr. Ali Merchant for his involvement in the development of CFD design tools that were essential for the project. I would also like to thank Dr. Gerald R. Guenette, Jr. for his suggestions during the experimentations.

In the end I would like to thank my wife Sarah and little cute son Arslan for their understanding and patience.

Funding for this research was provided by DARPA under the MAFC program.

Contents

List of Figures

List of Tables

Chapter 1

Introduction

The purpose of an aircraft inlet is to act as an interface between the free stream and the engine compressor. In supersonic airbreathing engines flying at cruise conditions, the inlet decelerates the free stream flow from flight Mach number to a Mach number required at the face of the compressor, recovering the energy in the form of increased pressure. Most compressors, in a supersonic propulsion system, require a flow at their face at around Mach 0.5. Since the flow decelerates from supersonic to subsonic, a normal shock is formed somewhere in the diffuser section of the inlet (where the flow Mach number crosses the value of 1). If the normal shock is formed outside the inlet then the inlet is called an external compression inlet, while if the normal shock is formed inside the inlet, behind the throat, then this type of inlet is called an internal compression inlet. A high efficiency inlet supplies the air to the engine, at the required operating conditions, with the minimum possible loss. The efficiency of the inlet is generally measured in terms of its total pressure recovery. Total pressure recovery is defined as the ratio of the total pressure at the face of the compressor (at some suitably defined point or average value) to the free stream total pressure. In a supersonic inlet the major sources of total pressure loss are the normal shock and the boundary layers. The total pressure loss across a normal shock wave as a function of upstream Mach number is shown in Figure 1.1 [4].

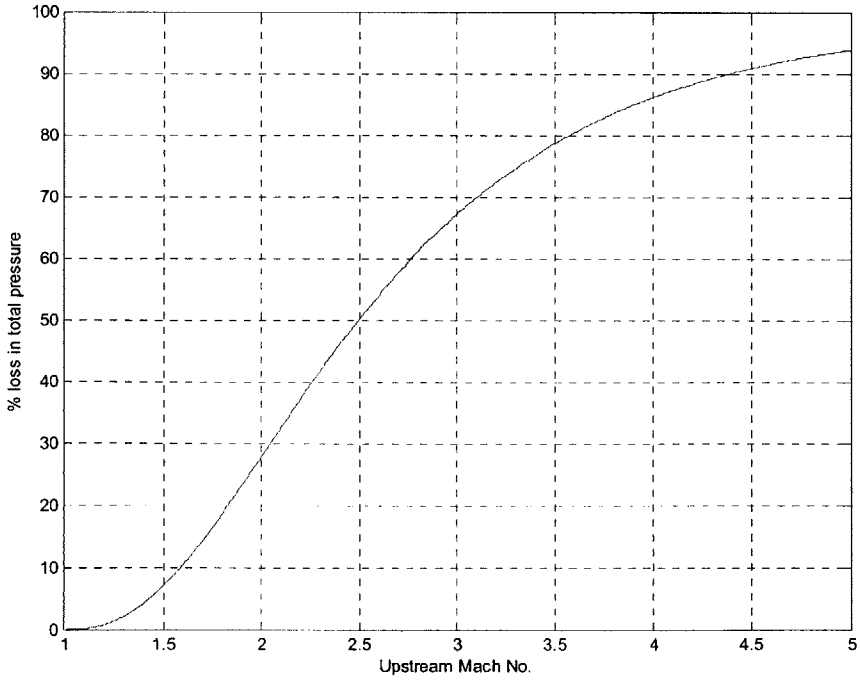

Figure 1.1: Total Pressure loss across a normal shock as a function of upstream Mach number.

Figure 1.1 shows that for low supersonic speeds an external compression inlet may give satisfactory performance as the total pressure loss is low, but for inlets flying at supersonic speeds above Mach 2.0, an internal compression inlet design gives better efficiency as compared to an external compression inlet as explained in the following paragraphs.

A near-isentropic supersonic inlet can be designed, using internal compression, by gradually slowing down the incoming flow through a series of oblique shock waves and a weak terminal normal shock just behind the throat [20]. With such a design one can achieve a total pressure recovery as high as 97%. The flow structure in such a design is shown in Figure 1.2.

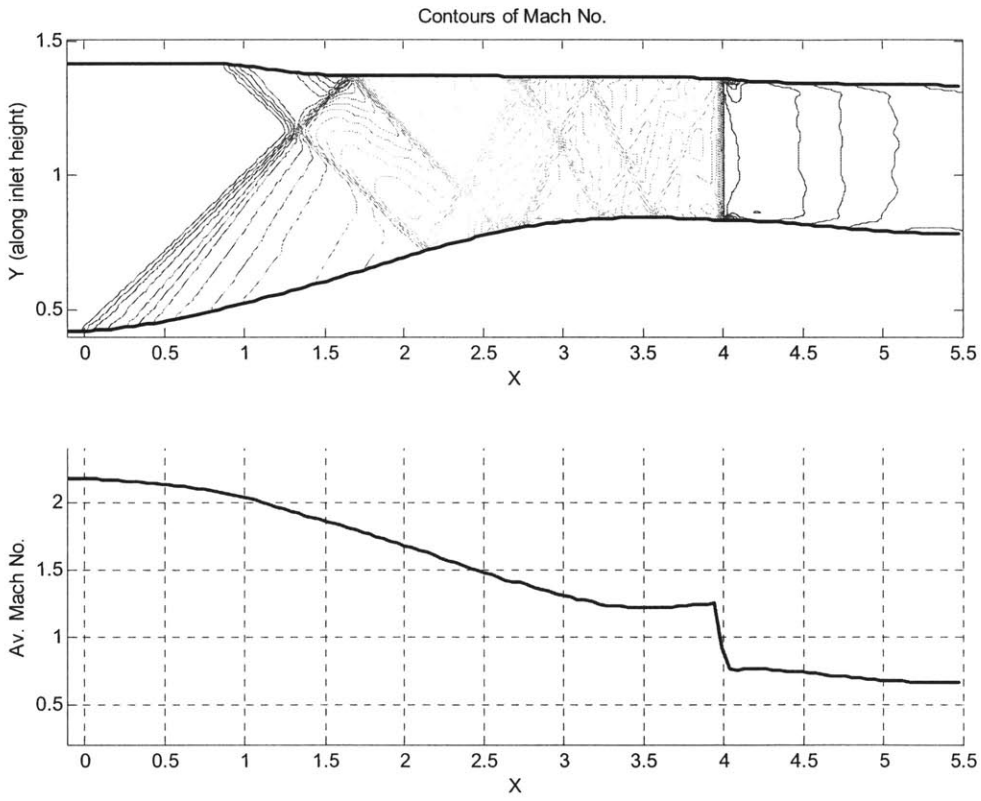

Figure 1.2: Internal compression inlet with oblique shock waves

With such a design the length of the inlet cannot be too small, as the flow has to decelerate gradually. This has implications for the growth of boundary layer losses. Specifically, although we can minimize the loss through the terminal normal shock, since it is weak, we get an increased boundary layer loss instead. It is clear that there is a trade-off between the loss in pressure recovery through the shock system and loss through the boundary layer growth. In order to minimize both, Merchant [2] carefully placed bleed valves at key locations in the inlet. The boundary layer growth is managed with the help of bleed valves situated at these locations. These valves bleed the air at the walls of the

inlet and prevent the boundary layer from growing. In this way we can achieve near-isentropic compression if we assume that we can dump the boundary-layer management bleed over-board with zero loss. But in practice this cannot be done ideally, and there is always some loss associated with bleed flow in the form of increased inlet drag. Thus from the system point of view there is a trade-off between pressure recovery and inlet drag, i.e. we can achieve near ideal pressure recovery but at the expense of increased inlet drag. In order to quantify these two parameters, data for Concord is shown in Table 1.1 [19] (this table gives the inlet efficiency in terms of the total pressure recovery and the aircraft drag includes the drag contributed by the inlet). From this table it is clear that in order to achieve higher performance of the propulsion system, a high inlet efficiency coupled with a low drag is required. A high efficiency inlet would be one that not only has high pressure recovery, but also uses as low bleed as possible to achieve high recovery.

Aerodynamic Loss	**Reduction of Payload (%)**
1% inlet efficiency (subsonic)	1
1% inlet efficiency (supersonic)	2.5
1% aircraft drag (subsonic)	1
1% aircraft drag (supersonic)	4.5
1% inlet efficiency (take off)	5

Table 1.1: Concord supersonic transport aircraft performance sensitivity to changes in inlet pressure recovery and aircraft drag.

Internal compression inlet operation is strongly affected by atmospheric disturbances as it has a 'bi-stable' operation. In the 'started' condition, the normal shock sits behind the throat as shown in Figure 1.2. Atmospheric disturbances can cause the normal shock to move upstream in such a way that it can even come out of the inlet completely, forming a bow-shock wave [1]. This shock blowout event is known as inlet unstart and results in a severe increase in aircraft drag; the mass flow through the inlet may also decrease below the engine's requirements and the engine itself may surge or shut off [2]. In order to 'start' the inlet again, one needs to suck the external shock and move it downstream behind the throat, where it remains in a stable condition in the absence of external disturbances. For this starting action one needs variable inlet geometry as discussed later in this chapter.

We can define the unstart tolerance of the inlet as the magnitude of the disturbance that can be tolerated without unstart. In other words, an inlet that has higher unstart tolerance is more robust in the face of disturbances. There is a tradeoff in inlet operation between robustness and efficiency (in terms of total pressure recovery) [3]. For a supersonic diffuser, behind the throat the flow re-accelerates to higher Mach numbers as given by the area velocity relationship for a converging diverging duct [4]:

$$\frac{dA}{A} = (M^2 - 1)\frac{du}{u} \tag{1.1}$$

Here A is the cross-section area along the inlet, M is the Mach number and u is the flow velocity. Equation 1.1 shows that, for a positive change in the area the change in the velocity is also positive for supersonic Mach numbers. Therefore, if the normal shock forms farther down the throat then it will be stronger (i.e., it goes subsonic from a higher value). For stable operation, the throat Mach number must be greater than one. If the throat Mach number is exactly one, then the flow downstream of the throat will be subsonic and there will be a very weak shock standing at the throat. This flow condition is marginally stable, as even a very small disturbance can move the shock either downstream or upstream. If the shock moves upstream then it enters the unstable region and it would continue to move upstream until the inlet unstarts. Combining this requirement with equation 1.1 we see that:

$$1 < M_{throat} < M_{shock} \tag{1.2}$$

From the discussion in the above paragraph, it is clear that a shock placed farther downstream of the throat is more immune to disturbances as compared to a shock placed nearer to the throat. Increased efficiency is achieved (at the expense of decreased robustness) with the normal shock closer to the throat. In this case the normal shock is very weak, consequently minimizing the losses across the shock. Similarly we can enhance the unstart tolerance, and inlet robustness, by placing the shock a bit farther downstream of the throat; in this case, however, we get a stronger shock resulting in increased pressure loss and lower efficiency. So it is clear that one can achieve enhanced recovery but at the cost of reduced inlet robustness. Therefore normal operation of the enhanced recovery inlet requires active stabilization during the cruise conditions to achieve an acceptable level of unstart tolerance.

In the design of an inlet, for the purpose of supplying air to the engine, the designer is primarily concerned with the properties of the internal flow such as mass flow, pressure recovery, static and dynamic distortion, flow angularity and flow stability [19]. For mixed compression inlets, the most important dynamic characteristic is the robustness of the shock system inside the inlet as discussed above. In order to achieve the required performance and robustness one has to vary the throat area of the inlet for different flight conditions while the overall structure of the inlet is optimized for the cruise conditions. In current supersonic internal compression inlet designs, the "operating point" of the inlet is varied with the help of a translating center body or mechanical system, called "ramp control". The ramp control is also required for "starting" the internal compression inlet as discussed earlier. It should be noted that bleeds are used only for boundary layer management and shock control, to reject disturbances in steady-state, and are not currently used for the atmospheric disturbance rejection in an unsteady fashion. The translating center body has large inertia; therefore if the inlet encounters a large atmospheric gust then the ramp control system cannot react in time to avoid unstart. This

means that during the cruise condition, where a transport aircraft engine operates most of the time, the operating point of the inlet has to be adjusted such that the terminal normal shock is placed sufficiently behind the throat to give acceptable level of unstart tolerance. Therefore, the inlet has to operate with a lower pressure recovery to account for the atmospheric gusts that are normally encountered during a flight.

This thesis suggests a control system on top of the "ramp control" to allow the designer to reduce the uncontrolled unstart tolerance further to achieve near isentropic operation of the inlet. The reduced static margin for unstarts is accounted for by the dynamic rejection of the atmospheric disturbances with the help of an active bleed control system.

In order to design an effective inlet stabilization control system we need to quantify the dynamic behavior of the inlet in the face of atmospheric and compressor disturbances. For that a quasi-1D and a 2D inviscid Euler simulations of the inlet were prepared by Ali Merchant [2] and integrated into Matlab and Simulink. The Euler simulation uses numerical solvers utilizing a second-order accurate finite-volume scheme for spatial discretization. Stabilization and shock capturing are enabled using Roe's scheme. A four stage Runge-Kutta method is used to time march the solution. Boundary conditions are applied using Riemann invariants. With the help of these tools we can model the dynamic behavior of the inlet quite accurately for the design and analysis of a control system.

During normal operation, many mechanisms such as aircraft maneuvers, back pressure, engine transients etc. can cause the inlet to unstart, but atmospheric disturbance is the least controllable and least predictable; therefore it is the most important factor in avoiding inlet unstarts [3]. To study the effectiveness of the control system we need to quantitatively express the worst-case atmospheric disturbances. A detailed study of atmospheric turbulence models was conducted as part of this work and worst-case PSD (Power Spectral Density) estimates were generated for inlet cruise conditions. The study of the atmospheric disturbances is important for a realistic evaluation of the performance of the inlet. The reason being that, the inlet itself does not dictate the bandwidth requirements for the control system. The inlet passes some of the disturbances un-attenuated even for higher frequencies. Thus it is the spectrum of the atmospheric disturbances that sets the bandwidth requirements for the actuators and controller.

This thesis presents a systematic way of predicting the dynamic behavior of a high-recovery supersonic inlet. Using the dynamic behavior, control schemes are presented that can be used to increase the robustness of the inlet in the face of atmospheric disturbances. In order to achieve that effectively, in chapter 2 of the thesis, we discuss different atmospheric disturbances and their characterization as applicable to our system. In chapter 3 we discuss dynamic characterization of the inlet itself. Different unstart mechanisms are also discussed. Different transfer functions for both 1D and 2D models are calculated and compared. In chapter 4 we discuss different control architectures for the stabilization of inlet. Chapter 4 also gives the results for the implementation of the control laws and their quantitative assessment in enhancing the inlet robustness. Finally chapter 5 provides some time-domain results and conclusions.

Chapter 2

Atmospheric Disturbance Characterization

As discussed in chapter 1, the bandwidth requirements of the inlet are not dictated by the inlet itself (that this is the case will be shown in chapter 3). This means that we have to look at the spectrum of disturbances affecting the inlet to find out the bandwidth requirements of the control system and actuators. Many different types of disturbances such as aircraft maneuvers, back pressure, engine transients etc. can cause the inlet to unstart but atmospheric turbulence is the least controllable and least predictable and therefore it is the most important factor in avoiding the inlet unstarts [3]. In this thesis we are not considering the downstream disturbances generated by the compressor; instead we concentrate entirely on the atmospheric disturbances.

2.1 Atmospheric Disturbance Types and Scales

Supersonic airplanes may encounter atmospheric turbulence comprised of four components: the three components of velocity and temperature. There is also pressure turbulence but it is related to velocity perturbations via the momentum equation, so we can eliminate it. In order to have a realistic study of the effects of atmospheric disturbances on the inlet, we need to express the disturbances in some quantitative form.

Atmospheric disturbances come in all sizes, from the macroscale (sizes greater than a few hundred kilometers) through mesoscale (from a few hundred km to tens of km) to microscale (tens of km to a few cm) [5, 6]. By "scale" we mean the horizontal distance over which the disturbance parameter, say velocity, changes by its own order of magnitude. For the purpose of quantitatively expressing the disturbances we can treat them as quasi-steady, since the change in the atmospheric disturbance properties takes place at a very slow rate and the aircraft is flying at a high Mach number. This means that as the airplane is flying through the disturbances, we can treat them to be stationary for an observer not moving w.r.t. the atmosphere. Therefore, for an observer sitting on the airplane, moving with a true air speed U, the atmosphere presents different turbulence lengths from a few hundred km down to a few cm, corresponding to different spatial wavelengths. Under this "frozen field" assumption we can convert between spatial wavelengths or corresponding wavenumbers to temporal frequencies using the following relationship:

$$f = \frac{\text{True Air Speed in m/s}}{\text{Spatial Wavelength in m}} = \frac{U}{\lambda} = \frac{Ma}{\lambda} = kMa \tag{2.1}$$

Here M is the flight Mach number, a the local speed of sound in m/s and k is wavenumber in cycles/m.

We will be interested primarily in mesoscale and microscale disturbances as the macroscale disturbances are adequately handled by the flight control and ramp control systems as discussed in the following sections.

2.2 Atmospheric Disturbance Models

Assuming the disturbances to be stationary, as discussed above, we can describe the atmospheric disturbances statistically in terms of their power spectral density (PSD) functions. In the micro and meso-scales the 3D turbulence is isotropic and we can use the Kolmogorov's spectrum for turbulence modeling [6]. A brief review of Kolmogorov's theory and its application to atmospheric turbulence is given in this section.

From the first law of thermodynamics we know that the total energy of an isolated gas volume remains constant over time. But the total kinetic energy of the turbulent eddies of an isolated gas decreases with time due to viscous dissipation. Hence a turbulent fluid can be maintained in steady state, in the kinetic sense, only if the energy injection rate equals the rate of dissipation.

Kolmogorov's theory is based on the notion that large eddies in a turbulent gas can feed energy to the smaller eddies, which in turn feed energy to smaller scales, resulting in a cascade of energy from the largest eddies to the smallest ones. That this notion is true can be seen from the fact that large eddies of size say l have large Reynolds number lV/ν where V is the typical velocity associated with the eddy (which may be small but l is very large). This large Reynolds number allows us to treat this flow as inviscid and from an application of Kelvin's vorticity theorem [7] we see that vorticity is conserved across different scales and thus we can imagine different fluid elements "carrying" the vorticity to smaller dimensions. For very small eddies the Reynolds number becomes small and thus viscous dissipation occurs at very small scales, resulting in the loss of kinetic energy. Thus according to Kolmogorov's theory an isolated turbulent gas would have an energy dissipation rate, ε, called the eddy dissipation rate, per unit mass per unit time (having units of energy/(mass x time) = m^2/s^3) in order to maintain equilibrium. Kinetic energy does not build up at any scale and the intermediate eddies merely transmit this energy ε to the smaller scales to be dissipated there. From the above discussion we see that the concept of energy cascade is applicable to some range of wavenumbers between very large eddies and some small eddy scale. Within this range of wavenumbers, called the inertial subrange, the energy is transferred to smaller eddies without dissipation and hence total energy remains constant. Using this constraint of constant energy and a constant eddy dissipation rate ε, of transport of turbulent kinetic energy from smaller wavenumbers to higher wavenumbers, for an isotropic turbulence, we can show using dimensional analysis that the power spectral density of atmospheric turbulence is given by [6]:

$$S_t(k) = \alpha_t \varepsilon^{2/3} k^{-5/3} \tag{2.2}$$

Where the subscript t denotes the type of disturbance being modeled. The coefficient α_t is a constant for each type of disturbance and given by:

$\alpha_l = 0.15$	(longitudinal wind velocity gust, dimensionless)
$\alpha_v = 0.2$	(vertical or horizontal wind velocity gust, dimensionless)
$\alpha_T = 0.39$	(temperature disturbance, $°K^2s^2m^{-2}$)
$\alpha_P = 0.0005(p_0/T_0)^2$	(pressure disturbance, $Pa^2s^2m^{-2}$)

Note that these values of the coefficients α_t and ε are determined experimentally using a large number of actual wind gust measurements as described by [6].

Data indicate that the –5/3 law spectral behavior, described above, extends uninterrupted to an outer scale disturbance wavelength of around 400 km [5]. This means, for a study of the effect of atmospheric disturbances on inlets only one parameter, i.e., ε the eddy dissipation rate, sets the spectral intensity over the entire frequency range of our interest. The eddy dissipation rate is a function of terrain, altitude, latitude and different times of the year. A typical value for ε is 2.0×10^{-5} m^2s^{-3} and can vary by as much as a factor of 10.

Using the given model spectra for different atmospheric disturbances we can use the Fourier Series method for the generation of random time series that have the same spectra as those of atmospheric disturbances [8]. Using the turbulence model developed by William Tank [6], as described above, a code was developed at UTRC [21], which simulates such time histories of the atmospheric turbulence. This code allows one to adjust different parameters (as given above) in the atmospheric turbulence model such as eddy dissipation rate, flight speed etc. A typical output of the code, along with the relevant spectra, is shown in Figure 2.1. This figure shows the spectra for forward or longitudinal velocity gust and the temperature gust. The time histories of the gusts are also shown in the figure. These time histories are generated by the code for the worst case setting of the eddy dissipation rate, ε. Gust histories such as those shown in the Figure 2.1 will be used for the time-domain testing of control algorithms in chapter 4 and 5. For frequency domain studies analytical spectra, such as those denoted as "model", will be used in chapter 3 and 4.

2.3 Transformation of atmospheric disturbances to Characteristic Canonical Form

From the discussion in the previous section it is clear that the atmospheric disturbances can be broken down into three types for our purposes:

1. Forward velocity disturbances.
2. Vertical velocity disturbances.
3. Temperature disturbances.

These disturbances in the atmosphere appear at the face of the inlet and travel down the inlet as three distinct modes, namely a fast acoustic wave $J+$, a slow acoustic wave $J-$ and

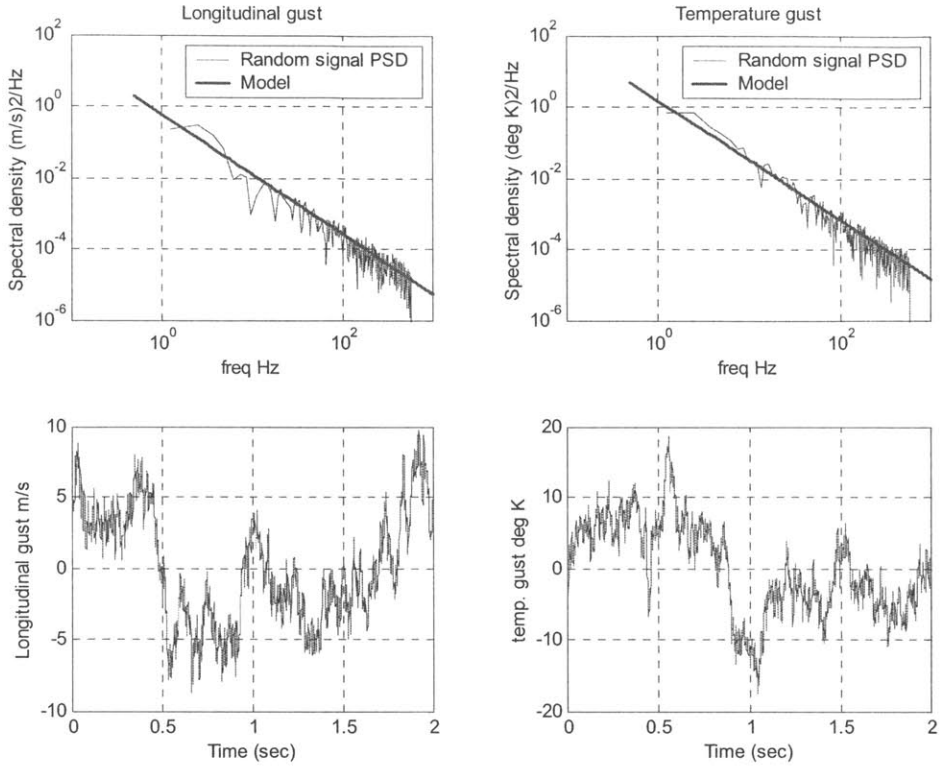

Figure 2.1: Forward velocity and temperature gust time histories and their spectra for an aircraft flying at Mach 2.2 at altitude of 60000 ft. (Note that the worst case empirical values of ε, 7×10^{-5}, were used.)

an entropy disturbance. We can represent each of the atmospheric disturbances as a combination of these 'canonical' or characteristic forms, namely $J+$, $J-$ and entropy. Each of the canonical disturbances can be regarded as a fundamental mode of the disturbance. Therefore, from the standpoint of control system design, these modes are to be controlled or rejected for the stabilization of inlets.

One comment is needed here about the canonical form of the disturbances: these canonical forms are not really independent of each other, e.g., if we have an entropy perturbation at the face of the inlet then it will also result in variations of $J+$ and $J-$ in the inlet. This can be seen from Equations (2.3) and (2.4), below, as a coupling between speed of sound change and $J+$ and $J-$. Therefore these are not really independent modes of the disturbances. But still studying the inlet response to disturbances in canonical form reveals very useful information as discussed in chapter 3 and we can even implement a control law based on canonical form as described in chapter 4. The reason being that the coupling between different modes is relatively weak as the rate of travel of each disturbance is different, so from the point of view of control law design these modes are fairly decoupled and we can treat them as independent modes of the disturbances. From

this discussion it is clear that it would be useful to transform the atmospheric disturbances to these characteristics canonical disturbances for the study of control law design.
We will break the atmospheric disturbances into three independent parts:

- Isothermal Horizontal Gust Δu.
- Isothermal Vertical Gust Δv.
- Temperature Gust ΔT.

For a calorically perfect gas the Riemann Invariants, $J+$ and $J-$, along the characteristic lines are defined as [4]:

$$J+ = u + \frac{2a}{\gamma - 1} \tag{2.3}$$

$$J- = u - \frac{2a}{\gamma - 1} \tag{2.4}$$

Here u is forward velocity, a is speed of sound and γ is the ratio of the specific heat at constant pressure and specific heat at constant volume, i.e., $\gamma = c_p/c_v$.

Let us define the entropy as:

$$s = pv^{\gamma}, \tag{2.5}$$

where p is the pressure and v is specific volume i.e., volume per unit mass.

2.3.1 Isothermal Horizontal Gust

For an isothermal horizontal gust Δu we have only forward velocity perturbation and from Equations 2.3 to 2.5 we obtain:

$$\begin{aligned} \Delta J+ &= \Delta u \\ \Delta J- &= \Delta u \\ \Delta s &= 0 \end{aligned} \tag{2.6}$$

2.3.2 Isothermal Vertical Gust

If we have an isothermal vertical gust without any forebody (i.e., no fuselage above or below the inlet) then the vertical gust simply transforms into an angle of attack change. But if a forebody is present, as it is in our case, whether above or below (Figure 2.2), the flow in front of the inlet is turned onto itself, isentropically, through a series of weak oblique shocks. Thus a change in vertical velocity is transformed into a change in forward velocity. Note that, due to the presence of the forebody, the vertical velocity of the flow cannot change due to the boundary condition imposed by the forebody.

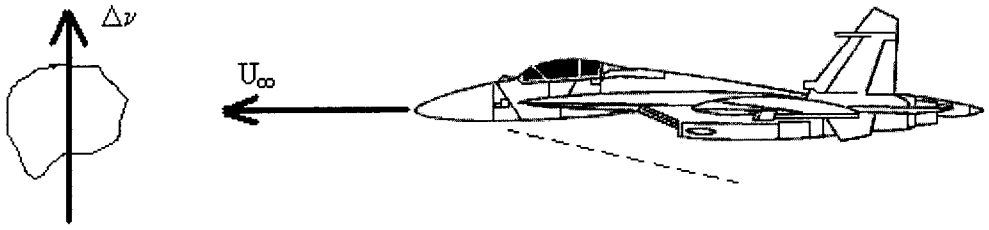

Figure 2.2: Effect of forebody on the vertical gust.

From the Prandtl-Meyer wave relation [4] we can write for a turning flow through a compression wave:

$$\frac{\Delta u}{U_\infty} \approx \frac{-\Delta\theta}{\sqrt{M_\infty{}^2 - 1}} \tag{2.7}$$

Here $\Delta\theta$ is the flow turning angle which would equal the change in the free stream flow direction due to the vertical gust given by:

$$\Delta\theta \approx \frac{\Delta v}{U_\infty} \tag{2.8}$$

From equations 2.7 and 2.8 we get the change in the forward velocity due to an isothermal vertical gust as:

$$\Delta u \approx \frac{-\Delta v}{\sqrt{M_\infty{}^2 - 1}} \tag{2.9}$$

Since the vertical gust velocity is very small as compared to the forward free stream velocity, the turning angle would also be very small. Also, for smooth turning the oblique shocks are vanishingly weak and we get isentropic compression. For an isentropic compression we have a constant total enthalpy H across the compression. Thus:

$$H = h + \frac{1}{2}u^2 = H_\infty \tag{2.10}$$

The speed of sound a is related to static enthalpy h as:

$$h = \frac{a^2}{\gamma - 1} \tag{2.11}$$

Combining Equations 2.10 and 2.11 with 2.9, for small perturbations Δu we obtain:

$$\Delta a \approx \frac{\gamma - 1}{2} \frac{M_\infty}{\sqrt{M_\infty{}^2 - 1}} \Delta v \tag{2.12}$$

hence the characteristics variables become:

$$\begin{aligned} \Delta J+ &= \frac{(M_\infty - 1)}{\sqrt{M_\infty{}^2 - 1}} \Delta v \\ \Delta J- &= -\frac{(M_\infty + 1)}{\sqrt{M_\infty{}^2 - 1}} \Delta v \\ \Delta s &= 0 \end{aligned} \tag{2.13}$$

Note that these relations are accurate only for small vertical velocity perturbations, which is necessarily the case in atmospheric disturbances.

2.3.3 Temperature Gust

A temperature gust ΔT is the same as a speed of sound change for and ideal gas. We can write:

$$\Delta a = \frac{\gamma R}{2a} \Delta T \tag{2.14}$$

For a temperature gust the forward velocity perturbation would be zero and combining Equation 2.14 with Equations 2.3 and 2.4 we get:

$$\begin{aligned} \Delta J+ &= \frac{\gamma R}{(\gamma - 1) a_\infty} \Delta T \\ \Delta J- &= -\frac{\gamma R}{(\gamma - 1) a_\infty} \Delta T \end{aligned} \tag{2.15}$$

From the definition of the entropy (Equation 2.5) we obtain for a pure temperature gust (the pressure is constant),

$$\Delta s = \gamma p_\infty v^{\gamma - 1} \Delta v \tag{2.16}$$

$$a^2 = \gamma R T = \gamma p v \tag{2.17}$$

Combining Equations 2.17 and 2.11 we get:

$$\Delta v = \frac{\gamma - 1}{\gamma p_\infty} \Delta h = \frac{\gamma - 1}{\gamma p_\infty} c_p \Delta T \tag{2.18}$$

From Equations 2.18 and 2.16 we obtain finally:

$$\Delta s = \frac{\gamma R}{\rho_\infty^{\gamma-1}} \Delta T \tag{2.19}$$

We can write the transformation from the atmospheric disturbance variables to the characteristic variables in matrix form as follows:

$$\begin{bmatrix} \Delta J+ \\ \Delta J- \\ \Delta s \end{bmatrix} = \begin{bmatrix} 1 & \frac{M_\infty - 1}{\sqrt{M_\infty^2 - 1}} & \frac{\gamma R}{(\gamma-1)a_\infty} \\ 1 & -\frac{M_\infty + 1}{\sqrt{M_\infty^2 - 1}} & -\frac{\gamma R}{(\gamma-1)a_\infty} \\ 0 & 0 & \frac{\gamma R}{\rho_\infty^{\gamma-1}} \end{bmatrix} \begin{bmatrix} \Delta u \\ \Delta v \\ \Delta T \end{bmatrix} \tag{2.20}$$

For a full scale inlet flying at 60,000 ft with a speed of Mach 2.2 in standard atmosphere, we get the above transformation matrix in SI units as:

$$\begin{bmatrix} \Delta J+ \\ \Delta J- \\ \Delta s \end{bmatrix} = \begin{bmatrix} 1 & 0.6124 & 3.4046 \\ 1 & -0.6124 & -3.4046 \\ 0 & 0 & 936.11 \end{bmatrix} \begin{bmatrix} \Delta u \\ \Delta v \\ \Delta T \end{bmatrix} \tag{2.21}$$

For the Euler simulation of the inlet we assume a stagnation speed of sound and stagnation density of 1.0 (for normalization purposes), thus the transformation matrix for the simulation becomes:

$$\begin{bmatrix} \Delta J+ \\ \Delta J- \\ \Delta s \end{bmatrix} = \begin{bmatrix} 0.0024 & 0.0015 & 0.0082 \\ 0.0024 & -0.0039 & -0.0082 \\ 0 & 0 & 0.0046 \end{bmatrix} \begin{bmatrix} \Delta u \\ \Delta v \\ \Delta T \end{bmatrix} \tag{2.23}$$

Here the transformation matrix is scaled such that the characteristic disturbance variables are non-dimensional while the atmospheric disturbance variables are dimensional, i.e., the non-dimensionalization factor is included in the transformation matrix (2.23).

2.4 Spectra of atmospheric disturbances in Characteristic form

In order to find the spectra of atmospheric disturbances in characteristic form we see that any disturbance in characteristic form is a linear combination of forward velocity, vertical velocity and temperature disturbances, e.g., in the case of $J+$ we get:

$$\Delta J+ = \beta_u \Delta u + \beta_v \Delta v + \beta_T \Delta T \tag{2.24}$$

Where the scaling coefficients, β's, are given by the transformation matrix. The spectra of $J+$ in terms of spatial wavenumbers is given by definition as:

$$S_{J+}(k) = \int_{-\infty}^{\infty} R_{J+}(l) e^{-i2\pi kl} dl \tag{2.25}$$

Where $R_{J+}(l)$ is the spatial autocorrelation function of $J+$ disturbance given by:

$$R_{J+}(l) = \left\langle \Delta J^+(x) \Delta J^+(x+l) \right\rangle \tag{2.26}$$

Here $\langle\ \rangle$ denotes the expectation. Assuming that the expectations of the products of forward velocity with other disturbances is zero or in other words the atmospheric disturbances are independent of each other, the autocorrelation function for $J+$ reduces to:

$$R_{J+}(l) = \beta_u{}^2 R_u(l) + \beta_v{}^2 R_v(l) + \beta_T{}^2 R_T(l) \tag{2.27}$$

From the above it is clear that the spectrum of $J+$ disturbance is given by:

$$S_{J+}(k) = \beta_u{}^2 S_u(k) + \beta_v{}^2 S_v(k) + \beta_T{}^2 S_T(k) \tag{2.28}$$

Since all the spectra have the same relationship with only the scaling coefficient different as given by Equation (2.2), we can write the above expression in a more compact form as:

$$S_{J+}(k) = \alpha_{J+} \varepsilon^{2/3} k^{-5/3} \tag{2.29}$$

Where the coefficient is given by:

$$\alpha_{J+} = \beta_u{}^2 \alpha_l + \beta_v{}^2 \alpha_v + \beta_T{}^2 \alpha_T \tag{2.30}$$

Similarly we can define the spectra for $J-$ and entropy s.

2.5 Non-dimensionalization of disturbance variables

We can convert a quasi-steady spatial disturbance to temporal disturbance for an aircraft flying at some Mach number M using relation (2.1). Suppose that we want to test a scaled version of an inlet at some different local conditions. For that we need to non-dimensionalize all the variables so that we can have a correspondence between different scales and test conditions. To non-dimensionalize length we use inlet height H, for speed we use local stagnation speed of sound a_0. Thus for time the factor is a_0/H. We can non-dimensionalize the frequency as follows:

$$\text{dimension - less wavelength} = \lambda^* = \frac{\lambda}{H} = \frac{Ma_0}{fH}$$

$$f = \frac{Ma_0}{\lambda^* H} \tag{2.31}$$

Thus we can relate the frequency of disturbance as seen by the full-scale inlet to some scaled experimental inlet using the above relationship as follows:

$$f_{sim} = f_{full} \frac{a_{0sim}}{a_{0full}} \frac{H_{full}}{H_{sim}} \tag{2.32}$$

Here f_{full} is the actual frequency of disturbances as seen by a full-scale inlet while f_{sim} is the reduced frequency for the scaled inlet of height H_{sim} used in the simulation or experiments.

To non-dimensionalize temperature we use the relationship:

$$T_0 = \frac{a_0^{\,2}}{\gamma R} \tag{2.33}$$

Where R is the universal gas constant and T_0 is the local stagnation temperature. Thus for the simulation we get:

$$T_{0sim} = T_{0full} \frac{a_{0sim}^{\,2}}{a_{0full}^{\,2}} \tag{2.34}$$

The atmospheric disturbance spectra in the characteristic form are shown in Figure 2.3 after scaling the actual disturbance velocities and temperature.

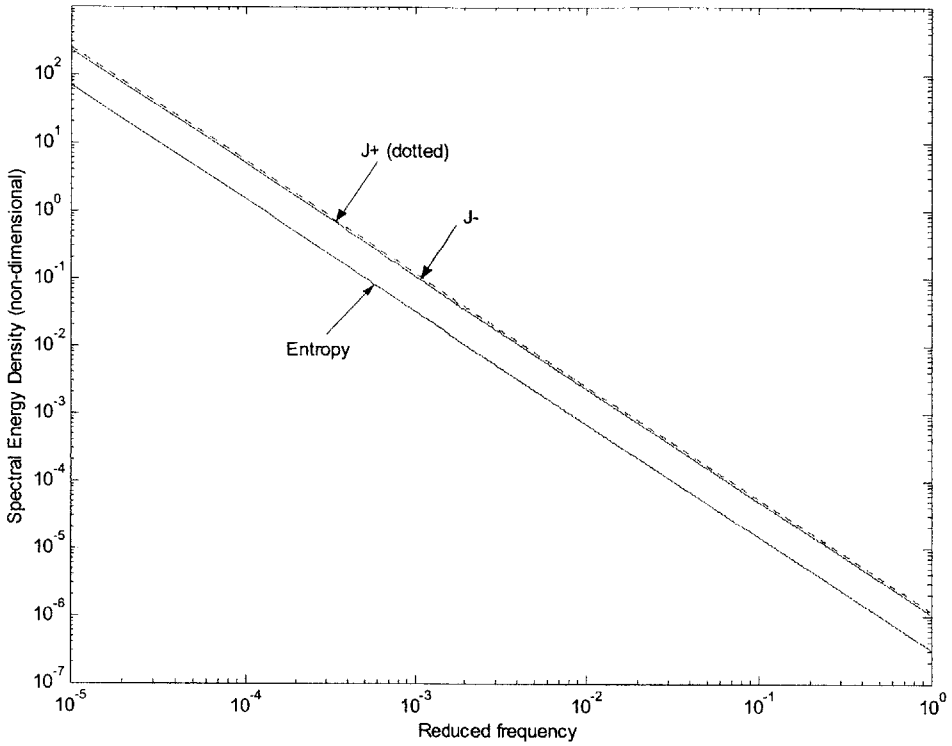

Figure 2.3: Atmospheric disturbance spectra in characteristic form.

2.6 Modification of disturbance spectra by velocity hold and ramp control

Atmospheric disturbances having very large wavelengths in the macroscale regions can exhibit large variations in gust velocities as discussed previously. From the point of view of inlet control we can assume that these large scale disturbances (> 6-20 km or frequencies below 0.03 to 0.1 Hz) will be absorbed by the aircraft velocity hold system. We also require a ramp control system in the inlet as discussed in chapter 1, which can modify the area properties of the inlet depending on the engine demand and atmospheric turbulence to avoid the unstart. Thus the inlet control system will see the atmospheric disturbance spectra attenuated by the vehicle velocity hold system and the inlet ramp control system.

2.6.1 Estimate of the Attenuation due to Ramp Control System

We assume a second order closed-loop response of the ramp control system with a slew rate of 60 deg/sec. Assuming a transfer function of the ramp control from the atmospheric disturbances to the throat Mach number as a second order system given by:

$$G_R(s) = \frac{s^2}{s^2 + 0.8376s + 1.0962} \tag{2.35}$$

Where the natural frequency is 1.047 (corresponding to a slew rate of 60 deg/sec) and damping ratio is assumed to be 0.4. Thus we see that the ramp control system acts as a high pass filter and attenuates the larger scale disturbances.

2.6.2 Estimate of the Attenuation due to Velocity/Mach Hold System

To get a quick estimate of the closed loop performance of a typical velocity/Mach hold system for the class of aircraft we are interested in, the data from [9] of a supersonic aircraft in the same weight class was used to estimate the velocity hold cutoff at around 0.33 rad/s (corresponding to a closed loop settling time of 15 sec giving an approximate time constant of 3 sec). For simplicity a full state feedback LQR controller was designed to get the step response in forward velocity as shown in Figure 2.4.

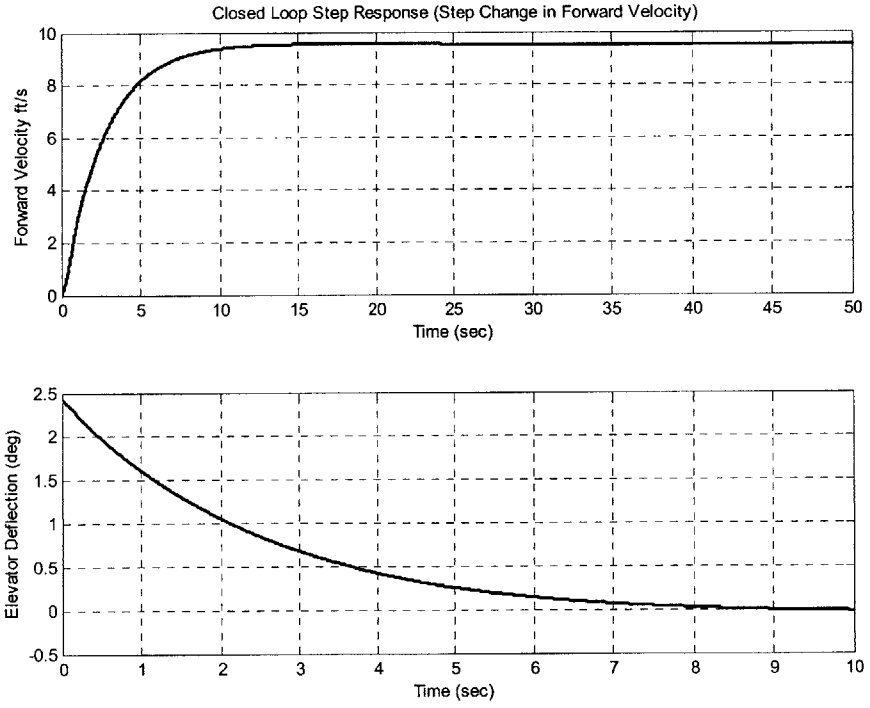

Figure 2.4: Closed loop bandwidth estimation for the velocity hold control system for a typical (39000 lb) supersonic aircraft at Mach 2 at an altitude of 55000 ft.

Assuming a dominant first order closed loop transfer function from atmospheric disturbance to forward velocity:

$$G_V(s) = \frac{s}{s + 0.33} \tag{2.36}$$

Using these transfer functions we can modify the spectra of atmospheric disturbances according to the following relationship [10]:

$$S_{out}(s) = |G(s)|^2 S_{in}(s) \tag{2.37}$$

Where $S_{in}(s)$ is the input spectrum to a system with transfer function $G(s)$ and $S_{out}(s)$ is the spectrum at the output of the system. A modified spectrum for the forward gust is shown in Figure 2.5.

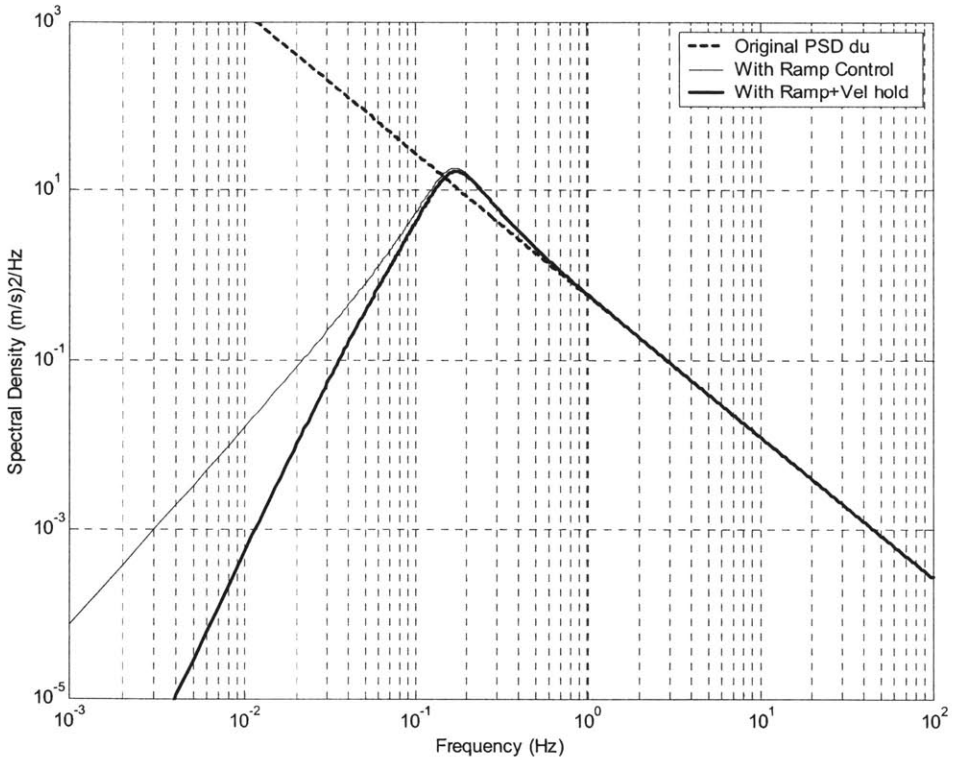

Figure 2.5: Spectrum for forward gust velocity and its modification due to ramp control and velocity hold systems.

From this modified spectrum we can calculate the maximum frequency of interest for the inlet disturbance rejection control system. This maximum frequency is calculated as that frequency which gives 99% of the spectral energy. For this particular spectrum it turns out to be approximately 18 Hz. Thus frequencies up to 18 Hz contribute 99% of the energy in the disturbance while higher frequencies only contribute the remaining1%. So from the point of view of the inlet control system we need only consider frequencies up to 18 Hz. Also as can be seen from the modified spectrum on the lower side, the

frequencies below 0.01 Hz are cutoff by the ramp control and velocity hold systems. Thus the range of frequencies of interest in the study of control system effectiveness in rejection of atmospheric disturbances is approximately from 0.01 Hz to 18 Hz for the full scale and 4.4×10^{-5} to 0.088 for the non-dimensional case.

It should be noted that the effective gain of the ramp and velocity/Mach hold systems is not infinity thus for very low frequencies we may not get the roll-off as shown in Figure 2.5. But the atmospheric spectra also do not obey the –5/3 law for very low frequencies; rather it gives an overestimate as compared to the actual measurements of the disturbances [6]. We also assume that although we get a flattened spectrum at very low frequencies, it is attenuated enough that the effect of disturbances at these low frequencies is negligible.

2.7 Summary

We need to express the atmospheric disturbances in terms of canonical variables. We can represent the disturbances in terms of power spectral densities. The inlet sees the disturbances modified by the ramp control and velocity/Mach hold systems. Thus in order to have a realistic estimate of the disturbances to be rejected by the control system, one should use the modified power spectral density functions.

Chapter 3

Inlet Dynamic Characterization

As mentioned in previous chapters, in order to design an effective control system architecture for the stabilization of the inlet during all flight regimes, it is necessary to be able to predict the dynamic behavior of the inlet with reasonable accuracy. If we can predict the dynamic behavior of the inlet using a relatively small number of parameters, then it is easier to design a control system based on these parameters. Keeping this in mind, this chapter first describes the creation of the necessary tools for the prediction of dynamic behavior. Then using these tools the dynamic behavior of the inlet is characterized in the form of transfer functions. Then simple models are fitted to these transfer functions to extract the parameters necessary for the understanding of the dynamic characteristics of the inlet.

3.1 Unsteady Quasi-1D Euler Simulation

An unsteady quasi-1D numerical code was developed by Merchant [2] and was used in the study of the dynamic characterization of the inlet. Area variation at the throat and exit boundary was used in the simulation to match the steady state Mach profile of the 1D simulation with the designed Mach profile for the actual 2D inlet design. In order to use this code for dynamic characterization of the inlet it is necessary to be able to excite the inlet with different disturbances and apply some control to analyze the control system design. For this purpose, the code was embedded in Simulink and integrated into Matlab to generate routines with the help of which different transfer functions can be generated and different control schemes can be tested and analyzed.

A block diagram of the Simulink model (called an S-function) of the inlet is shown in Figure 3.1. As can be seen in the figure, we can excite the inlet with a number of different disturbances. Also we can apply control through upstream and shock bleed perturbations. Atmospheric disturbances are introduced in terms of forward velocity, vertical/up velocity and temperature perturbations. As discussed in the previous chapter, from the point of view of the dynamic behavior of the inlet it is important to be able to study the characteristic form of the disturbances. Thus we also have the option of applying the disturbances in the form of Riemann's Invariants J+ and J-. For the temperature or speed of sound change an entropy perturbation input is also provided. Thus we can excite the inlet using the characteristic form. As discussed later in this chapter, this capability reveals very useful information about the dynamic response of the inlet to atmospheric disturbances. The physical interface of the Simulink model is explained pictorially in Figure 3.2.

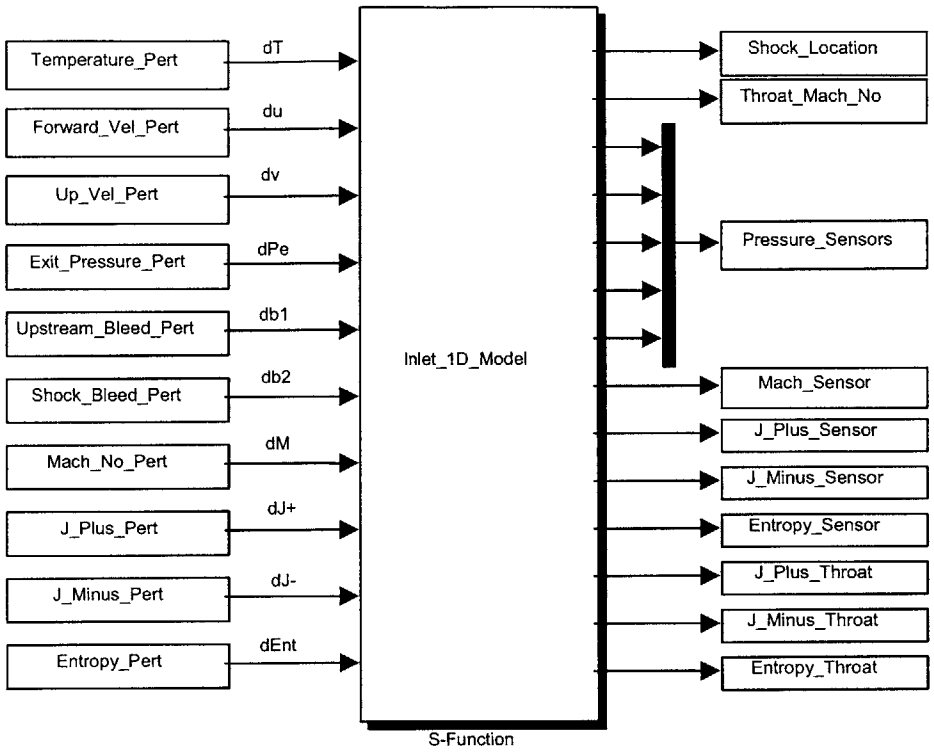

Figure 3.1: 1D Simulink Model of the inlet.

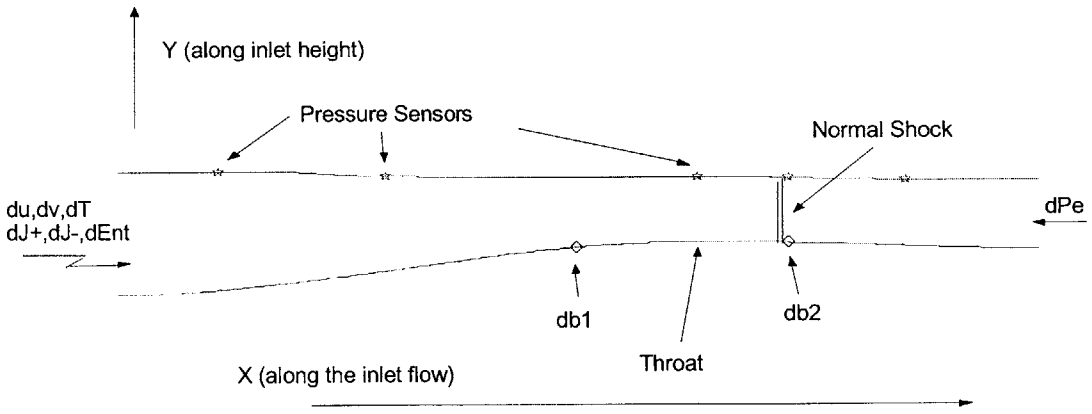

Figure 3.2: Pictorial representation of inlet physical interface.

3.2 Frequency Response Study of the Inlet

Using the Simulink model we can excite each input with a small sinusoidal signal at different frequencies and find out the frequency response of the inlet at any desired output. Such numerically obtained frequency responses provide good physical insight into the dynamic operation of the inlet under consideration but they are parameter free. Thus they do not provide insight into the physics of the problem at hand, i.e., we cannot generalize the results. For this reason we will study the frequency response of the inlet for the disturbances in characteristic form and try to fit the responses with simple models to get an understanding of the physical phenomena.

The following transfer functions are studied and are described in detail in following sections:

1. Inlet lip fast acoustic wave perturbations (dJ+) to static pressure sensor, throat Mach number (M_{th}) and shock position.
2. Inlet lip slow acoustic wave perturbations (dJ-) to static pressure sensor, throat Mach number (M_{th}) and shock position.
3. Inlet lip entropy perturbations to static pressure sensor, throat Mach number (M_{th}) and shock position.
4. Inlet lip forward velocity perturbations (du) to static pressure sensor, throat Mach number (M_{th}) and shock position.
5. Inlet lip vertical/up velocity perturbations (dv) to static pressure sensor, throat Mach number (M_{th}) and shock position.
6. Inlet lip temperature perturbation (dT) to static pressure sensor and throat Mach number (M_{th}) and shock position.
7. Upstream bleed perturbations (db1) to throat Mach number (M_{th}) and Shock.

The static pressure sensor is located upstream of the throat near to the lip of the inlet. For this study a location of 0.5 inlet heights from the inlet lip was used (first star in Figure 3.2).

For the 1D study the following nominal values of the inlet parameters were used:

Inlet Mach No. = 2.2
Mean Upstream Bleed = 1% of inlet mass flow
Mean Shock Bleed = 2% of inlet mass flow
Shock Location = 4.0
Throat Location = 3.5
Inlet Height/Length = 1.0/5.5
Exit Pressure Boundary Condition = Constant Exit Pressure

These nominal values are based on the steady-state inlet design as described in [2]. For a detailed description of non-dimensionalization of different variables see chapter 2.

3.2.1 Fast Acoustic Wave Perturbations (dJ+)

As discussed in chapter 2, the fast acoustic wave perturbation can result from a perturbation in forward velocity or vertical velocity, or from a perturbation in the speed of sound, as given by expression (2.3). The perturbation in the speed of sound is equivalent to a temperature perturbation since the speed of sound, in a perfect gas, is related to the temperature according to:

$$a = \sqrt{\gamma RT} \tag{3.1}$$

The frequency response from the inlet lip J+ disturbance to throat Mach number is shown in Figure 3.3. Similarly Figure 3.4 gives the response from the inlet J+ disturbance to the $J+$ value at the sensor and throat. From the plot it can be seen that the inlet actually passes the disturbance with very little amplification at the throat. It can be seen that low frequencies are most important as far as the throat Mach number is concerned.

3.2.2 Shock Motion due to J+ Perturbations

Normal shock motion is affected by the J+ perturbations but it is a highly non-linear

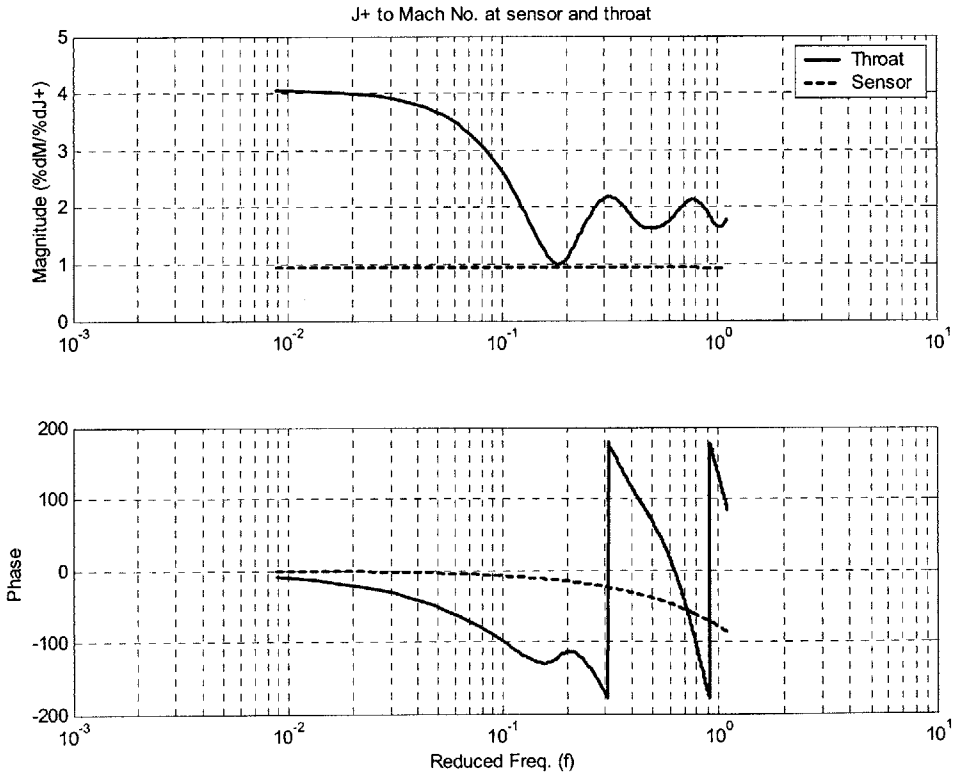

Figure 3.3: Frequency response of the inlet J+ disturbance to throat Mach number.

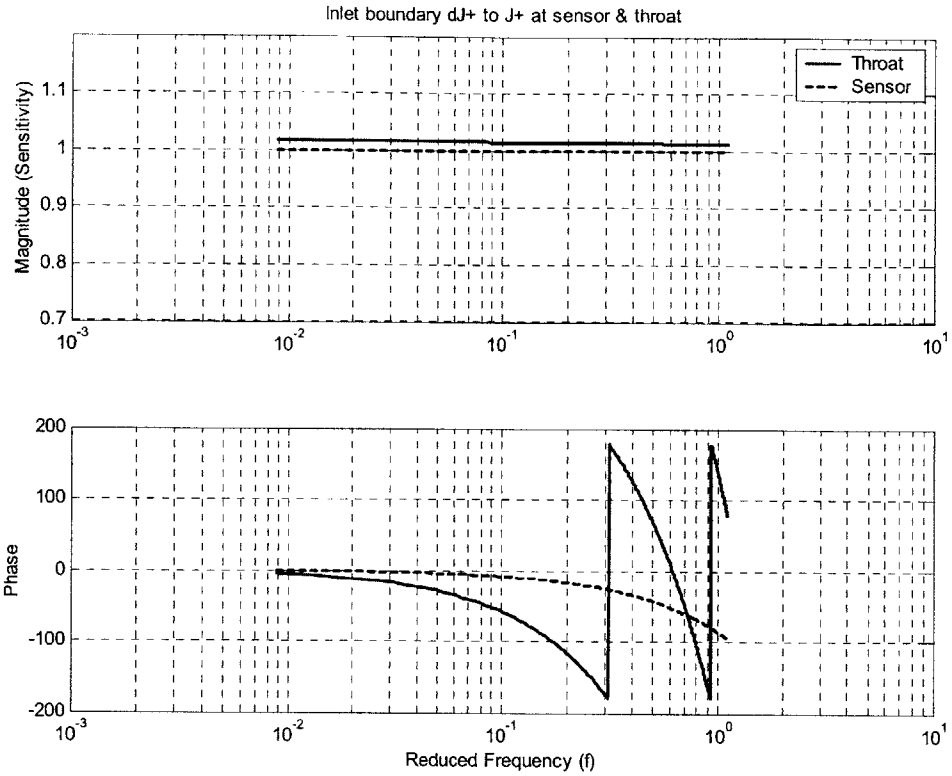

Figure 3.4: Frequency response of the inlet J+ disturbance to sensor and throat J+.

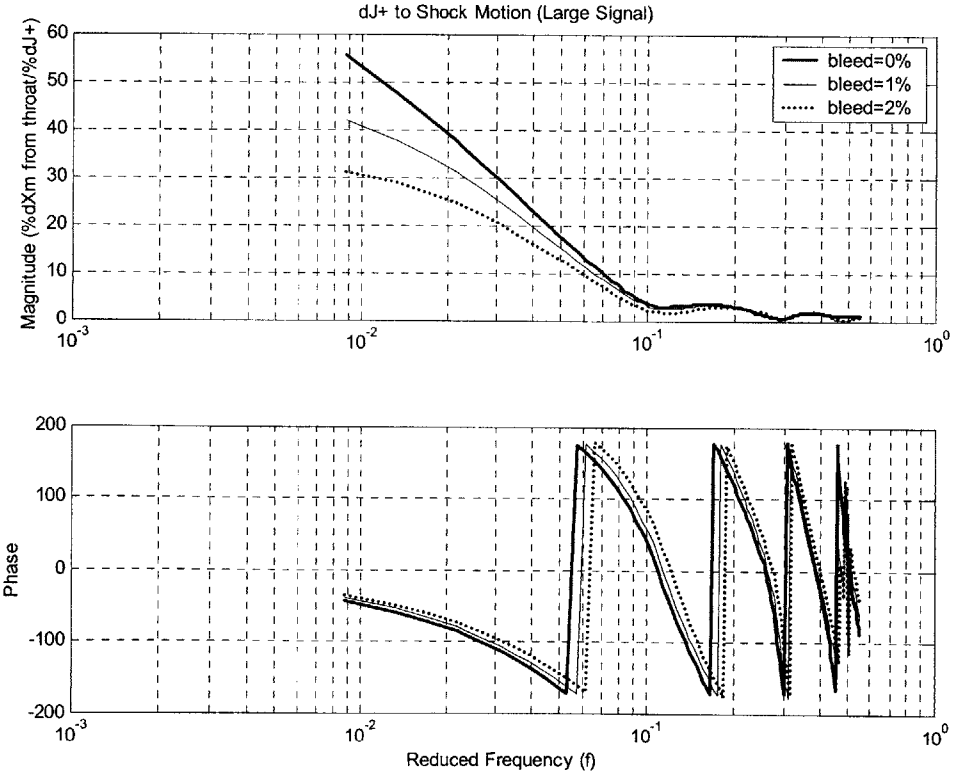

Figure 3.5: Shock Motion as a function of frequency for J+ perturbation at the inlet lip.

function of different parameters such as shock bleed, distance of normal shock from throat etc. In order to study the effect of J+ perturbations on shock motion the large signal frequency response of the shock motion is obtained for different mean shock bleed values. The results are shown in Figure 3.5.

The reason for using large excitation signals for the generation of the frequency response in Figure 3.5 is the grid size used in the discretization of the inlet. For small perturbations the shock motion is negligibly small and the number of grid points required to resolve the shock motion is prohibitively large. Hence in order to get an estimate of the response of shock motion to the disturbances, large input signals that are typical of the worst-case atmospheric perturbations, were used. Although these large signals result in the non-linear operation of the inlet and thus are not true representation of the linear frequency response of the system, nevertheless these plots still reveal some useful information about the dynamic characteristics of the shock motion.

The motion of the shock is a non-linear function of both perturbations and bleed control as shown in Figure 3.6 for a sinusoidal J+ input perturbation. For instance in Figure 3.6 we see that the shock not only oscillates according to the input, it also has a tendency to shift towards the throat after each oscillation. Nevertheless, such a frequency response study (as in Figure 3.5) still provides very useful information regarding the dynamics of the shock motion. It is very clear that the shock motion is a strong function of the frequency of the perturbation. The shock is most severely affected by the zero frequency or DC perturbation. As the frequency increases the shock amplitude becomes smaller and

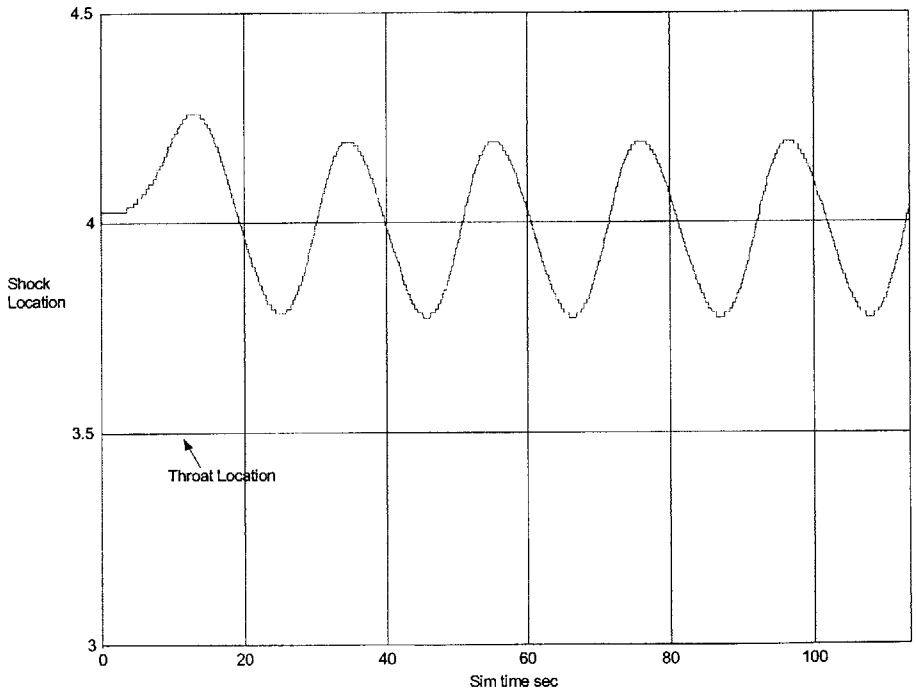

Figure 3.6: Shock Motion for sinusoidal J+ perturbation at inlet lip.

for non-dimensional frequencies of values higher than 0.1 we get almost negligible shock motion. Secondly, the shock motion is an inverse function of the steady-state bleed level.

Thus for higher values of steady-state bleed the shock motion is reduced. This immediately suggests a simple form of controller for shock motion control. We can simply employ a controller that provides shock motion control by a bleed that is proportional to the distance of the shock from its nominal position. This type of controller is presented in detail in [15] and will be discussed further in chapter 4.

3.2.3 Slow Acoustic Wave Perturbations (dJ-)

Slow acoustic wave perturbations also result from all the atmospheric perturbations that we are considering, namely forward velocity, vertical velocity and temperature perturbations as given in chapter 2. The frequency response of the inlet from J- perturbations to throat Mach number is given in Figure 3.7. Figure 3.8 gives the frequency response for J- at the static presser sensor location and the throat. It can be seen that the inlet has almost a flat response for J- perturbations. Throat Mach number is affected to a higher non-dimensional frequency of approximately 1.0. Also from Figure 3.8 we see that the inlet amplifies the J- perturbations at the throat by a factor of almost 2.25. From the spectra of J+ and J- disturbances shown in Figure 2.3 in chapter 2, we see that incoming J+ and J- disturbances have almost equal magnitudes; therefore (comparing Figures 3.4 and 3.8) from the point of view of the control of throat Mach number J- perturbations are more important than J+ perturbations.

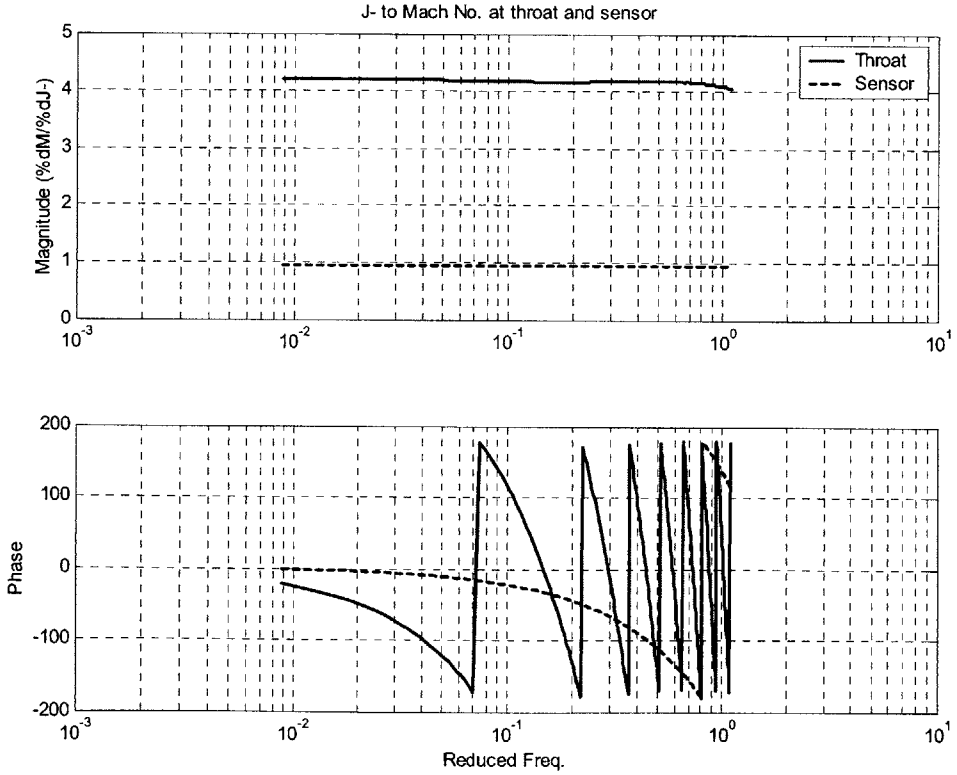

Figure 3.7: Frequency response of inlet J- to Mach No. at Throat and Sensor.

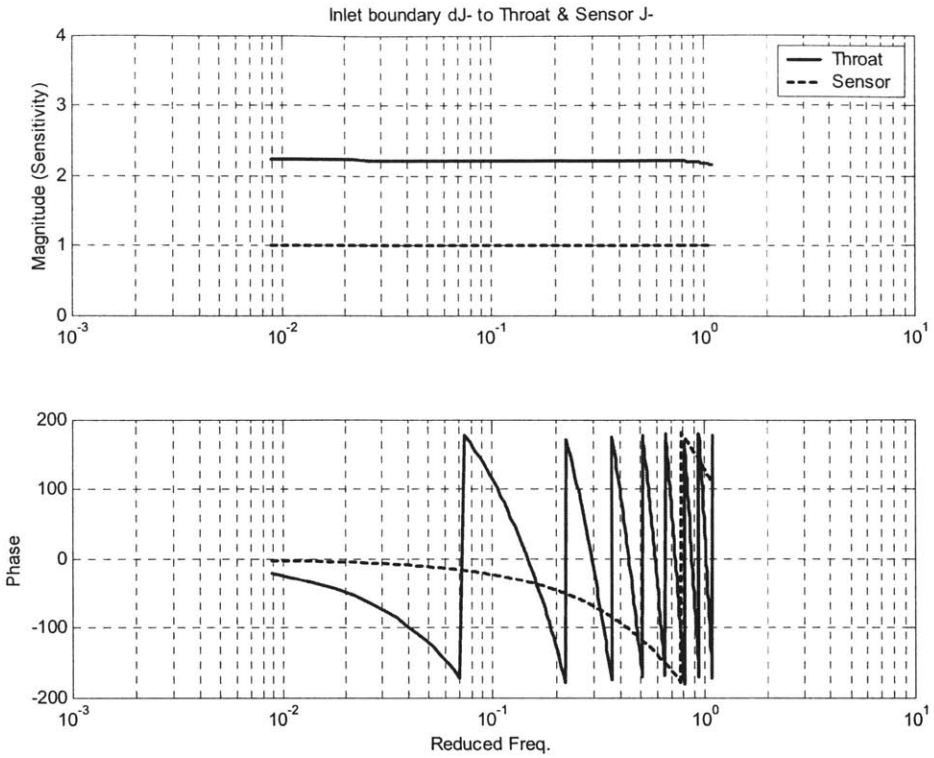

Figure 3.8: Frequency response of the inlet J- disturbance to sensor and throat J-.

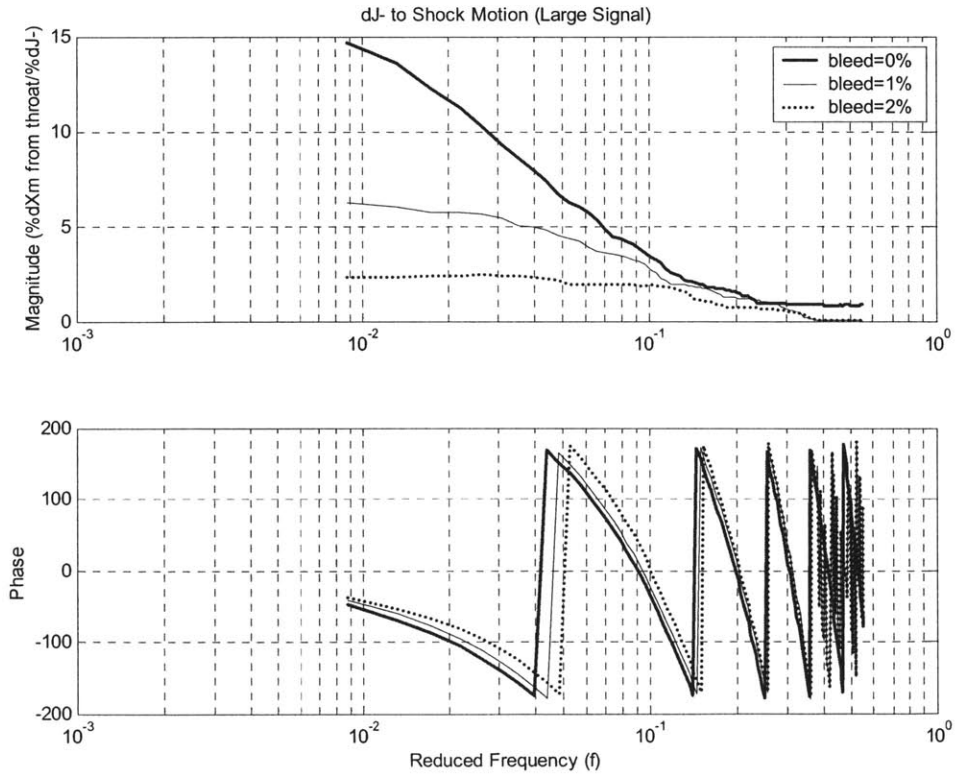

Figure 3.9: Shock Motion as a function of frequency for J- perturbations at inlet lip.

3.2.4 Shock Motion due to J- Perturbations

Shock motion is also affected by J- perturbations and a large signal frequency response of shock motion for J- perturbations is shown in Figure 3.9.

Comparing Figures 3.5 and 3.9, it is immediately clear that as far as shock motion is concerned J- perturbations have far less affect (by almost an order of magnitude) as compared to J+ perturbations. Also shock motion is again severely affected by the amount of bleed, which has a much stronger attenuating effect in this case as compared to J+.

3.2.5 Entropy Perturbations

Entropy perturbations result from a speed of sound or temperature change in the atmosphere as discussed in chapter 2. The frequency response plots for throat Mach number and values of entropy at a static pressure sensor, located 0.5 inlet heights downstream of the inlet lip, and at the throat are shown in Figures 3.10 and 3.11 respectively.

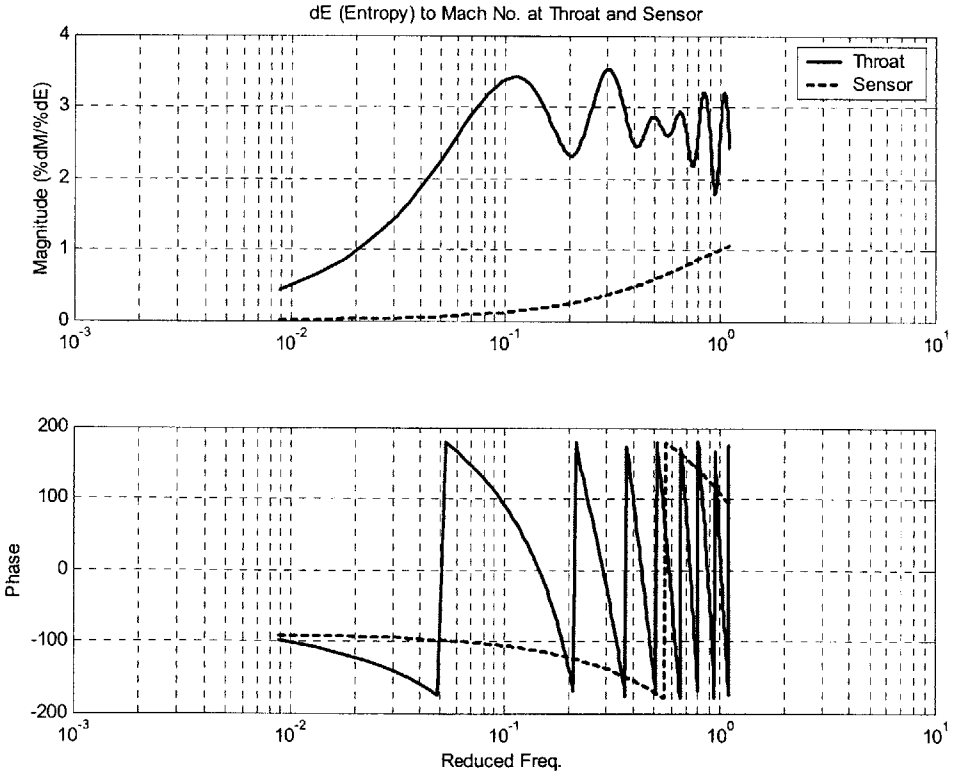

Figure 3.10: Throat and Sensor Mach number as a function of frequency for inlet lip entropy perturbations. (Sensor is located 0.5 inlet heights downstream of inlet lip).

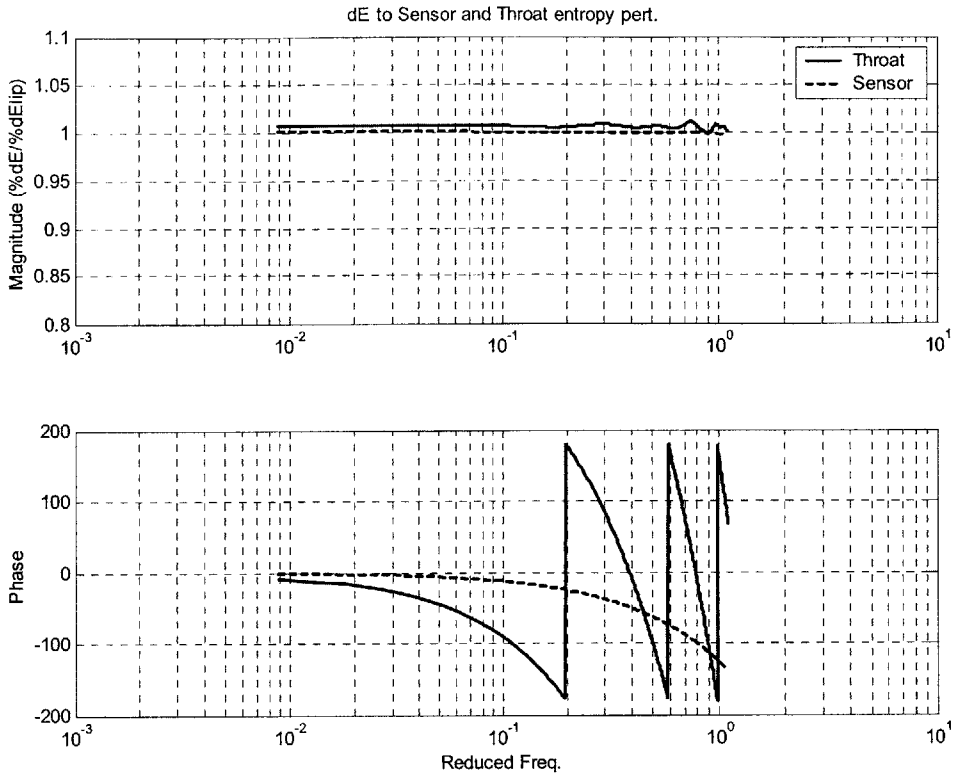

Figure 3.11: Inlet lip entropy perturbations to entropy perturbations at Throat and sensor (located at 0.5 inlet heights downstream of inlet lip).

As can be seen from Figure 3.10, the throat Mach number is not affected much by the low frequency components of the entropy perturbations; it is affected mostly by perturbations that have a non-dimensional frequency higher than about 0.1. By looking at the entropy, as an output, at the static pressure sensor location and at the throat we can see that the inlet does not amplify the entropy perturbations; and it remains almost constant from the lip of the inlet to the throat.

3.2.6 Shock Motion due to Entropy perturbations

Figure 3.12 shows the large signal frequency response for the entropy perturbations. This response is almost identical to that for J+ except for a phase reversal, i.e., for positive entropy perturbations at the inlet lip we get negative shock motion which means the shock moves away from the throat.

From the transfer functions of shock motion for different canonical perturbations it is clear that J+ and entropy perturbations are most important from the point of view of shock motion control. Similarly for the control of throat Mach number the J- perturbation is most important.

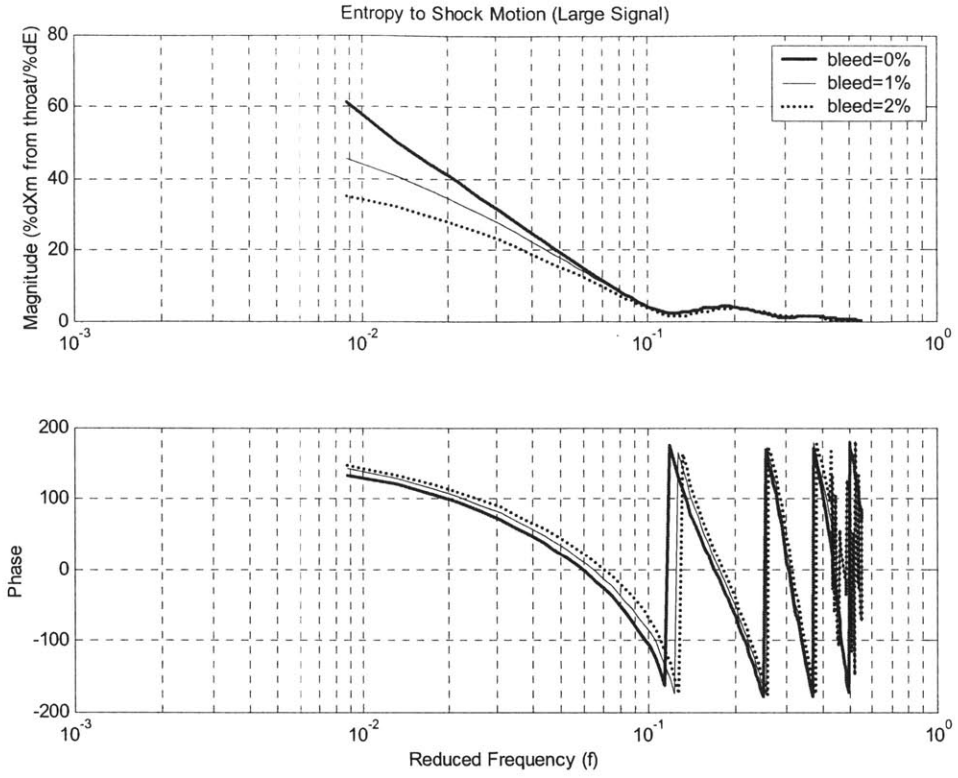

Figure 3.12: Shock Motion as a function of frequency for Entropy perturbations at inlet lip.

3.2.7 Frequency Response Plots for Atmospheric Perturbations

The frequency response plots for atmospheric perturbations in forward velocity, vertical velocity and temperature are also computed and are given in Figures 3.13 to 3.15 respectively for comparison purposes.

Note that the temperature perturbation results in all three canonical perturbations i.e., J+, J- and entropy and thus its frequency response plot is a combination of all three canonical plots scaled by different factors. From a comparison of the effect on throat Mach number response to different atmospheric disturbances it is apparent that the temperature perturbation has the smallest affect on the throat Mach number. Throat Mach number perturbations due to the temperature perturbations are significant up to a non-dimensional frequency of around 0.4, while other atmospheric perturbations are significant up to and beyond a non-dimensional frequency of 1.0.

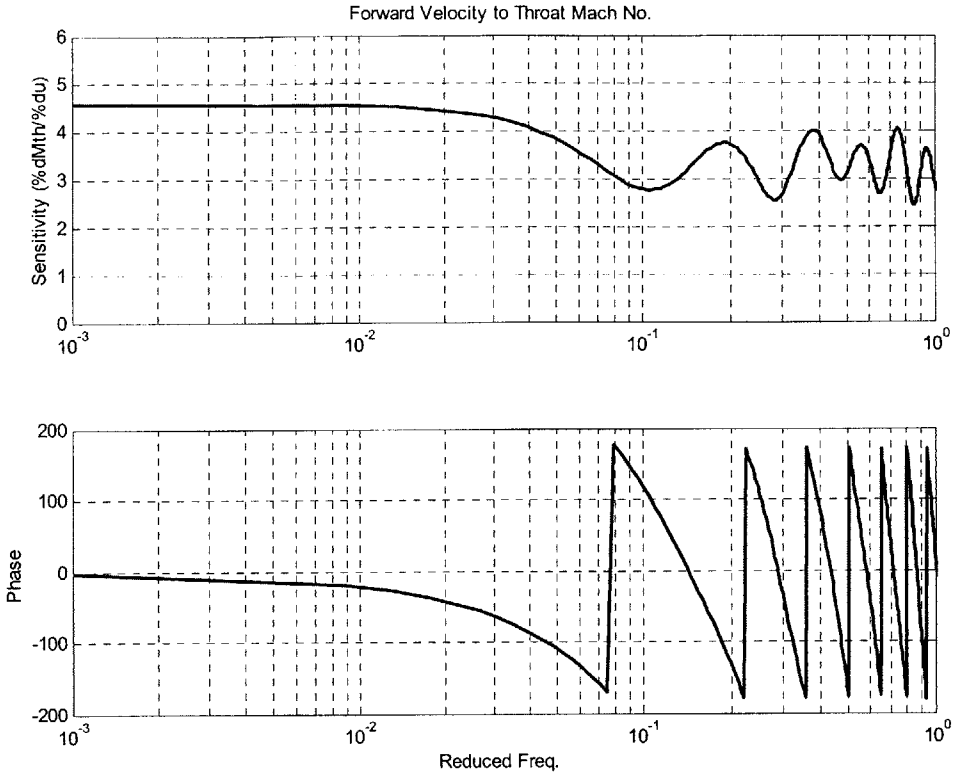

Figure 3.13: Frequency response of forward velocity to Mach number at throat.

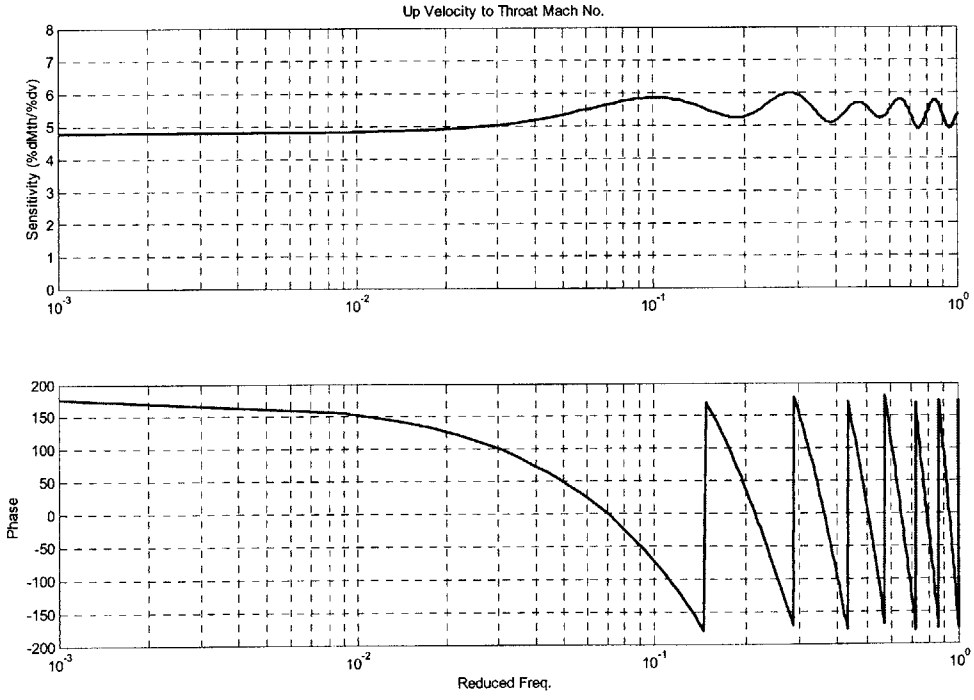

Figure 3.14: Vertical velocity to throat Mach number frequency response.

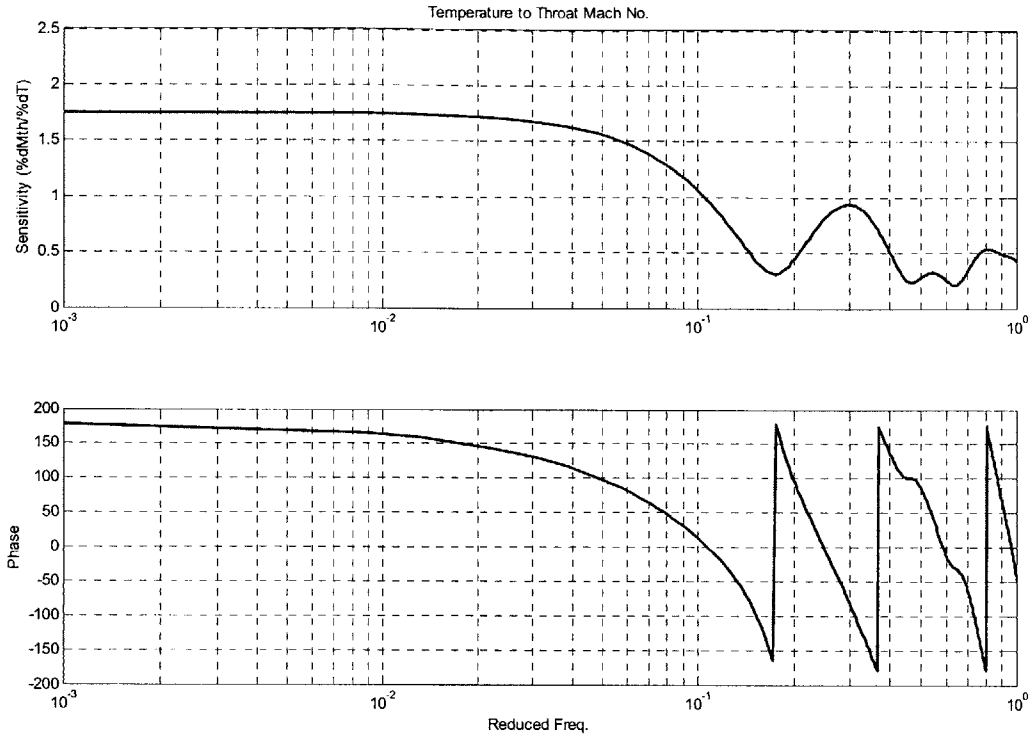

Figure 3.15: Temperature perturbations to throat Mach number frequency response.

3.2.8 Upstream Bleed Perturbations

In order to control the throat Mach number an upstream bleed or suction valve is used to cancel the disturbances propagating through the inlet. The purpose of the upstream suction is to launch a counter disturbance with the right magnitude and timing so that by the time the incoming disturbance reaches the throat the counter disturbance is there to cancel it. In this way we can use the upstream bleed to act as a disturbance rejection actuator. In order to perform this function we need its dynamic characteristics or more specifically its transfer function to throat Mach number as given in Figure 3.16. From this we see that if we bleed 1% of inlet mass flow we get around 2.5% variation in throat Mach number, which comes out to be around 0.03. This does not give us enough control authority to control throat Mach number variations due to atmospheric disturbances, which cause around 3% to 5% variation in throat Mach number for worst-case inputs. From this discussion it is apparent that in order to reject the worst-case atmospheric disturbances we need to bleed around 2% of the inlet mass flow. The main purpose of the upstream bleed is to prevent the inlet unstart by not allowing the throat Mach number to fall below unity due to incoming disturbances (see inlet unstart mechanisms in section 3.7). From Figure 3.16 it is clear that we need to bleed more to prevent the throat Mach number from falling below its nominal value. This means that we can have a mean bleed value of 1% and then allow the control system to bleed up to 3% (i.e. 2% perturbation) or

more to prevent the throat Mach number from falling. At the other extreme, we can at most completely close the valve, therefore we can only decrease the bleed by 1% (i.e. by mean bleed value). This gives us less control authority to prevent the throat Mach number from rising. However, an increased throat Mach number, due to incoming disturbances, is not as critical as a decrease in throat Mach number as it would push the shock downstream and would not result in unstart of the inlet.

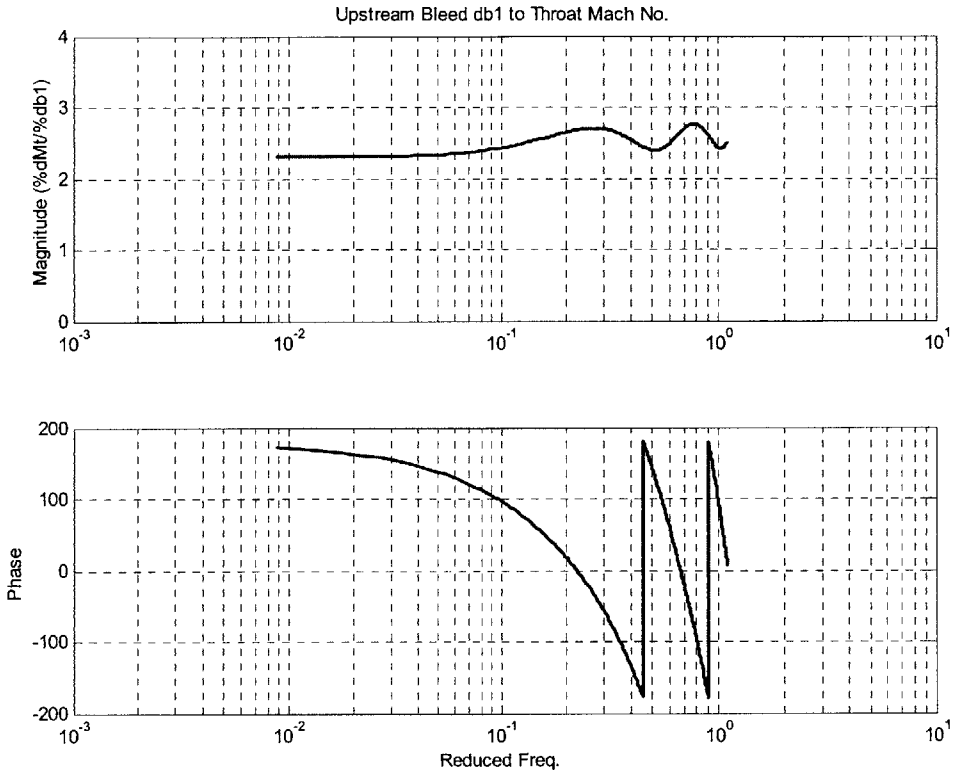

Figure 3.16: Frequency response of the throat Mach for upstream bleed perturbations.

Another way to look at the upstream bleed effectiveness for canceling disturbances is to look at the transfer function from upstream bleed to characteristic disturbances at the throat. Figures 3.17 to 3.19 show the ability of the bleed to change the J-, J+ and entropy at the throat respectively and hence give a measure of effectiveness of the bleed in canceling these disturbances. As can be seen in these figures the upstream bleed is very poor for canceling the fast acoustic wave and entropy perturbations at the throat; it is most effective in canceling the slow acoustic waves. The throat Mach number is most strongly affected by the slow acoustic waves, so it is fortunate that we can control it most effectively.

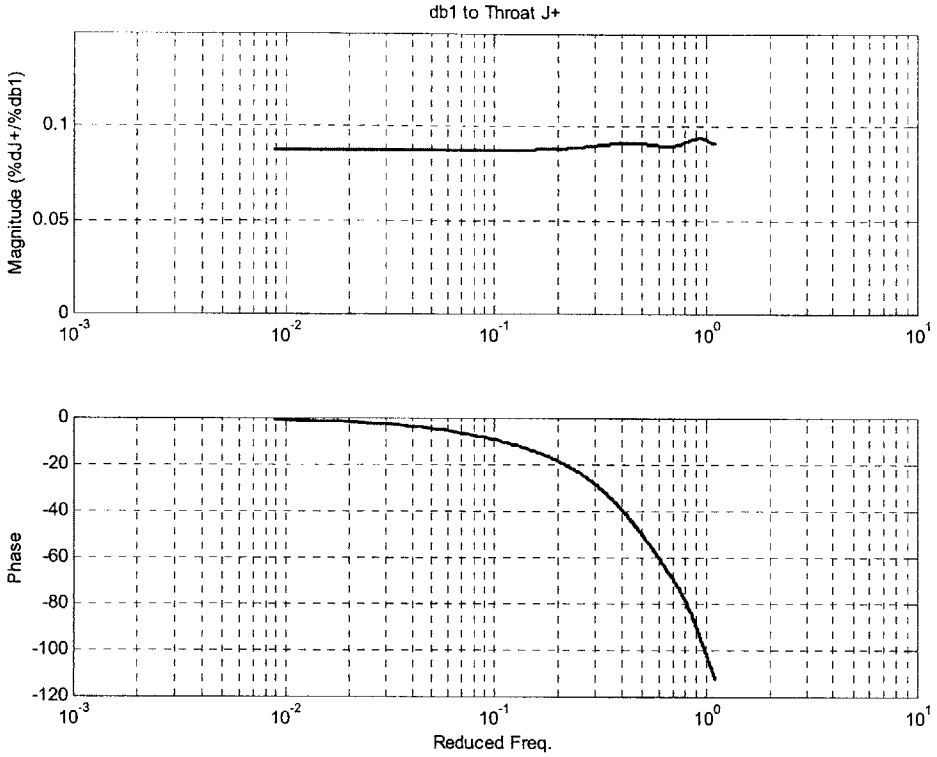

Figure 3.17: Upstream bleed perturbations to throat J+ variations as a function of frequency.

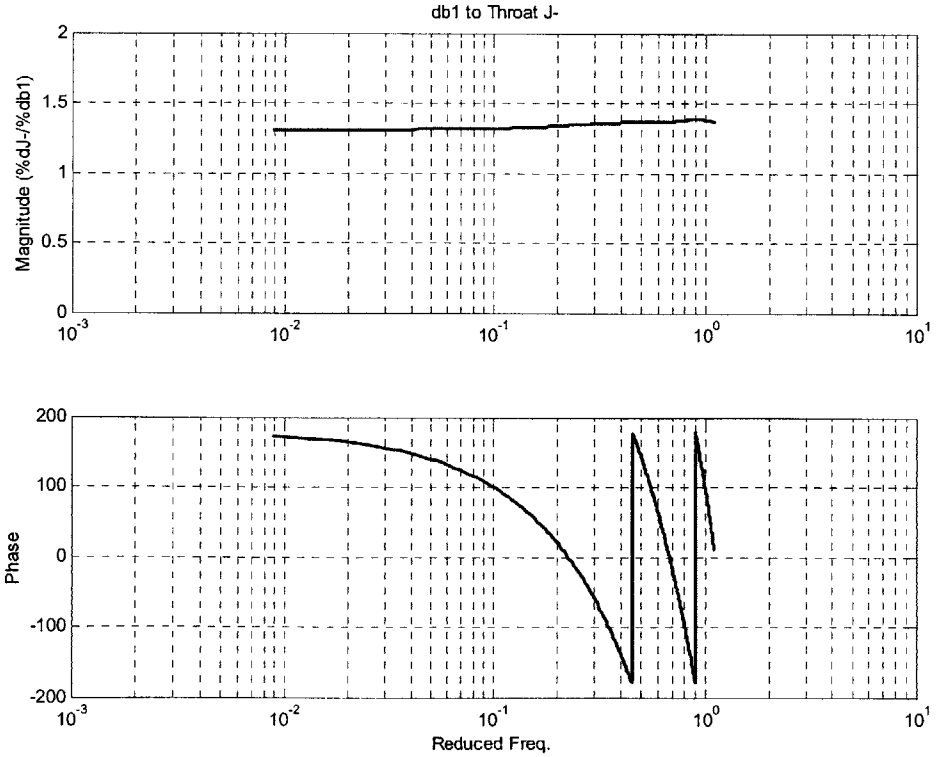

Figure 3.18: Upstream bleed perturbations to throat J- variations as a function of frequency.

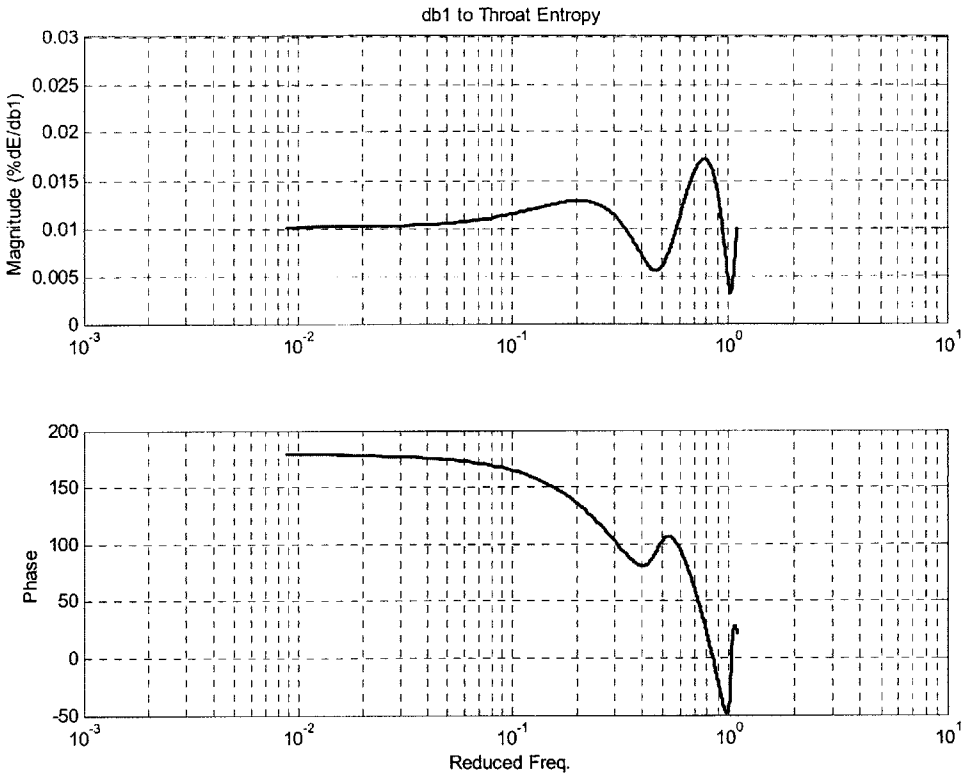

Figure 3.19: Upstream bleed perturbations to throat Entropy variations as a function of frequency.

3.3 Effect of Back Pressure on Shock Location

For mixed compression, high recovery supersonic inlets the dynamics of the inlet and engine are coupled [11] in the sense that inlet unstart can cause engine-compressor surge/stall and vice versa. Therefore, it is very important to have a quantitative idea about the effect of the back pressure on the shock location. Back pressure cannot affect the throat Mach number as the throat is in the supersonic flow region; therefore, the back pressure perturbations affect only the subsonic flow region after the shock. Varying the back pressure also affects the shock location, because it changes the exit boundary condition. The transfer function of back/exit pressure to shock location is shown in Figure 3.20.

To investigate the effect of shock bleed on the ability of the exit pressure to move the shock, transfer functions were calculated for different mean bleeds at the shock. As can be seen in Figure 3.20, at low frequencies the effect of bleed on shock motion is significant and the shock becomes less sensitive to the exit pressure perturbations. But at higher frequencies from a non-dimensional value of about 0.08 onwards, steady bleed has almost no effect. But since the shock motion is small at higher frequencies, this ineffectiveness of the bleed at high frequencies is not a problem.

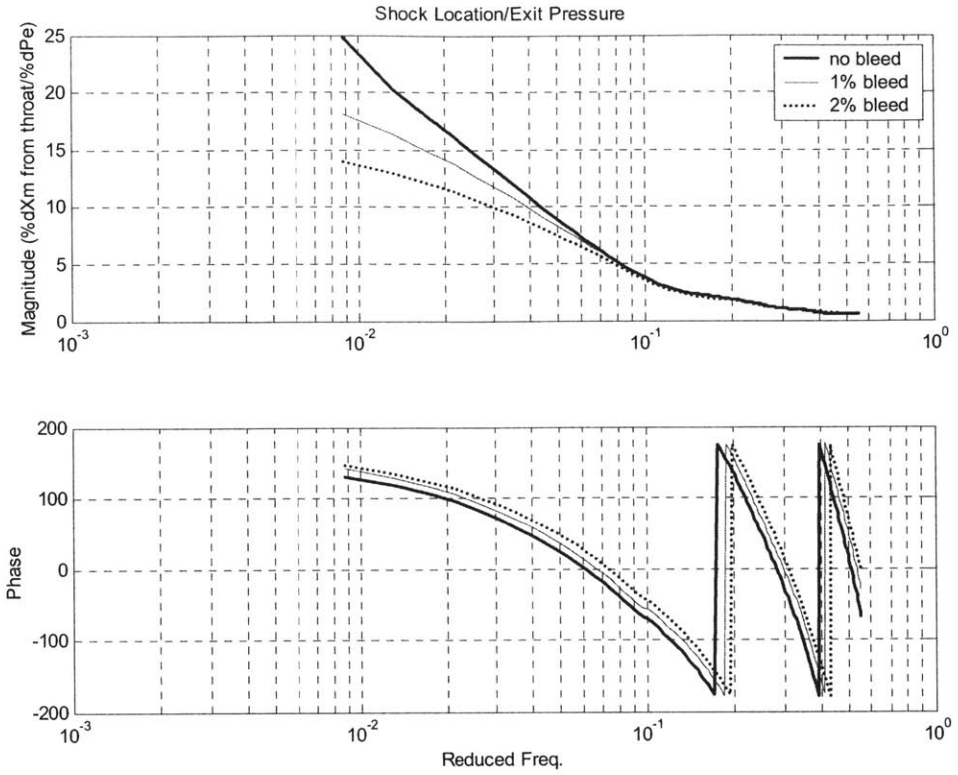

Figure 3.20: Exit pressure to Shock Location transfer function. Magnitude is the percentage of the shock movement of its distance from throat for 1% change in exit pressure from its nominal value.

Not shown by the linear response plots is the fact that the bleed effectively adds a deadband effect to the shock motion, especially at DC and very low frequencies. For higher frequencies the dead band almost vanishes. A typical hysteresis plot for shock motion due to exit pressure perturbation at DC is shown in Figure 3.21. From this figure it is clear that the shock has more tendency to move towards the throat as compared to move away from it. Also, increasing the bleed at the nominal position tends to keep the shock fixed and requires a larger perturbation to actually start the shock moving.

Another aspect of the effect of back pressure on shock motion is its comparison with other disturbances. From the sensitivity magnitudes one can readily conclude that back pressure has a smaller effect on shock motion. But while we can reduce the shock motion due to atmospheric disturbances to quite low values using both upstream and shock bleeds, the shock motion due to back pressure is only affected by shock bleed and hence must be taken into account in an unstart control architecture.

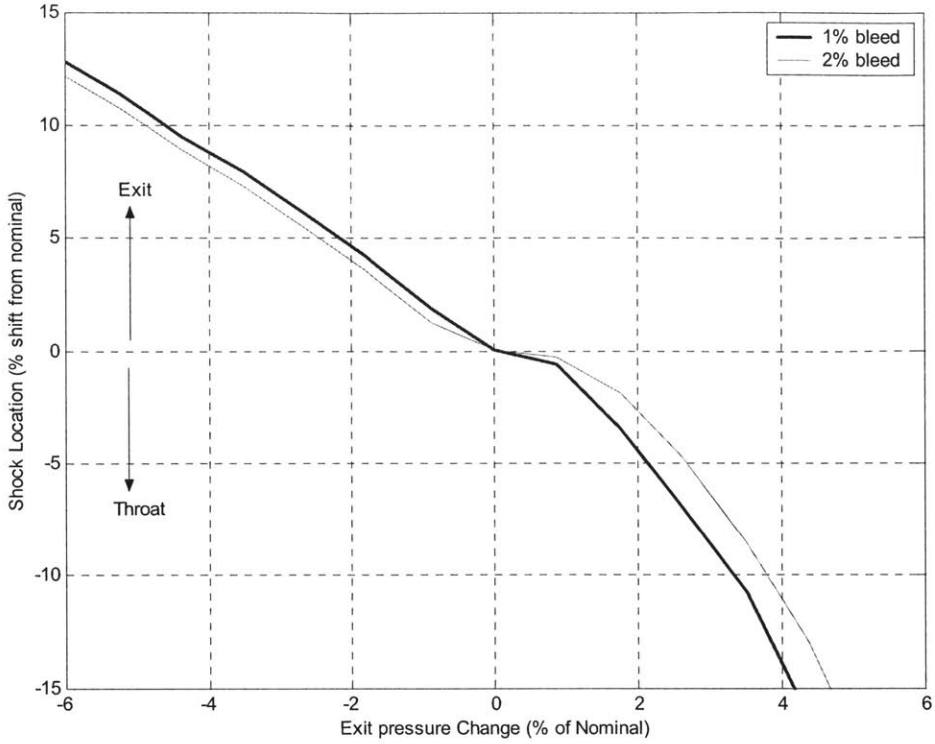

Figure 3.21: Dead band at DC, of shock motion, due to 1% and 2% bleed at nominal shock location.

3.4 Constant Exit Pressure Boundary Condition Assumption and its Implications on Shock Motion

To understand the shock motion as a function of different parameters it is useful to have a simplified model of the shock motion that captures the dynamics of the shock with reasonable accuracy. Such models are based on a linearization approach described in [12]. This method is used to analyze the acoustic reflection and transmission properties of normal shocks in ducts [13, 14]. Using these analytical techniques MacMartin [15] has derived an ODE that captures the shock dynamics with reasonable accuracy. From the model it is apparent that the transmission coefficient of upstream fast acoustic disturbances, or J+, is nearly unity. Thus J+ disturbances effectively pass through the shock and have almost negligible effect on shock motion. But from Figure 3.5, we see that in our 1D simulation the shock is very strongly affected by the upstream J+ disturbances. This can be explained by the fact that we are using a fixed exit pressure boundary condition for the inlet. Thus in the simulation, the exit pressure boundary condition is such that it gives a reflection coefficient of –1 for downstream propagating disturbances. Thus a J+ disturbance, although it passes through the shock almost unchanged, gets reflected at the exit boundary and thus appears as upstream propagating

pressure disturbance, as though the exit pressure generated it. Thus Figure 3.5 is showing the shock motion due to perturbations in J+ if we keep the exit boundary pressure constant. If we make the exit boundary condition such that there are no reflections from the boundary then the shock motion is reduced, as shown in Figure 3.22:

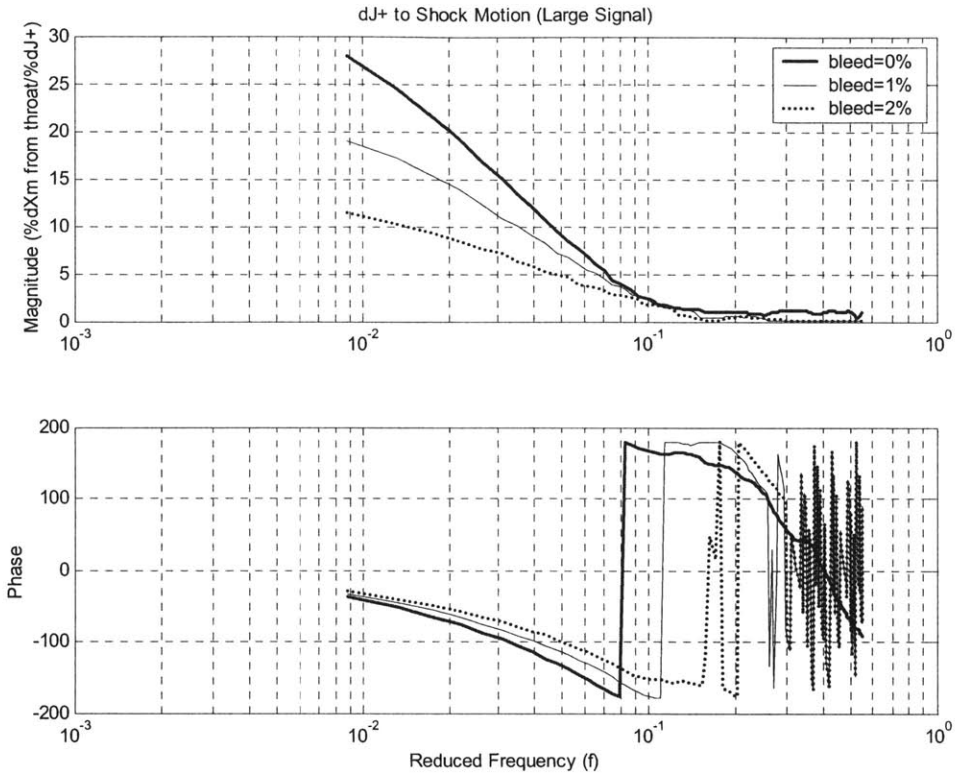

Figure 3.22: Shock motion due to J+ as function of frequency with no reflection condition at the exit boundary.

We see that even after implementing a no reflection boundary condition at the exit, the shock is still strongly affected by the J+ disturbances which is contrary to the conclusion drawn in [15]. From a comparison of Figure 3.5 and Figure 3.22 it is clear that the shock motion is a strong function of both upstream and exit boundary perturbations.

In the real operating environment we need to interface the inlet with a compressor. In order to have realistic exit boundary conditions at the inlet-compressor interface we need a coupled inlet-engine dynamic model [16]. Using such a model we can define Compressor-Face Boundary Conditions (CFBC) that are a simplified representation of the dynamic response of the compressor to the incoming disturbances arriving from upstream. There have been a number of studies to create simplified models for the prediction of unsteady CFBC [17, 18]. Sajben [18] presented a simplified model for the computation of transmission and reflection coefficients accounting for compressor

configuration and Mach number. His results show that for different compressor configurations and Mach numbers the reflection coefficient can vary widely from –1 to 1. In a small-scale wind tunnel experiment, we can reasonably assume the exit pressure to be constant and thus for these conditions the frequency response plots of the shock motion given in previous figures are applicable. Moreover in any real scenario with inlet compressor interface there are bound to be some J+ reflections, and although they may not have a reflection coefficient value of –1, assuming a value of –1 for the reflection coefficient gives us the worst-case scenario. Thus from the point of view of the study of the effect of atmospheric disturbances on inlet stability, assuming a constant pressure exit boundary condition gives us a worst-case scenario (as it reflects back all the incoming disturbances) and stabilization of inlet for this condition will ensure stability for other compressor face boundary conditions (CFBC) except for the disturbances that are generated by the compressor or engine surges.

3.5 Constant Delay approximations of the Transfer Functions

Acoustic wave perturbations ΔJ+ and ΔJ- travel with speeds $u(x,t)+c(x,t)$ and $u(x,t)-c(x,t)$ in a duct, where u is the local stream velocity and c is the speed of sound. Note that both u and c are functions of space and time. Thus in the frame of reference of the inlet the acoustic waves may travel at different speeds at different locations. The area variation appears as a source term and these characteristic acoustic perturbations may change their amplitude as they are propagating down the inlet. An acoustic perturbation traveling down an inlet with or without amplification can be modeled as a constant time delay in the frequency domain. The value of the time delay depends upon the distance along the inlet and the speed of propagation of the disturbance. The amplitude at any given point along the inlet depends upon the amplification factor of the given disturbance.

This immediately suggests a simplified model for the transfer functions of different perturbations. It is apparent from Figure 3.4 that J+ perturbations travel down the inlet with almost no change in amplitude at different frequencies, as the magnitude of the transfer function is almost the same at the static pressure sensor location and at the throat. The phase difference at the sensor and throat signifies different time delays corresponding to their physical location along the inlet.

We can represent the transfer function of a given disturbance by using one or more constant delay terms over the range of frequencies of interest. For example forward velocity perturbations comprise J+ and J- disturbance. Thus a constant velocity perturbation would travel down the inlet with velocities $u+c$ and $u-c$. Thus we need to approximate the forward velocity transfer functions with at least two constant delay terms. Therefore we can write:

$$TF = \sum_{i=1}^{N} A_i \exp(-j2\pi f T_i) \tag{3.2}$$

Where A_i is the amplitude and Ti is the constant delay. The delay T_i for each perturbation depends upon the propagation speed of the mode. N is the number of terms with which we need to approximate the transfer function. For fast and slow modes the delays can be evaluated as:

$$T^{+} = \int \frac{dx}{u + c}$$
$$T^{-} = \int \frac{dx}{u - c} \tag{3.3}$$

Where T^{+} is the time delay for fast acoustic waves and T^{-} is the time delay for slow acoustic waves. The integral is taken from the start of the inlet to the point where we want the transfer function such as sensor or throat. Once the time delays are evaluated the amplitudes A_i's can be evaluated by doing a least squares fit with the numerical transfer function (see appendix A for the code listing). Flow velocity u and speed of sound c in the inlet are the steady-state values established by the nominal operating conditions. For an inlet Mach number of 2.2, the quasi-1D solution gives the following profiles for the isentropic inlet:

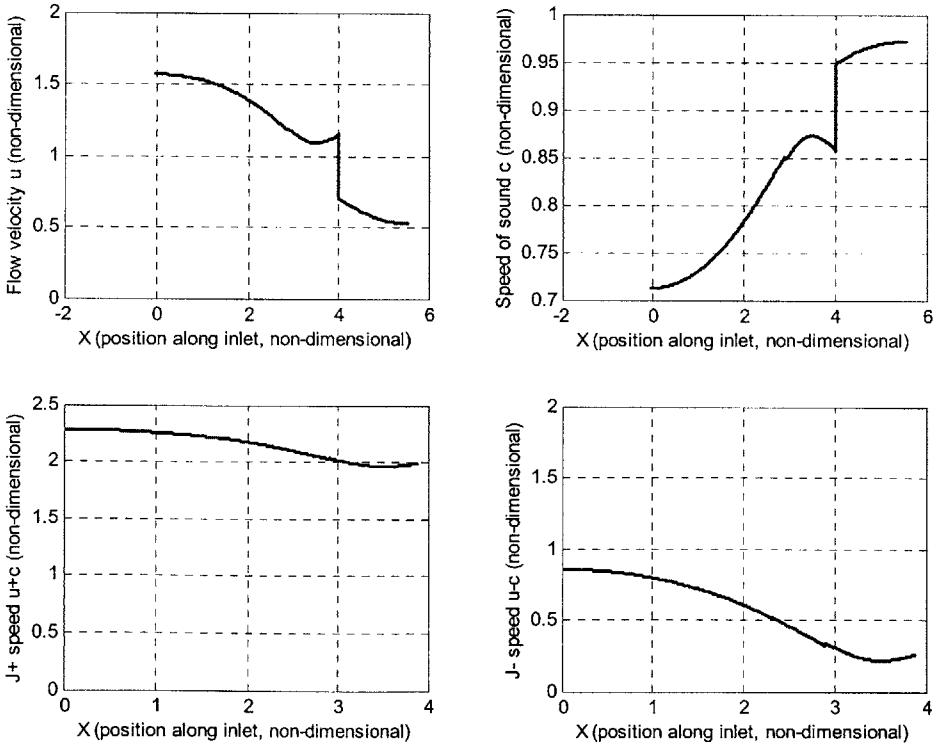

Figure 3.23: Flow velocity and speed of sound from quasi-1D simulation. The speed of fast and slow waves as a function of inlet position is also shown.

Using these values of u and c we can calculate the time delays at different locations along the inlet as shown in Figure 3.24. From the Figure 3.23 it can be seen that, in the frame of reference of the inlet, the change in the speed of fast waves is not significant while the slow wave exhibit a considerable decrease in the velocity near the throat. This change is reflected by an increase in the time delay for the slow waves near the throat.

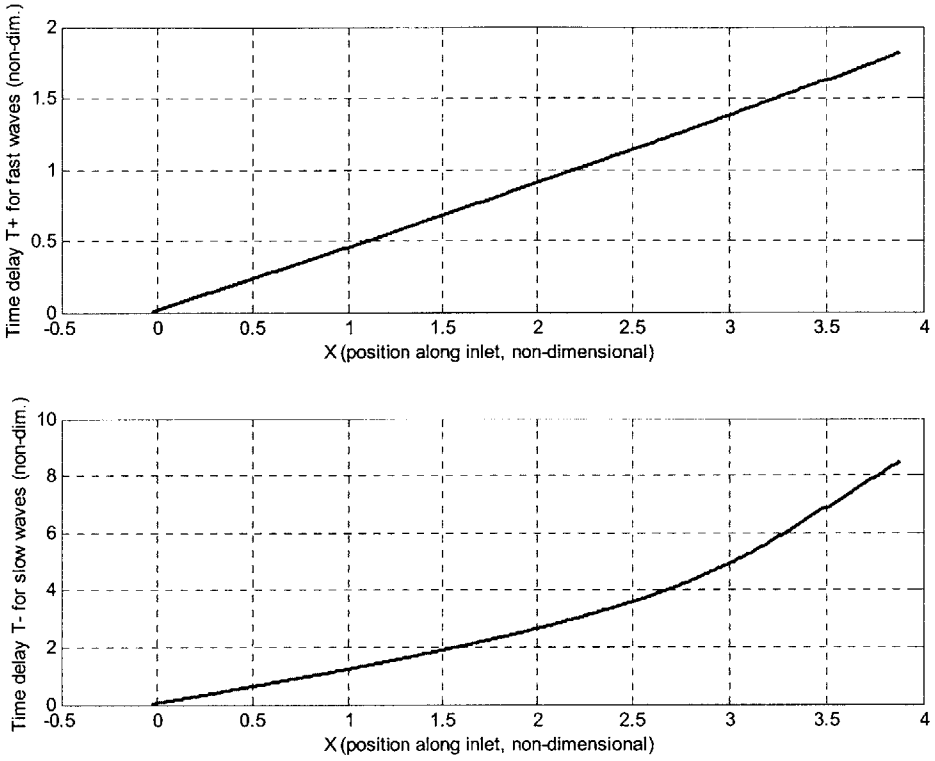

Figure 3.24: Time delays for fast and slow waves in the inlet.

A few sample transfer function approximations using the method described above are given in the following paragraphs.

3.5.1 Transfer Function from Inlet dJ+ to Sensor and Throat

Using the integral for fast acoustic wave perturbations (or from Figure 3.24 for approximate values) we find the following time delays for the sensor located at X=0.5 along the inlet:

T^+ for TF at throat = 1.615
T^+ for TF at sensor = 0.2380

For J+ perturbations we expect only one term in the constant delay approximation, as it is the characteristic disturbance. Thus the transfer function from inlet lip J+ perturbations to sensor or throat can be written as:

$$\frac{dJ_{th}^{+}(j\omega)}{dJ_{in}^{+}(j\omega)} = A_{th}\exp(-j\omega T^{+}) \tag{3.4}$$

We can determine the amplitude A_{th} from theory[1] or from the numerical transfer function (Figure 3.4). As expected the constant delay model of the transfer function is in good agreement with the numerical transfer function as shown in Figure 3.25.

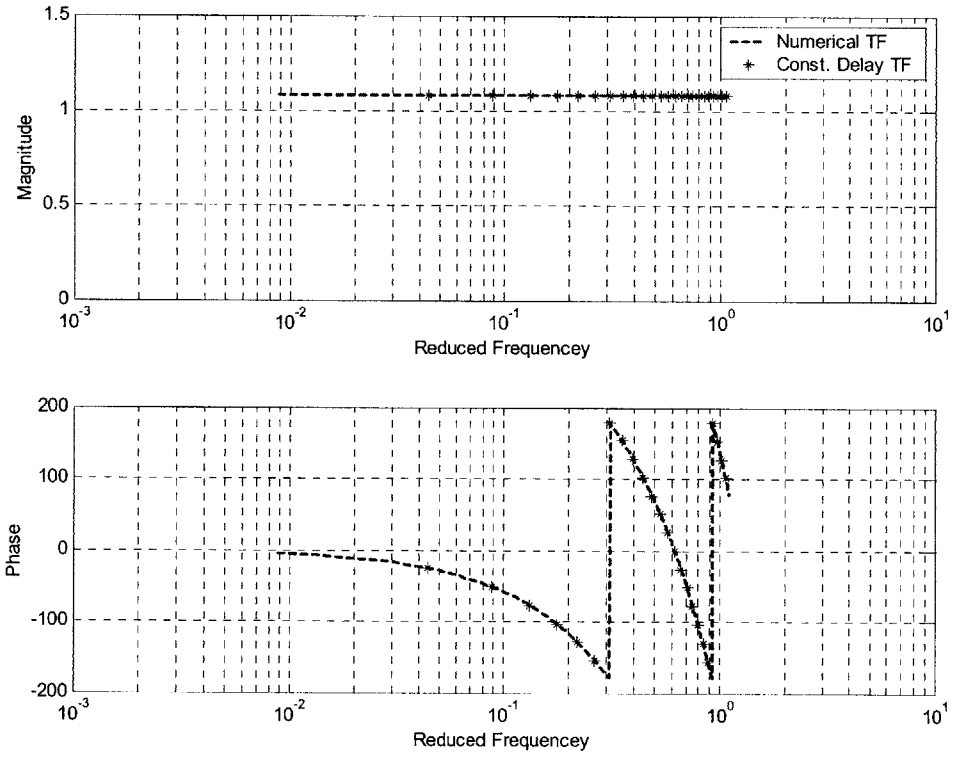

Figure 3.25: Comparison of the numerical and constant delay TFs from inlet lip J+ to Throat J+ perturbations.

3.5.2 Transfer Function from Inlet dJ- to Sensor and Throat

Similarly as in the case of fast waves we can model the slow waves transfer function as a constant delay. Using the integral for slow waves (3.3) we get:

[1] This can be done by linearizing the Euler equations as described in [2].

T^- for TF at throat = 6.81
T^- for TF at sensor = 0.6390

The fitted and numerical transfer function at the throat is shown in Figure 3.26. It can be seen that the fitted and numerical TFs are in good agreement.

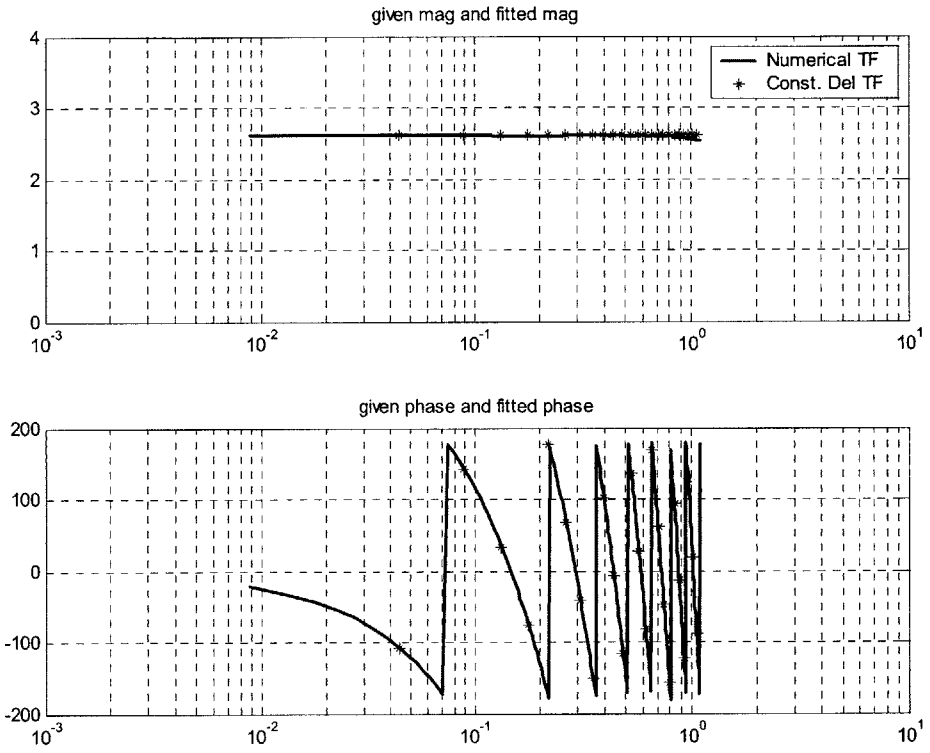

Figure 3.26: Comparison of the numerical and constant delay TFs for inlet lip J- to Throat Mach number perturbations.

3.5.3 Transfer Function from Inlet Forward Velocity to Throat Mach Number

As discussed in chapter 2, the forward velocity perturbations result in the perturbations of both fast waves and slow waves. Therefore from Equation 3.2, we expect the transfer function to be of the form:

$$\frac{dM_{th}(j\omega)}{du(j\omega)} = A_{th}^{+}\exp(-j\omega T_{th}^{+}) + A_{th}^{-}\exp(-j\omega T_{th}^{-}) \tag{3.5}$$

Where:

A_{th}^{+} = Amplification of fast waves at the throat

A_{th}^{-} = Amplification of slow waves at the throat

T_{th}^{+} = Time delay of fast waves from the inlet lip to the throat

T_{th}^{-} = Time delay of slow waves from the inlet lip to the throat

From the transfer functions shown in Figures 3.3 and 3.7 we can estimate amplification factors for fast and slow waves respectively. The time delays are given in Figure 3.24. Using this data the constant delay approximated TF along with the numerical TF is shown in Figure 3.27. Although the amplification factor for fast waves is not constant as a function of frequency, but still the approximation is reasonably accurate.

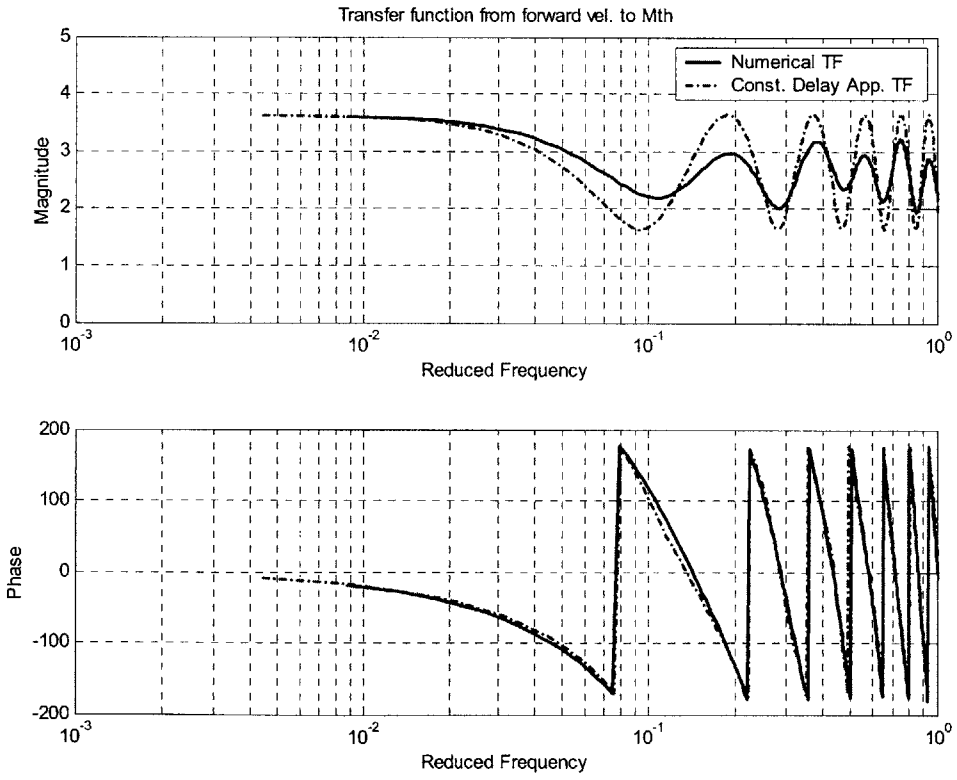

Figure 3.27: Comparison of constant delay approximation to the numerical TF from inlet lip forward velocity to throat Mach number.

3.6 Unsteady 2D Euler Simulation

As discussed earlier the isentropic inlet essentially uses oblique shocks to slow down the incoming flow gradually and there is a weak normal shock after the throat to get subsonic flow. The presence of an oblique shock structure makes the inlet flow essentially two-dimensional in the supersonic part of the inlet. Thus using a quasi-1D approximation for the dynamic analysis may be misleading. Thus it is important to use the 2D analysis to see the effects of the oblique shock structure on the dynamic characteristics of the inlet.

An unsteady 2D Euler code was developed by Merchant [2] and was embedded in Simulink to study the dynamic characteristics of the inlet. Its interface is essentially the same as the quasi-1D model and we can use the atmospheric perturbations as well as characteristic perturbations to get the dynamic response of the inlet in the form of transfer functions.

3.6.1 Frequency Response Study of the 2D Inlet

To analyze the effects of the 2D flow structure on the dynamic characteristics of the inlet, a frequency response study, similar to the quasi-1D case, was conducted using the 2D Euler Simulink model. In this case since we have flow variations along the inlet height, we must define the transfer functions along the inlet as a function of the inlet height. Thus we get transfer functions for the throat Mach number at each grid point along the inlet height at the throat. In order to compare the results with quasi-1D transfer functions we have to use area averaged transfer functions at the desired location. Different transfer functions obtained from the 2D frequency response study are discussed in the following paragraphs.

Figure 3.28 shows the area averaged 2D transfer function from the inlet lip fast waves to throat Mach number. It can be seen in Figure 3.28 that the area averaged 2D transfer function, for fast acoustic wave perturbations dJ+, matches very closely with the quasi-1D transfer function over the frequency range of interest. At higher frequencies the larger difference between the area averaged 2D transfer function and the quasi-1D transfer function is thought to be due to numerical dissipation in the Euler simulation.

Figure 3.29 shows the variation of the magnitude of the transfer function for different locations along the inlet height. It can be seen that there are large variations in the transfer function at different locations but the averaged response matches the 1D simulations. Note that in this figure the y-axis is normalized with the height of the inlet at the throat, therefore 1.0 along the y-axis represents the height of the inlet at the throat.

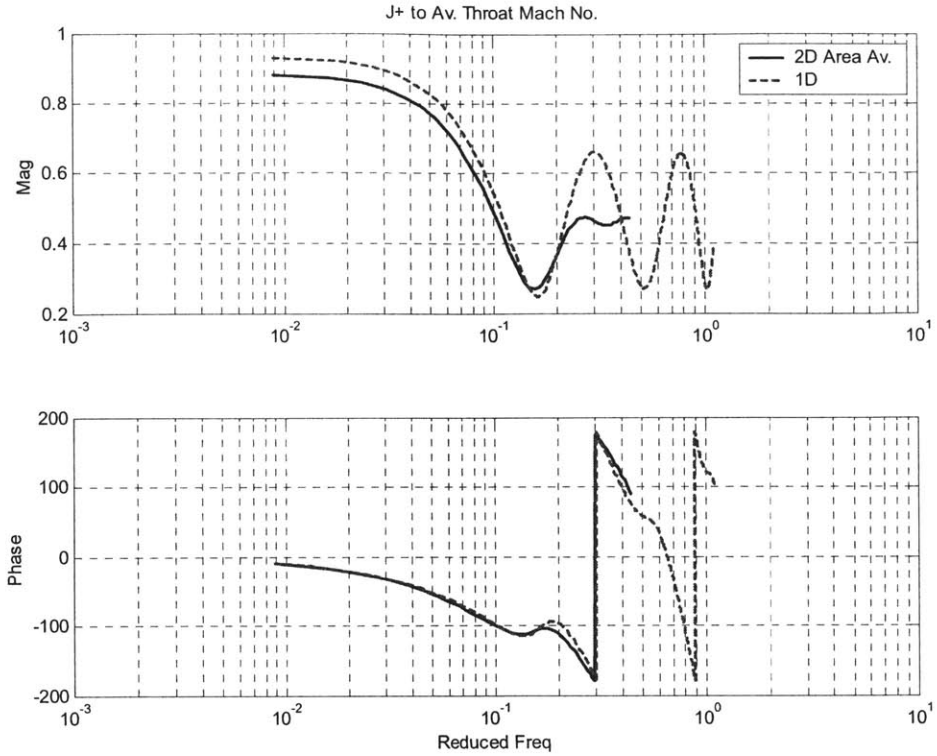

Figure 3.28: Inlet lip dJ+ to area averaged throat Mach number transfer function and its comparison with quasi-1D case.

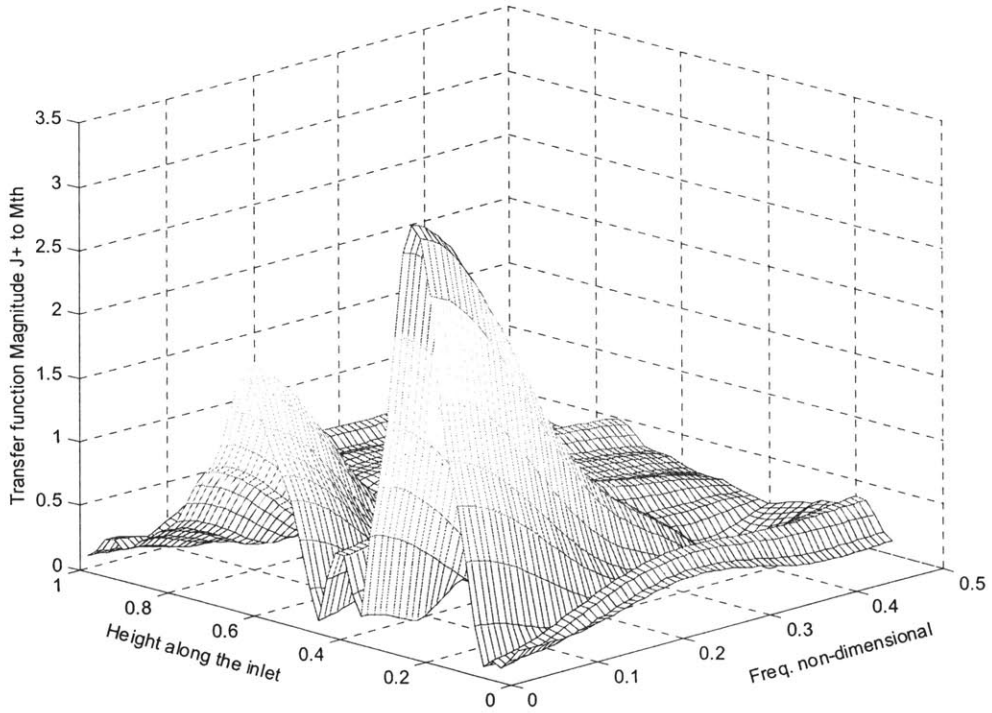

Figure 3.29: Inlet lip dJ+ perturbations to Throat Mach number perturbations and its variation along inlet height

For the slow acoustic waves Figure 3.30 shows the transfer function from inlet lip to throat Mach number. Again the area averaged solution matches closely with the quasi-1D case over the frequency range of interest. In the 2D case the phase delay is higher as expected; since in 2D the perturbation wave actually has to pass through a number of oblique shocks, a little bit longer time delay occurs due to change in the flow direction. It can be seen from Figure 3.31 that the throat Mach number transfer function magnitude for slow acoustic waves varies considerably along the inlet height. But still the average effect resembles closely the quasi-1D transfer functions. The variation of the transfer function over the inlet height is similar to the fast acoustic waves.

The frequency response from the upstream bleed perturbations to throat Mach number variations is shown in Figures 3.32 and 3.33. The area averaged value of the response can be seen to follow closely with the quasi-1D results, at least over the frequency range of interest. From Figure 3.33 it is clear that the upstream suction has greater effect along the inlet height where the atmospheric disturbances have the highest magnitudes of the transfer function. The variation of the phase as a function of inlet height and frequency is shown in Figures 3.34 and 3.35 for J+ and upstream bleed perturbations to throat Mach number. These figures again show that the control effectiveness follows the phase variations (except for a sign reversal) due to atmospheric perturbations. Thus variation of the effect of atmospheric disturbances along the inlet height is not an issue, since the effectiveness of control also follows the same variations.

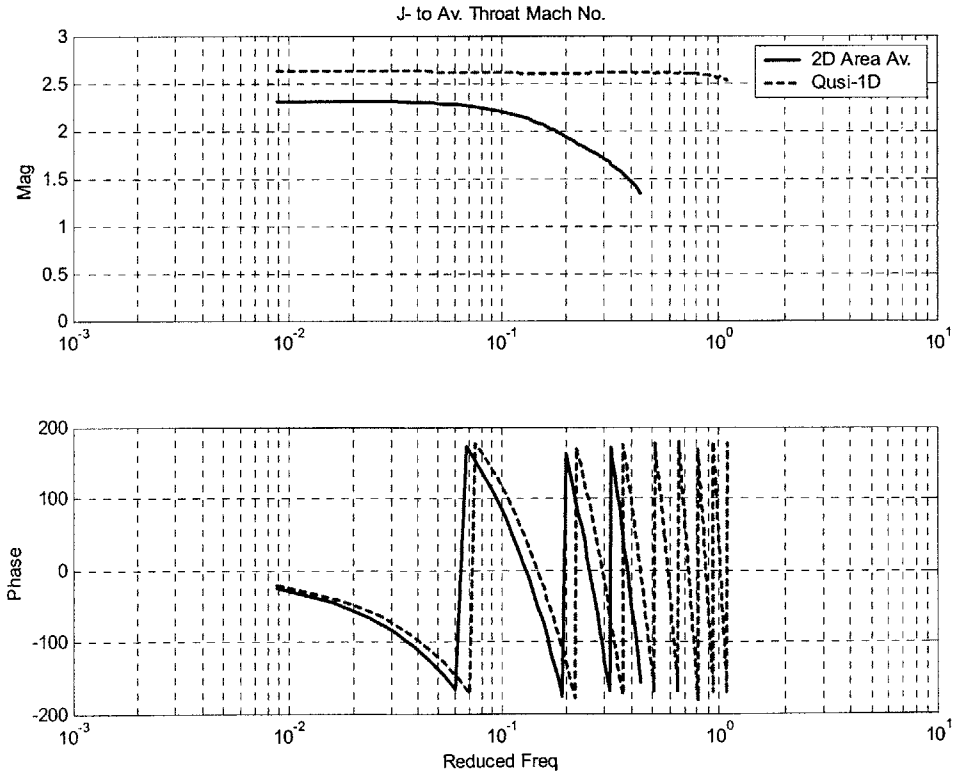

Figure 3.30: Inlet lip dJ- to area averaged throat Mach number transfer function and its comparison with quasi-1D case.

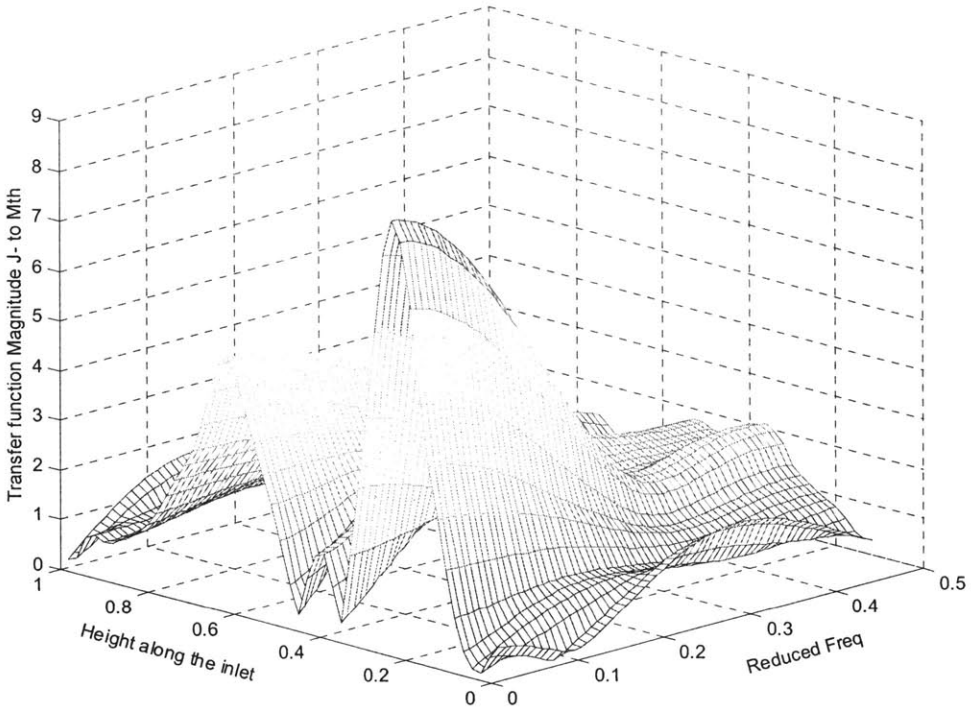

Figure 3.31: Inlet lip dJ- perturbations to Throat Mach number and its variation along inlet height.

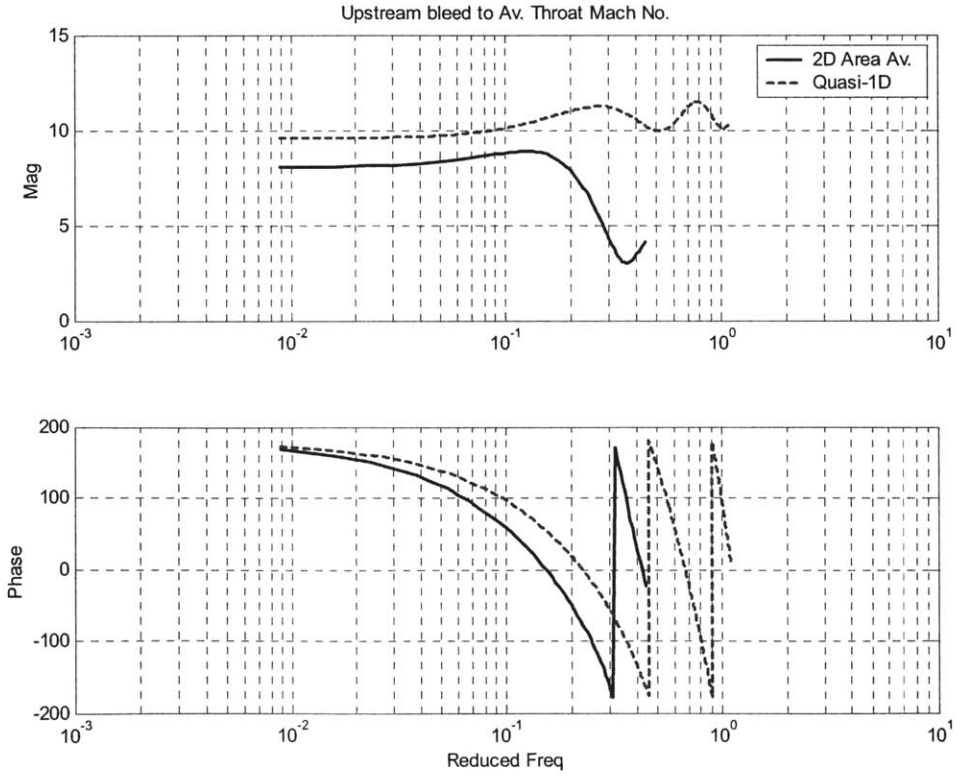

Figure 3.32: Upstream bleed to area averaged throat Mach number transfer function and its comparison with quasi-1D case.

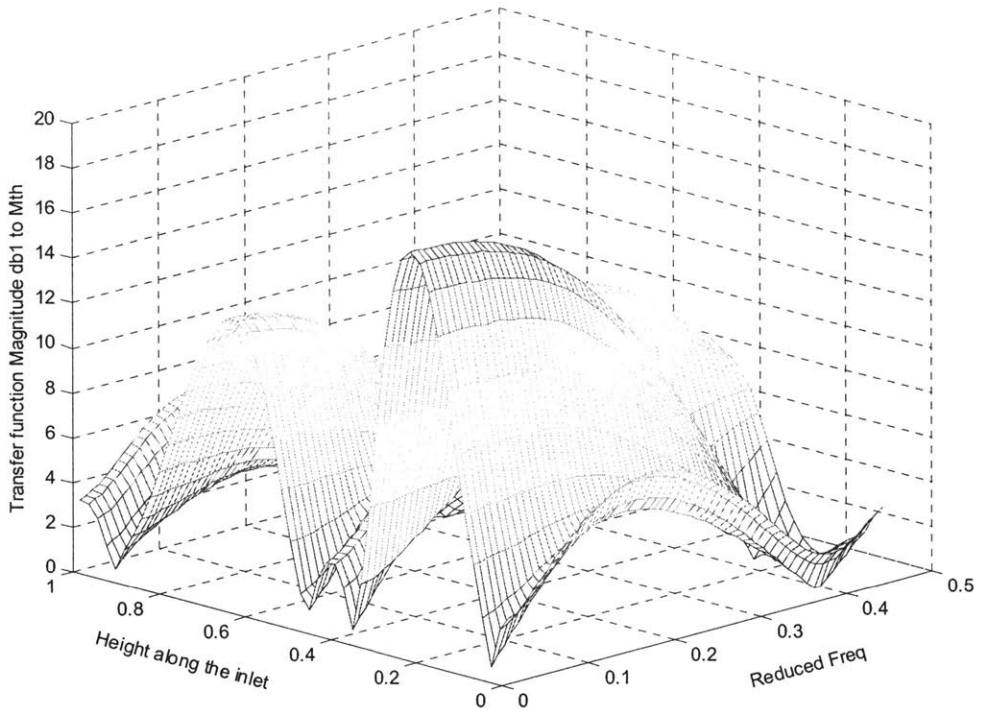

Figure 3.33: Transfer function from upstream bleed perturbations (using symmetrical bleed) to Throat Mach number and its variation along inlet height.

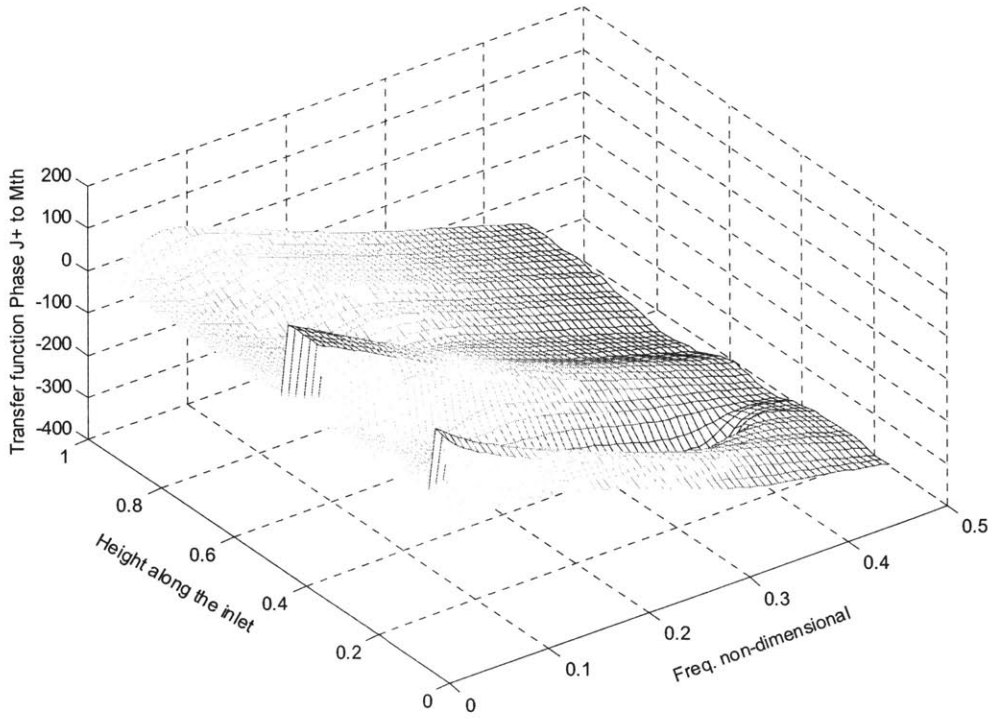

Figure 3.34: Transfer function phase from J+ perturbations to Throat Mach number and its variation along inlet height. (Phase is shown unwrapped.)

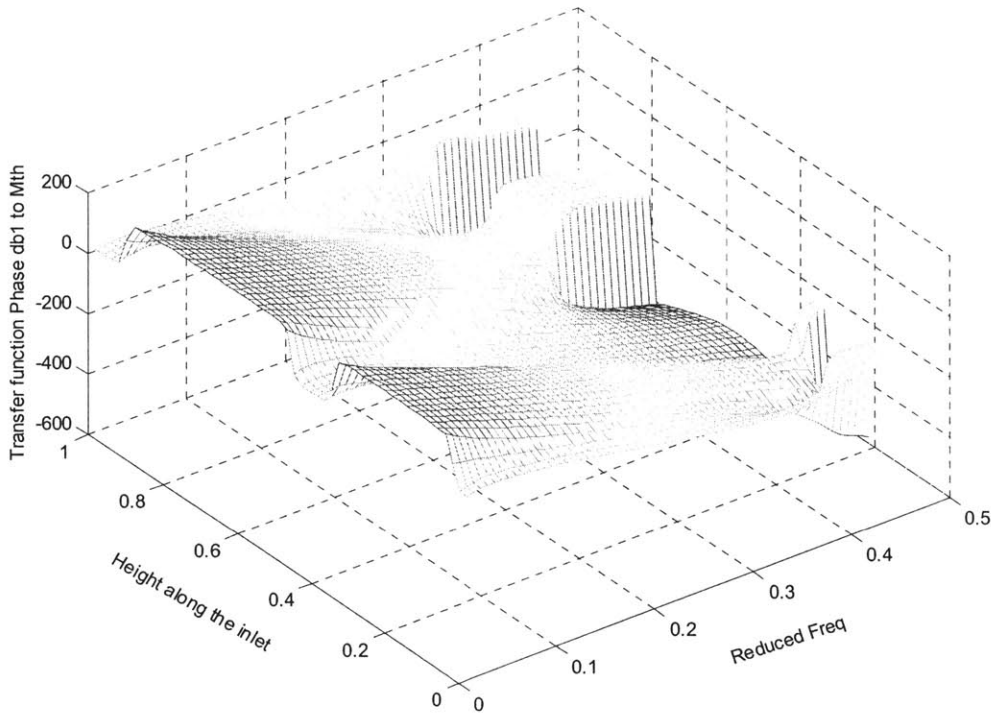

Figure 3.35: Transfer function phase from db1 perturbations to Throat Mach number and its variation along inlet height. (Phase is shown unwrapped.)

The plots shown in Figures 3.32 and 3.33 are generated by using a symmetrical upstream bleed, i.e., a bleed slot at the top wall and also at the bottom wall is used. If we just use a bleed at the bottom wall then the result is shown in Figure 3.36. It is clear that using an asymmetrical bleed results in much higher control authority in the bottom half of the inlet throat and a minimal control authority at the top half of the inlet throat. In contrast, the disturbances have large impact on the throat Mach number at the top half of the inlet throat; therefore using an asymmetrical bleed would not result in the response predicted by the quasi-1D simulations.

Frequency response plots for the inlet lip entropy perturbations to the throat Mach number are shown in Figures 3.37 and 3.38. Again it is clear from the figures, the area averaged results of the 2D simulation match closely with the quasi-1D results over the frequency range of interest. The variation of the transfer function magnitude along the inlet height at throat is also similar to that for the previous transfer functions.

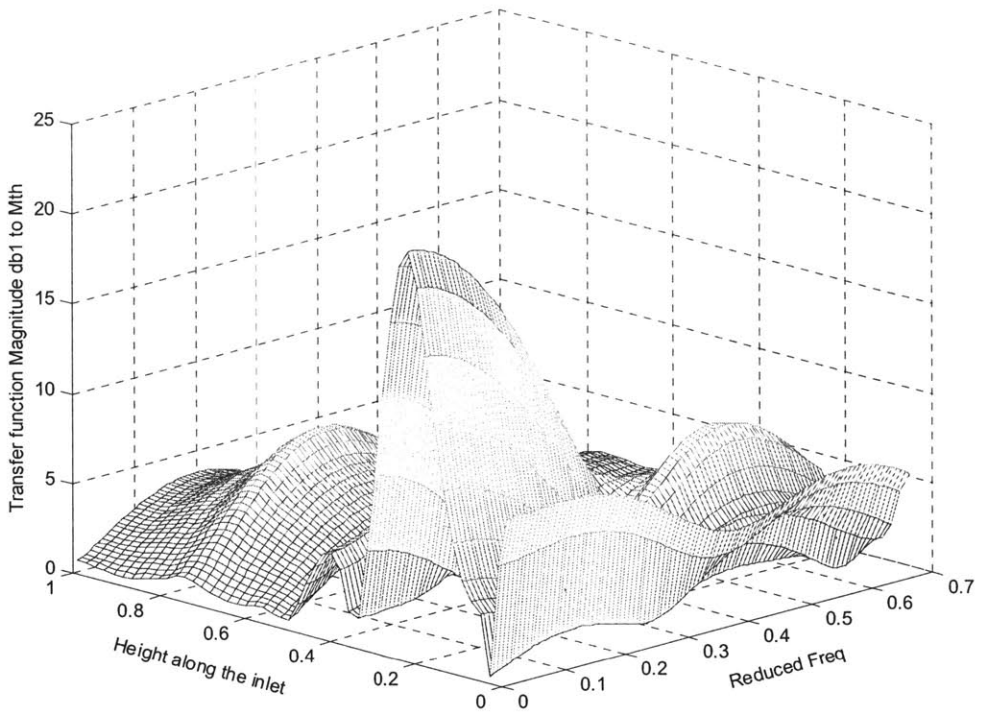

Figure 3.36: Transfer function from upstream bleed perturbations (using bottom bleed valve only) to Throat Machumber and its variation along inlet height.

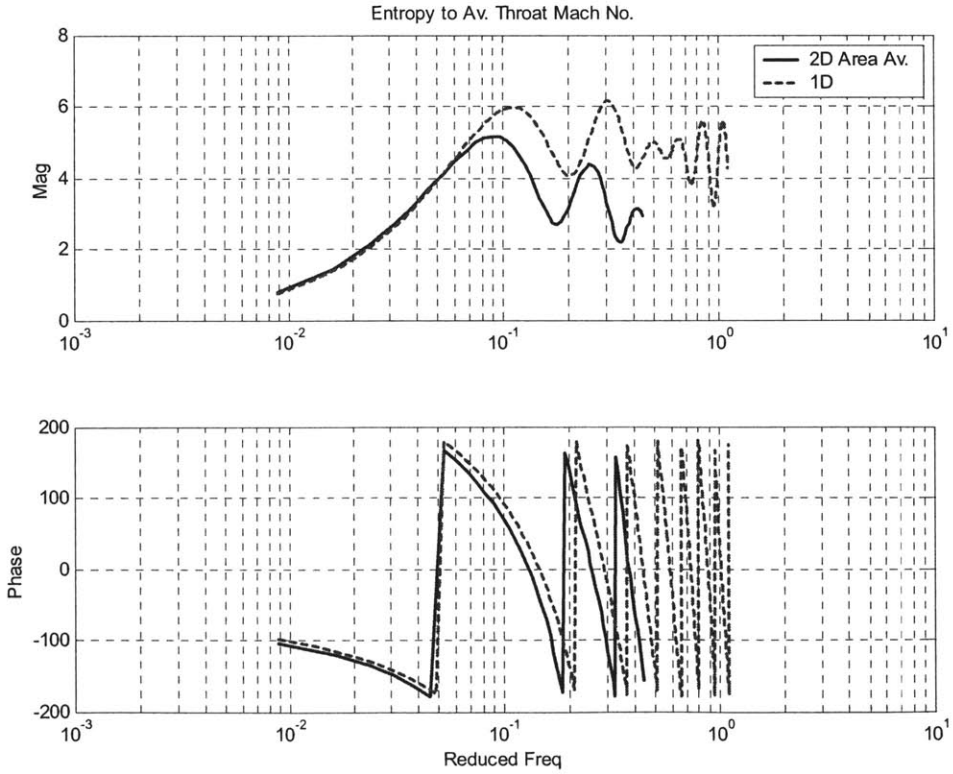

Figure 3.37: Transfer function from inlet lip Entropy perturbation to area averaged throat Mach number transfer function and its comparison with quasi-1D case.

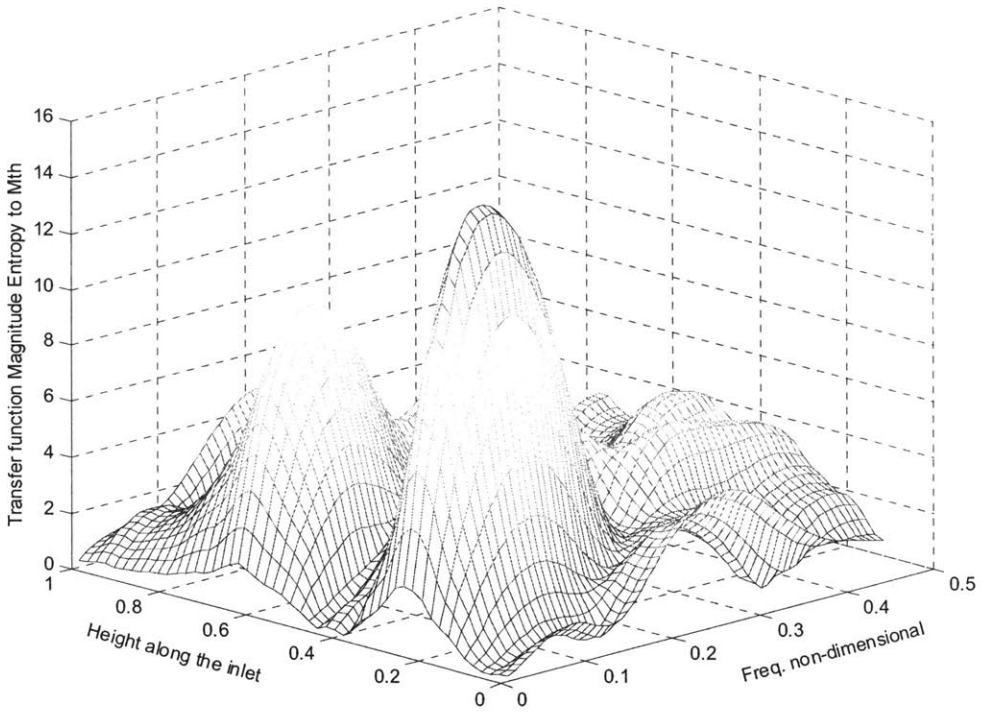

Figure 3.38: Transfer function from inlet lip Entropy perturbations to Throat Mach number perturbations and its variation along inlet height.

3.7 Inlet Unstart Mechanisms

As far as the dynamic behavior of inlet unstart is concerned, an inlet can unstart in two distinct ways. The disturbances that affect the shock directly, such as fast waves and entropy disturbances, tend to move the shock considerably, depending upon the magnitude of the disturbance, from its mean position. Thus a negative going fast acoustic wave pulse can cause the shock to move upstream towards the throat, as can be seen from Figure 3.5, and if this disturbance persists for enough time it can cause the shock to move forward and hence come out of the inlet completely, causing the unstart. Such an event is shown in Figure 3.39. A negative going fast acoustic wave step of magnitude 0.04 was used in the simulation, with controls off, to generate the response shown in Figure 3.39. Note that in this mode of unstart the shock continues to move upstream and as soon as it passes the throat it accelerates and completely comes out of the inlet as shown in Figure 3.40. This figure clearly shows that the shock continues to move towards the throat and its velocity increases with time.

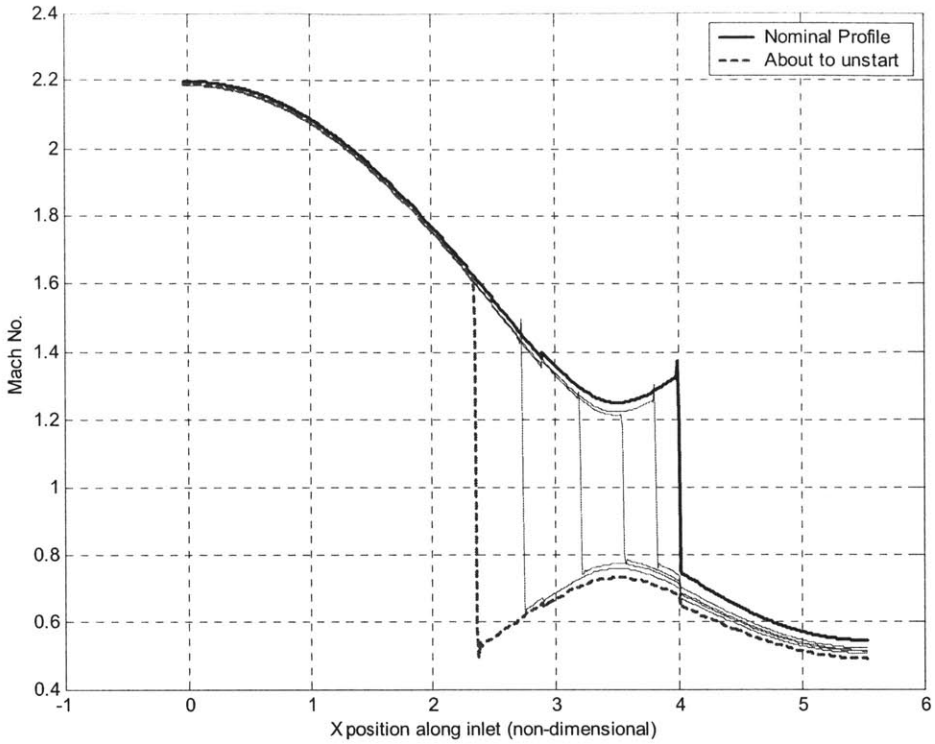

Figure 3.39: Mach number profiles for different time instants during an unstart event. The shock is moving towards the inlet lip due to an incoming atmospheric disturbance. Unstart due to shock motion.

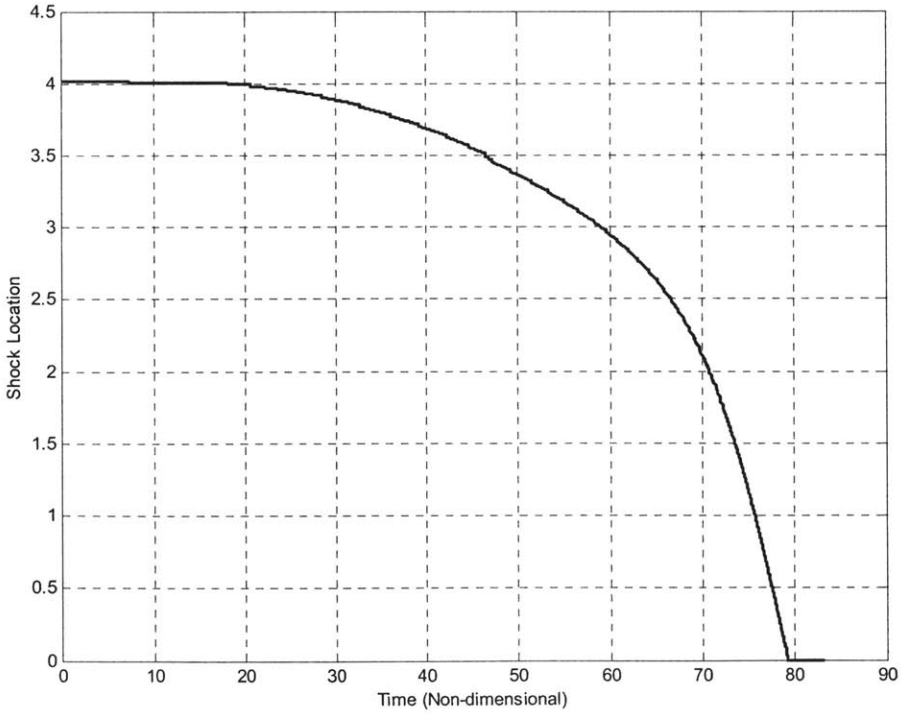

Figure 3.40: Location of the shock as a function of time for the unstart event due to shock motion.

There is another way in which inlet unstart can occur. The slow acoustic wave disturbances, J-, have much stronger effect on the throat Mach number than on the shock itself. Consequently when a pulse of slow acoustic wave disturbance hits the inlet, it tends to change the throat Mach number. For a negative going slow acoustic wave pulse the throat Mach number decreases, as can be seen in Figure 3.7. Therefore, for a strong J- disturbance, the throat Mach number may drop below 1, while the shock behind the throat has not appreciably moved. In this case a new shock forms at the throat and starts moving upstream as shown in Figure 3.41. The formation of the new shock is clear from the Figure 3.42, which shows the position of the first shock in the inlet. Figure 3.43 shows the 2D shock structure with a new shock just formed upstream of the throat.

From this discussion it is clear that in order to prevent the inlet from unstarting, it is not sufficient to keep the shock position stable. We also have to control the throat Mach number and prevent it from dropping below unity.

Another important factor affecting the shock motion, other than atmospheric disturbances, is the exit pressure perturbations due to the compressor. If there is a sufficiently strong positive going perturbation in the exit pressure then it can also cause the shock to move

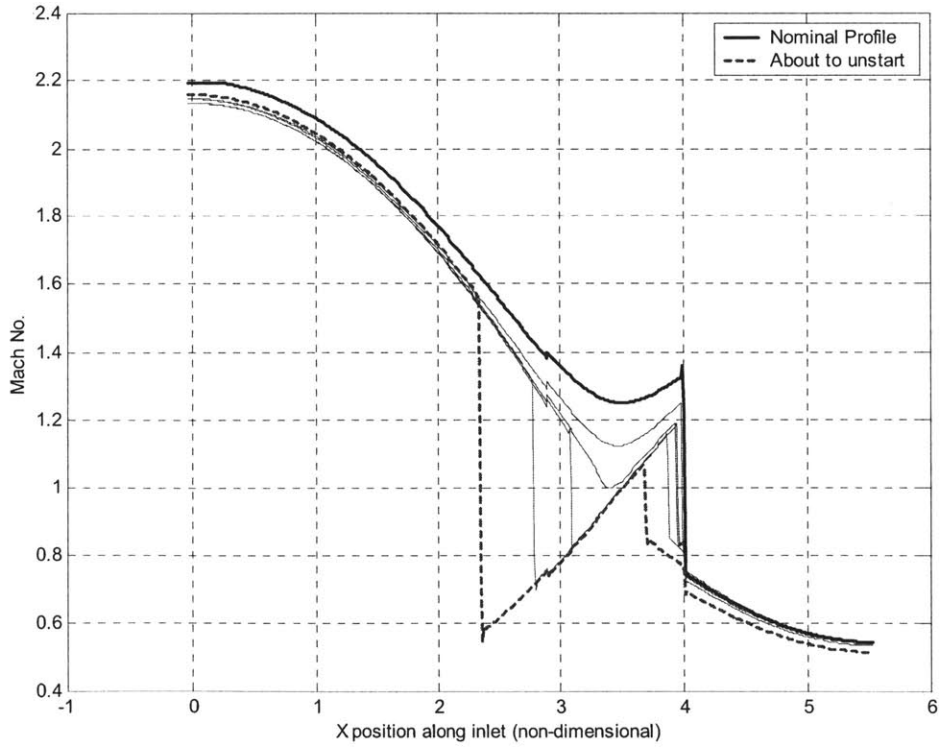

Figure 3.41: Mach number profiles for different positions of the shock. Shock is moving towards the inlet lip due to incoming atmospheric disturbance. Unstart due to new shock forming at throat.

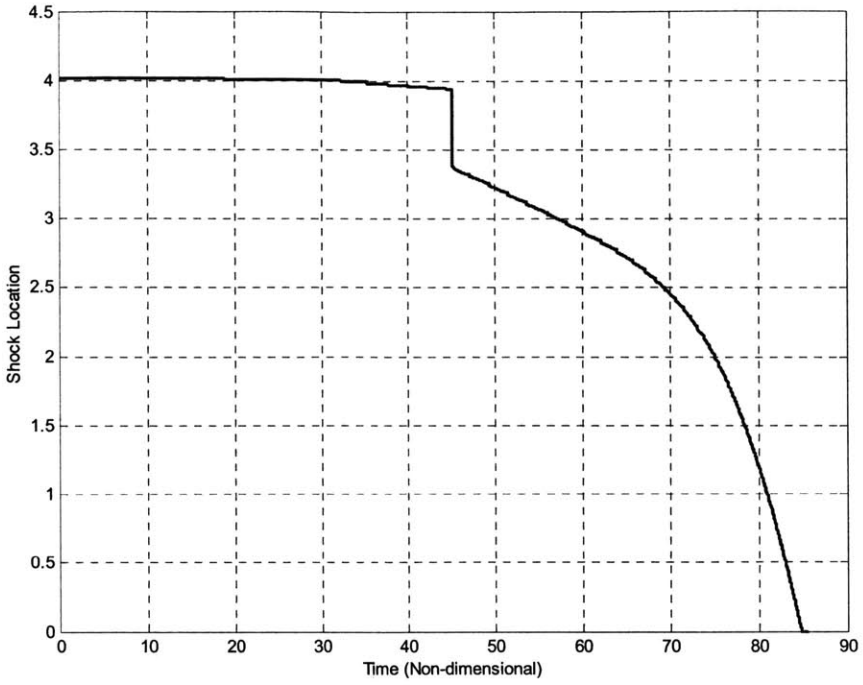

Figure 3.42: Location of the first shock as a function of time for the unstart event due to shock motion.

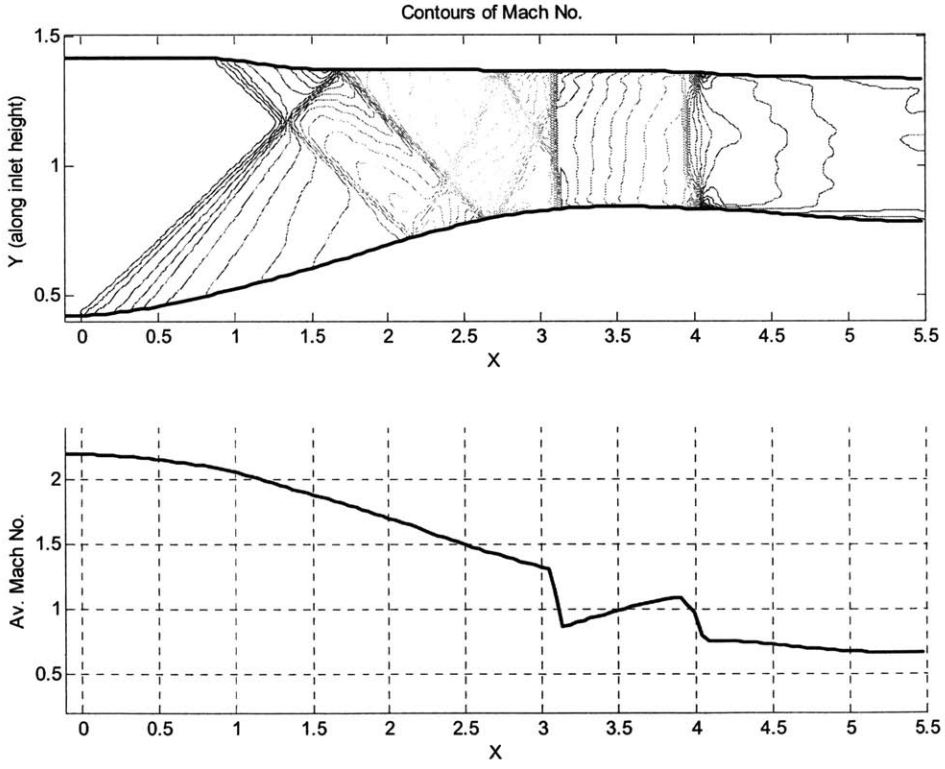

Figure 3.43: Contours of Mach number for the unstarting inlet due to new shock formation.

upstream and unstart the inlet. In this report the effect of atmospheric perturbations is considered mostly and effects due to exit pressure perturbations are generally ignored for the purpose of limiting the overall scope of the thesis.

3.8 Bandwidth Requirement of the Actuators

An important parameter from the point of view of the control system design is the bandwidth requirements of the control system and actuator. It can be seen from the transfer function plots (qausi-1D) of the atmospheric disturbances that the inlet has a flat response over reduced frequencies up to 1. The inlet actually tends to amplify the entropy perturbations for higher frequencies. Thus it is apparent that the atmospheric perturbation cut-off, rather than the inlet itself, sets the bandwidth requirement. From the previous chapter it is apparent that most of the atmospheric turbulence energy is concentrated at lower frequencies. Thus we see from the results that a dimensional frequency of around 25 Hz (corresponding to a non-dimensional frequency of approximately 0.11) is the upper cut-off as far as the atmospheric perturbations are concerned. Thus the bleed actuator has to have at least this bandwidth in order to cancel the affects of atmospheric perturbations. Equation 2.32, in chapter 2, gives the relationship between the full-scale frequency and the reduced frequency. Using this relationship, we can calculate the non-dimensional bandwidth for a simulation or for a wind tunnel test.

3.9 Throat Mach number Variations due to Characteristic Disturbances

From the 1D Euler simulations we have the transfer functions from different atmospheric disturbances in characteristic form to the throat Mach number as given in the previous sections of this chapter. Using these transfer functions, we can estimate the effect of atmospheric disturbances on throat Mach number without control. The modified spectra for each atmospheric disturbance in characteristic form are shown in Figures 3.44 to 3.46.

These figures show the original PSD for each of the disturbance in characteristic form, its modification due to ramp control and Mach hold system and also the resulting spectrum of throat Mach number variations. The vertical lines in these figures show the range of frequencies that are significant as stated in the previous section. Using these spectra we can calculate the RMS values of throat Mach number variations due to each type of disturbance. These RMS values are tabulated in Table 3.1.

From this table we see that, for throat Mach number, the most dominant or important atmospheric disturbance is J- or the slow acoustic wave. Although the entropy perturbation is large at the inlet boundary, it is attenuated by the inlet itself by virtue of its design and thus has only about $1/6^{th}$ of the impact of the J- disturbances. The only

disturbance that is significantly amplified by the inlet is J- disturbance and thus it is the disturbance that needs to be controlled most effectively for throat Mach number control.

Disturbance Type	RMS value of M_{th} ($\times 10^{-3}$)
J+	16.2
J-	48.3
Entropy	8.7

Table 3.1: Estimated RMS values for throat Mach number variations due to canonical atmospheric disturbances.

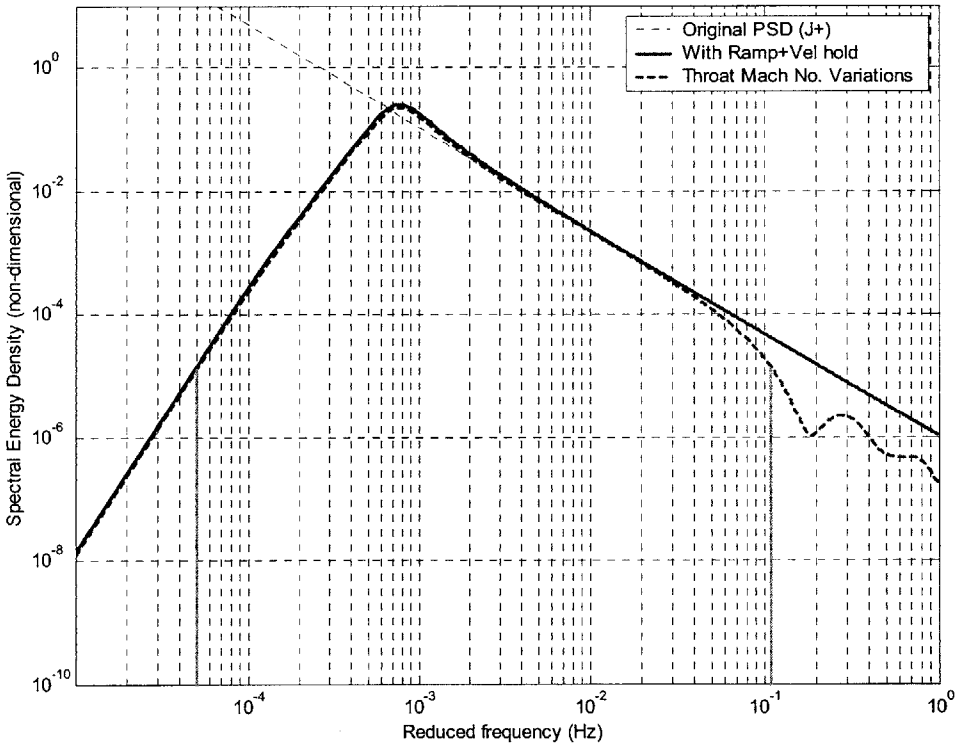

Figure 3.44: Throat Mach no. perturbation spectral density for (worst case) J+ disturbance at the inlet upstream boundary.

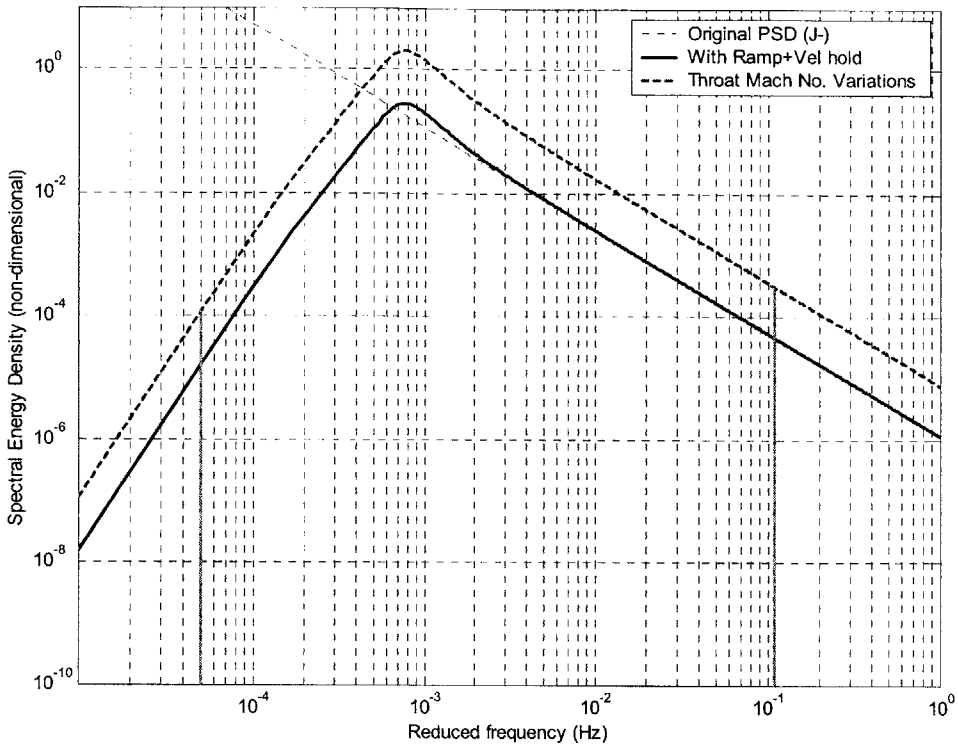

Figure 3.45: Throat Mach no. perturbation spectral density for (worst case) J- disturbance at the inlet upstream boundary.

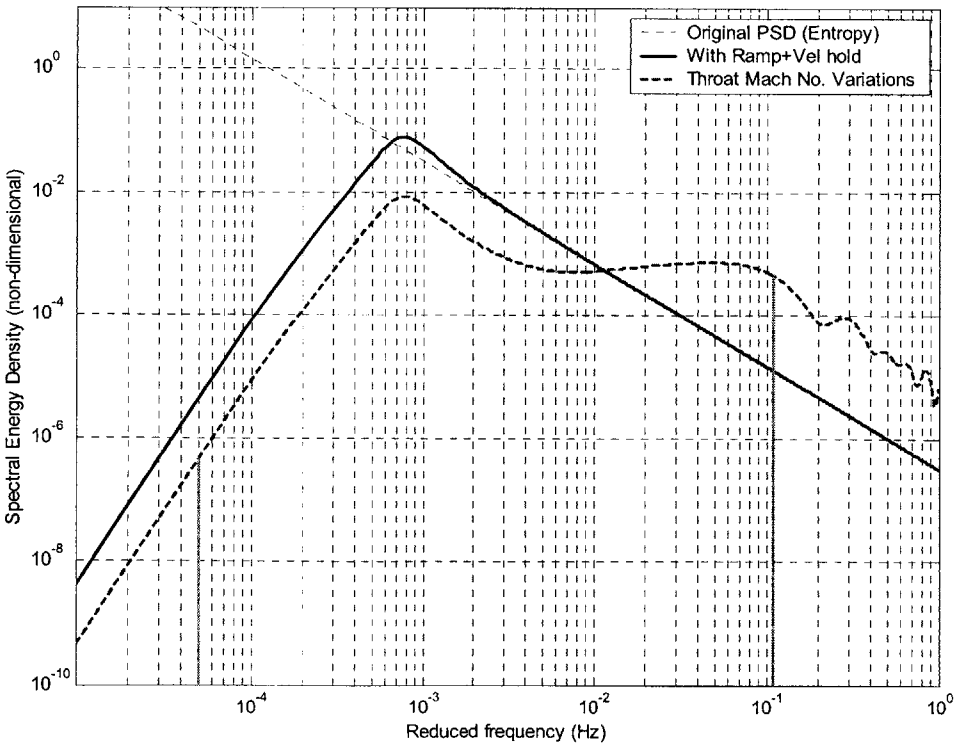

Figure 3.46: Throat Mach no. perturbation spectral density for (worst case) Entropy disturbance at the inlet upstream boundary.

Chapter 4

Control System Design and Testing

By examining the dynamic response of the inlet, we have shown in chapter 3 that, in the range of the frequencies of interest, the quasi-1D and area-averaged 2D transfer functions are almost identical. We have also shown that a symmetrical bleed implementation gives us control authority that closely mimics the non-uniformity of the atmospheric disturbance transfer functions across the inlet throat. Thus the frequency response of the inlet is represented well, to a good approximation, by quasi-1D simulation. Motivated by this observation, it is reasonable in this initial study to base the control architecture design on the quasi-1D simulation results, as it is easier and simpler to work with 1D simulation. Then the designed control law can be tested and verified in the full two-dimensional simulation.

As discussed in the previous chapter, there are two unstart mechanisms. Thus we need to take into account both of the mechanisms in order to prevent unstart. So the control part can be subdivided into two distinct parts, namely the throat Mach number control and shock motion control. Although the throat Mach number is controlled by the upstream bleed, that also helps to some extent in the control of the shock position and shock position control is done using the shock bleed that in turn also helps a little in the control of throat Mach number. But these effects are only secondary and to a first order approximation we can ignore them. This results in a decoupled design of control laws for throat Mach number and shock position and simplifies the problem.

4.1 Throat Mach Number Control

As discussed in the previous chapter, atmospheric disturbances can change the throat Mach number significantly. Thus throat Mach number may increase, pushing the shock downstream and reducing the inlet efficiency. Similarly the throat Mach number may decrease, resulting in shock motion toward the throat and eventual unstart. Both of these are undesirable and must be controlled to enhance the robustness of the inlet. We can control the throat Mach number by using the upstream bleed perturbations as mentioned in the previous chapter.

The upstream bleed perturbations result in mostly slow acoustic waves, as can be seen from Figures 3.17 to 3.19 and Table 3.1 in chapter 3. From the speed of the propagation of the slow acoustic waves, we can estimate a time delay of approximately 2.0 non-dimensional units. Therefore, a feedback control loop can be used to control the throat Mach number at very low frequencies. In a natural setting, this problem is a disturbance

rejection problem and a feedforward control is not only natural but much simpler to implement as well. Feedback control can be used on top of the feedforward controller to add robustness to the system especially at low frequencies. In this section a feed-forward control implementation for the throat Mach number control is discussed.

We can design a feed-forward controller based on canonical disturbances, namely J-, J+ and entropy, or we can use the atmospheric disturbances directly. We will discuss both approaches and controllers implemented using both techniques will be presented.

4.1.1 Throat Mach Number Controller Design Based on Atmospheric Disturbances

The response of an inlet to forward velocity atmospheric perturbations comprise both slow acoustic waves and fast acoustic wave perturbations. Therefore, by using forward velocity perturbations as our prime disturbance to be controlled, we can account for both J+ and J- perturbations. Moreover, since J- is the perturbation that we want to control most effectively, using forward velocity perturbation also satisfies this requirement. Using a static pressure sensor upstream of the bleed to estimate the Mach number perturbations, the feed-forward control architecture looks as shown in Figure 4.1.

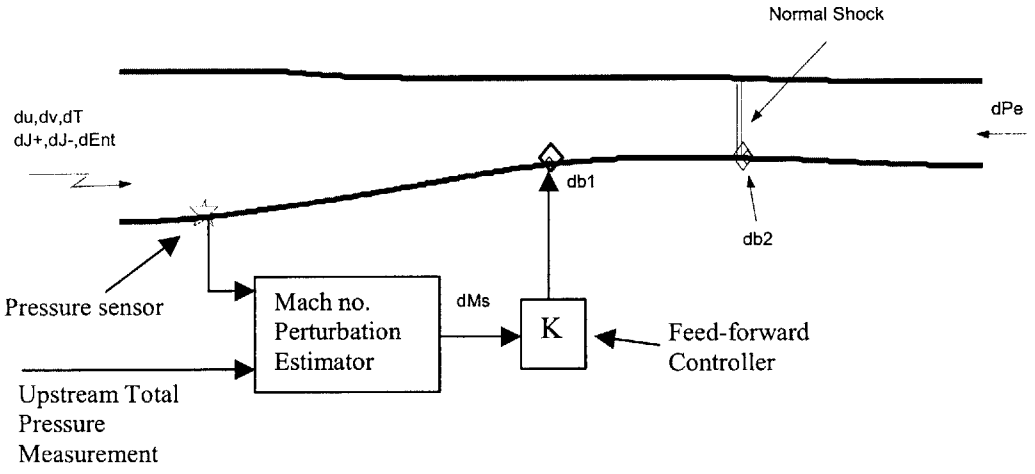

Figure 4.1: Feed-forward control law architecture, for throat Mach number control, based on Mach number estimation at the sensor.

The change in throat Mach number due to upstream forward velocity perturbation and upstream bleed perturbation is given as:

$$dM_{th} = \frac{dM_{th}}{du} du + \frac{dM_{th}}{db1} db1 \tag{4.1}$$

Here du is the forward velocity perturbation at the inlet face and $db1$ is the upstream bleed perturbation.

We can write Equation 4.1 in frequency domain using transfer function notation as:

$$dM_{th} = G_{Mth\_du}(j\omega)du + G_{Mth\_db1}(j\omega)db1 \tag{4.2}$$

Here $G_{Mth\_du}(j\omega)$ is the frequency response of the inlet from the forward velocity perturbation to the throat Mach number and $G_{Mth\_db1}(j\omega)$ is the frequency response of the inlet from the upstream bleed perturbation to the throat Mach number.

The bleed value can be written in terms of a postulated controller as:

$$db1 = KdM_s = K\frac{dM_s}{du}du \tag{4.3}$$

In frequency domain using the transfer function notation:

$$db1 = K(j\omega)G_{Ms\_du}(j\omega)du \tag{4.4}$$

Where $G_{Ms\_du}(j\omega)$ is the frequency response of the inlet from the forward velocity perturbation to the sensor located upstream of the bleed as shown in Figure 4.1. The sensor has to be located upstream as far from the bleed as possible. Locating the static pressure sensor far upstream of the bleed gives enough lead time to the actuator to respond to the incoming disturbances. But we cannot place the pressure sensor too close to the inlet face as it reduces the pressure sensor sensitivity to the incoming disturbances as shown in Figure 4.2.

Substituting Equation 4.4 into 4.2 we get:

$$dM_{th} = G_{Mth\_du}(j\omega)du + G_{Mth\_db1}(j\omega)KG_{Ms\_du}(j\omega)du \tag{4.5}$$

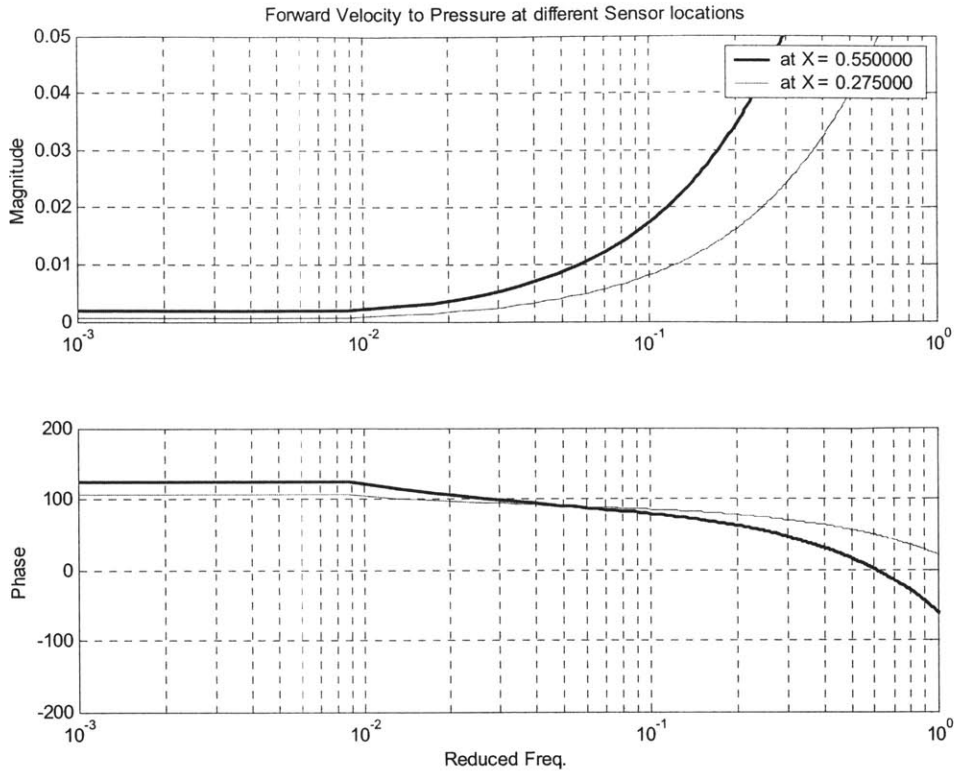

Figure 4.2: The sensitivity of the static pressure sensor at different sensor locations along the inlet.

For perfect cancellation we want:

$$dM_{th} = 0 \tag{4.6}$$

From Equation 4.5 we can solve for the controller K to be:

$$K = -\frac{G_{Mth\_du}(j\omega)}{G_{Mth\_db1}(j\omega)G_{Ms\_du}(j\omega)} \tag{4.7}$$

From Equation 4.7 it is clear that the controller transfer function, K, depends on the inverse of the transfer function from bleed to throat Mach number and transfer function from forward velocity to Mach number sensor. Thus if these transfer functions have non-minimum phase behavior, i.e., they have right half plane zeros, then the controller gain would contain right half plane poles and would be unstable. Also, if the transfer function has more poles than zeros (strictly causal) then its inverse will be acausal and therefore would not be realizable. Thus there is an issue of realizability and stability of the controller filter. That is the main reason for using the Mach number sensor to sense the upstream perturbations, rather than using the pressure sensor value directly. It was observed that if we use the pressure sensor value directly then the filter is very difficult to

realize due to non-minimum phase transfer functions. Also we want to place the pressure sensors as far as possible downstream from the throat, near to the inlet lip. This provides sufficient lead time for the actuators and the extra delay in the transfer functions makes the realization of the filters easier.

From the quasi-1D transfer functions for the inlet, shown in Figures 3.13 and 3.16, we can get the desired frequency response of the feed-forward controller. The desired frequency response of the feed-forward controller along with its realization, in both continuous and discrete cases, is shown in Figure 4.3. The realization was done in the continuous domain by doing a least squares fit, by a filter with the specified number of poles and zeros, to the desired frequency response. In the realization shown in Figure 4.3, a filter with 4 zeros and 5 poles was used to fit the desired frequency response data over the frequency range of interest. For the realization shown in Figure 4.3, a frequency range up to 0.4 was used, which is well beyond the highest frequency of interest. We can use a lower value for the maximum frequency, but unfortunately the resulting controller would be unstable. The Matlab command "INVFREQS" implements the least squares fit. Once the continuous domain filter is obtained we can transform it to a discrete time filter for testing in the inlet simulation. The discrete transfer function shown in Figure 4.3 was obtained by using a sampling frequency of 8.8 (corresponding to a dimensional sampling frequency of 2000 Hz for full scale inlet) and assuming that the inputs stay constant during each sampling interval (a zero-order hold approximation). The Matlab command "C2D" implements this transformation from the continuous time domain to the discrete time domain.

Figure 4.4 shows the pole-zero map for the discrete realization of the controller. It can be seen that it is stable as also shown by its step response in Figure 4.5. Note that the controller is realized well beyond the highest non-dimensional frequency of interest of 0.1.

We can see the effectiveness of the feed-forward controller in canceling the effect of incoming disturbances to the throat Mach number by plotting the frequency response of the incoming disturbances to the throat Mach number with controller and without controller. These plots are shown in Figures 4.6 and 4.7. The controller reduces the perturbations to throat Mach number due to forward-velocity and vertical-velocity but is not that effective, especially at higher frequencies, at rejecting temperature perturbations. We will discuss the implications of this in the next paragraphs.

The ineffectiveness of the controller for higher frequencies for temperature perturbations is not surprising, since we ignored the temperature perturbations in the design of the controller. Temperature perturbations comprise all three characteristic types, namely J+, J- and entropy, as discussed in section 2.3.3.

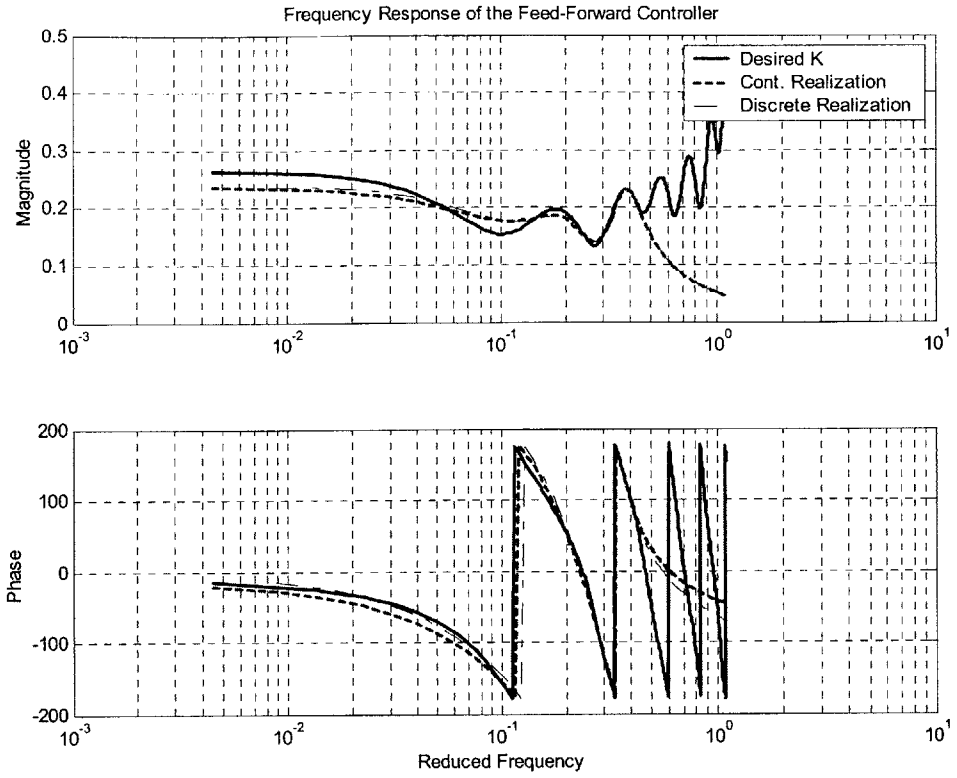

Figure 4.3: Frequency response of the feed-forward controller and its realizations.

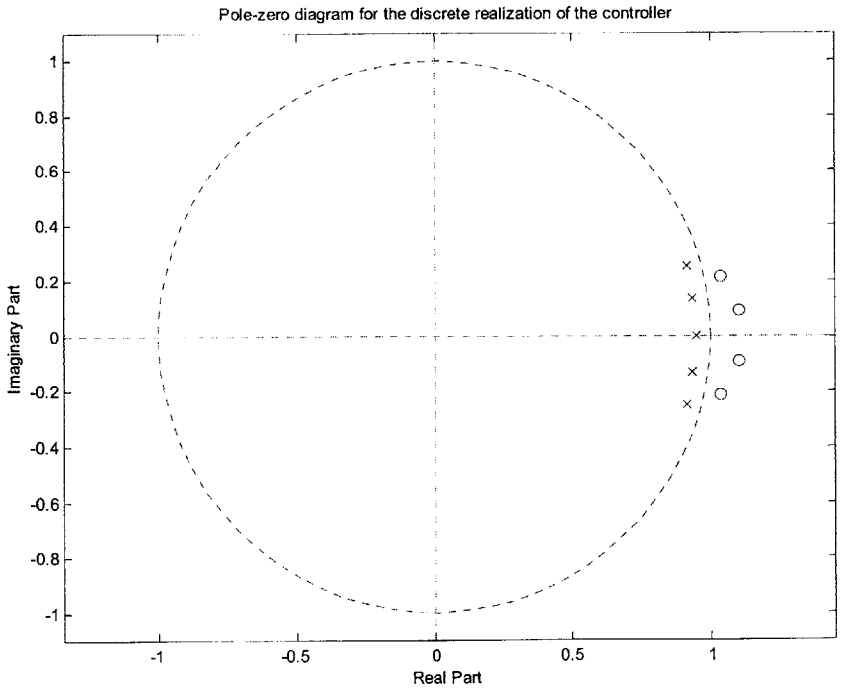

Figure 4.4: Pole-zero diagram for the discrete feed-forward controller.

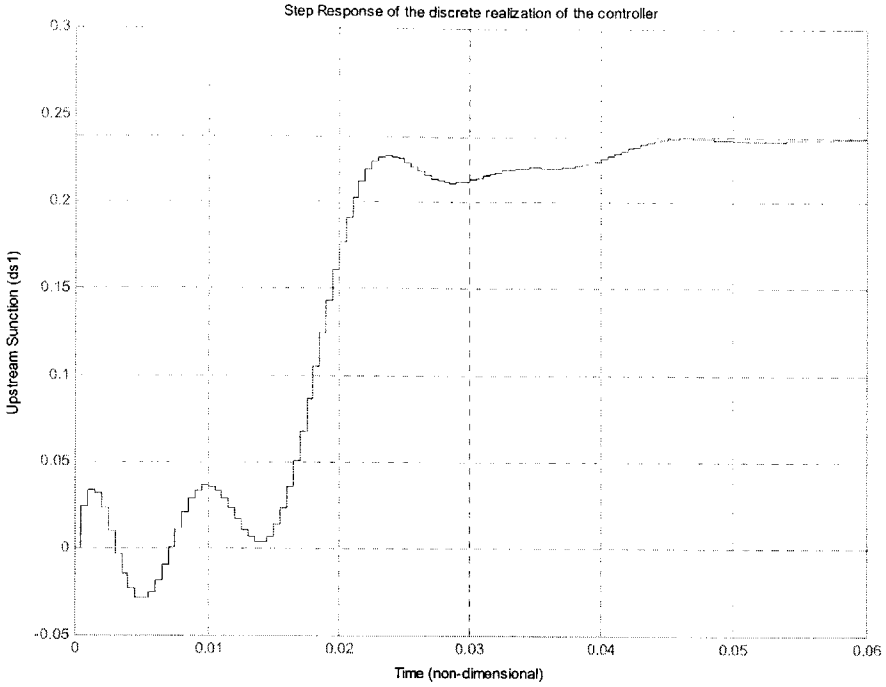

Figure 4.5: Step response of the discrete feed-forward controller.

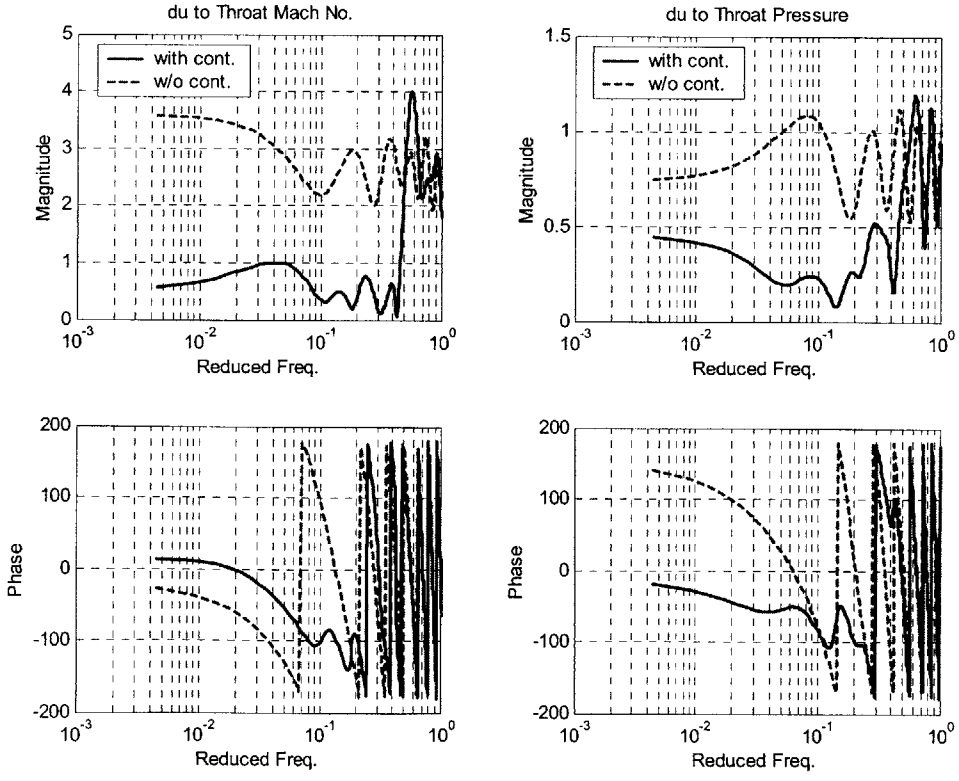

Figure 4.6: Controller effectiveness for changes in throat Mach number and pressure.

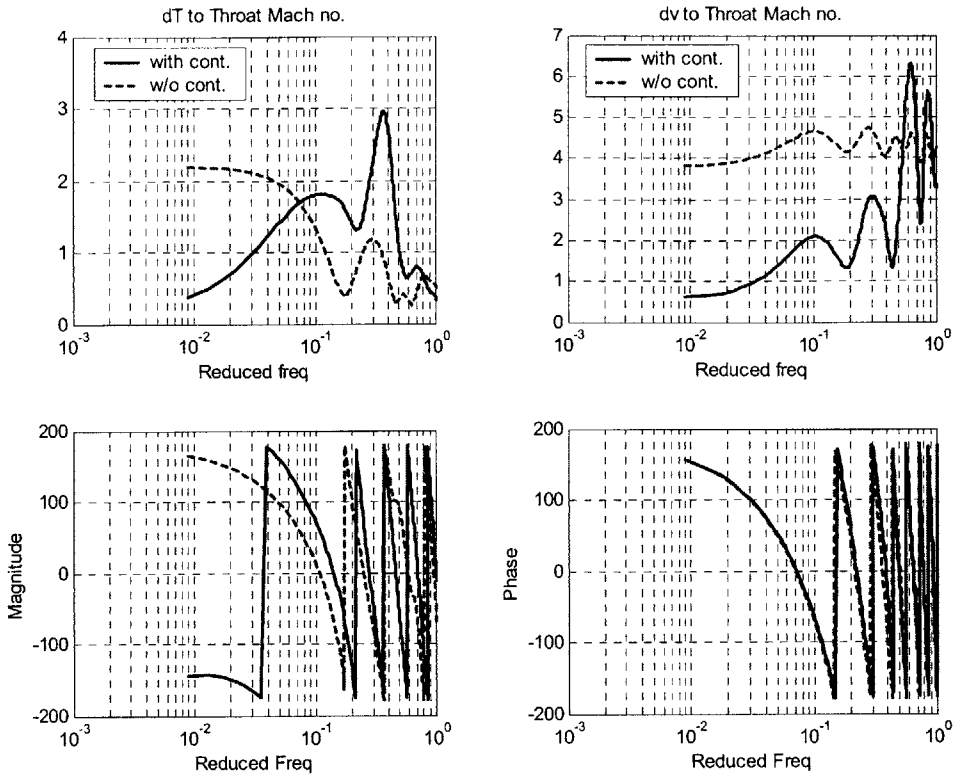

Figure 4.7: Controller effectiveness for changes in throat Mach number due to vertical velocity perturbations (dv) and temperature perturbations (dT).

Another way of looking at the controller effectiveness is to look at the spectrum of atmospheric disturbance effect at the throat with the controller on and with the controller off. Figures 4.8 through 4.10 give the spectra of variations in throat Mach number with the control off and with the control on. Figure 4.10 shows that the controller actually amplifies the temperature disturbance spectrum beyond the maximum frequency of interest of 0.1. But still the controller is effective for lower frequency disturbances, where the maximum energy is concentrated. Thus we see that although we ignored the temperature and vertical velocity perturbations in the design of the controller, the controller is still effective over the most important range of frequencies. Table 4.1 gives the RMS values of the throat Mach number variations due to different types of disturbances. From this table it is apparent that this control architecture is most effective for slow acoustic waves. The entropy perturbations are actually amplified a little bit by the controller. This is expected since the bleed cancels the slow acoustic perturbations most effectively as given in Figures 3.17 through 3.19 in the last chapter.

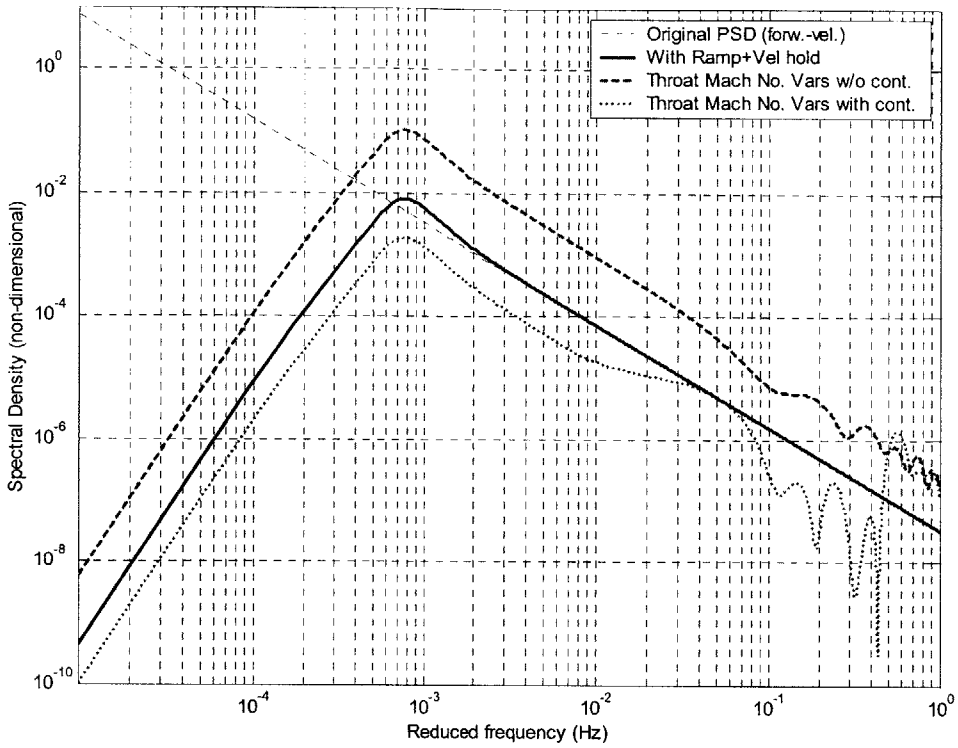

Figure 4.8: PSD of throat Mach number variations with control and without control for forward velocity.

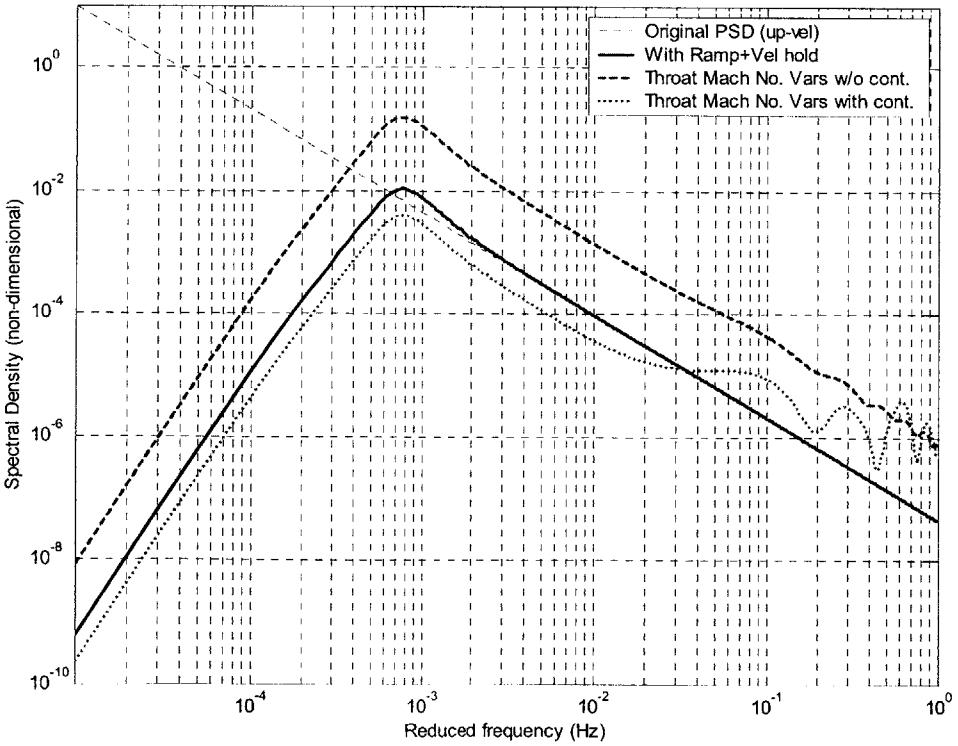

Figure 4.9: PSD of throat Mach number variations with control and without control for up velocity.

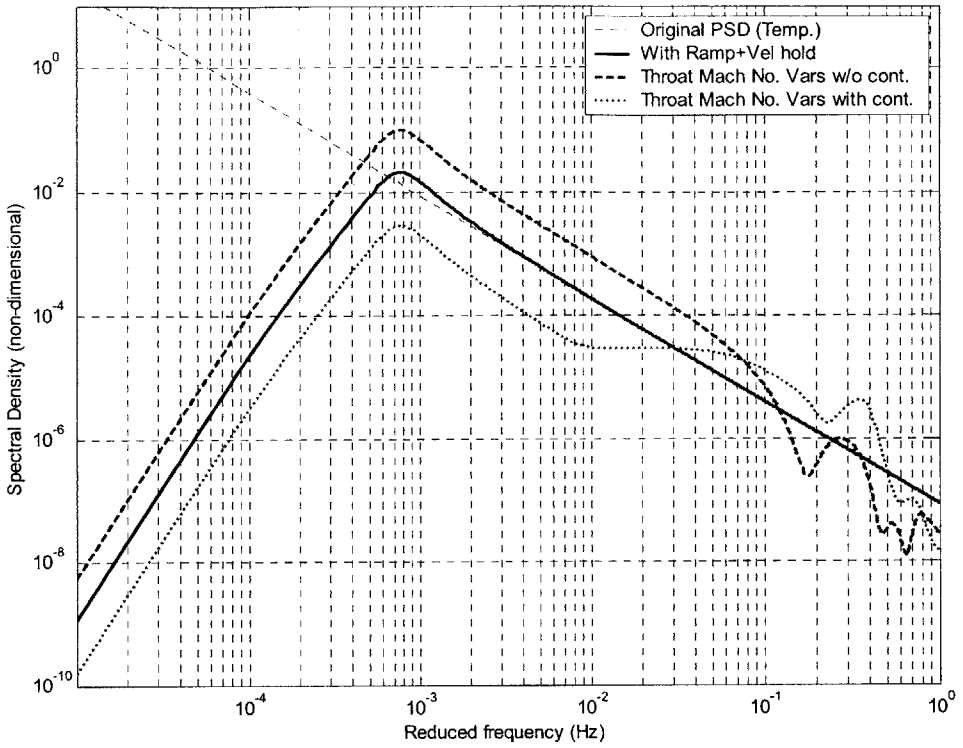

Figure 4.10: PSD of throat Mach number variations with control and without control for temperature.

Disturbance Type	RMS value of M_{th} without control ($\times 10^{-3}$)	RMS value of M_{th} with control ($\times 10^{-3}$)
Forwd. Vel.	11.0	1.7
Up Vel.	13.8	2.7
Temperature	10.8	2.6
J+	16.2	5.2
J-	48.3	6.4
Entropy	8.7	9.7

Table 4.1: RMS value of throat Mach number variations with control and without control.

4.1.2 Throat Mach Number Controller Design based on Characteristic Disturbances

We have observed that the design based on the atmospheric disturbances is not completely effective in controlling the temperature disturbance; in characteristic form we see that it actually amplifies the entropy disturbance. We can improve our controller by designing it specifically for each type of characteristic disturbance. For that we will need an estimator that gives us an estimate of the perturbation in each characteristic disturbance.

From the transfer function of the upstream bleed to the characteristic variables at the throat, shown in Figures 3.17 to 3.19, it is clear that the bleed affects the slow acoustic waves mostly and fast waves and entropy perturbations are not affected much by the bleed. Thus in this section a simple controller will be designed to cancel the slow acoustic wave perturbations at the throat. Since throat Mach number perturbations can be broken down into the characteristic perturbations, controlling the characteristic perturbations should ensure the stability of the throat Mach number. Using this approach the controller architecture looks as shown in Figure 4.11.

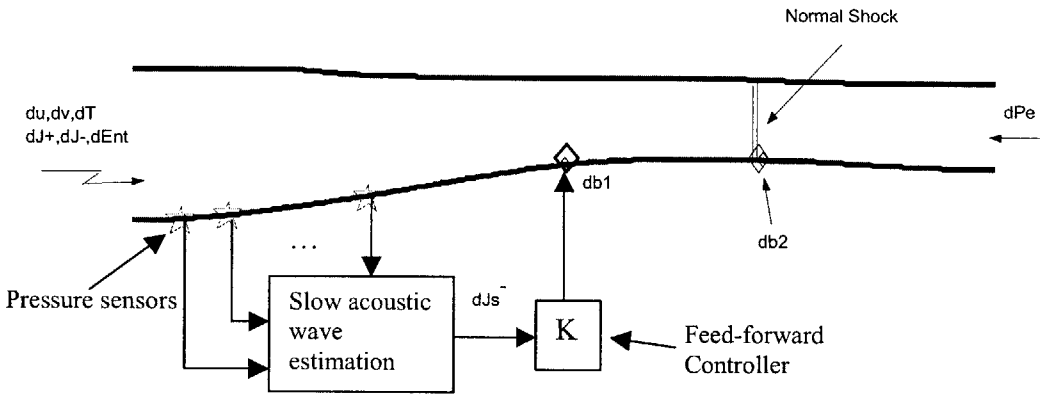

Figure 4.11: Feed-forward control law architecture, for cancellation of slow acoustic waves at the throat, using the characteristic disturbance estimation.

Using the same procedure as outlined in section 4.1.1, we can show that the controller gain required for a perfect cancellation of the slow acoustic wave disturbances at the throat is:

$$K = -\frac{G_{J_{th}\_J^-}(j\omega)}{G_{J_{th}\_db1}(j\omega)G_{J_s^-\_J^-}(j\omega)} \tag{4.8}$$

Where:

$G_{Jth\_J}(jw)$= The frequency response of the inlet form the J- perturbations at the inlet face to the J- perturbations at the throat (Figure 3.8).

$G_{Jth\_db1}(jw)$ = The frequency response of the inlet from the upstream bleed perturbations to the J- perturbations at the throat (Figure 3.18).

$G_{Js\_J}(jw)$ = The frequency response of the inlet form the J- perturbations at the inlet face to the J- perturbations at the output of the sensor estimator (Figure 3.8).

Each of the transfer function plots, in chapter 3, shown in figures as mentioned above, can be approximated by a constant delay function in the range of the frequencies of interest. Thus the controller also becomes simply a constant delay function with the constant gain and phase computed from Equation 4.8.

Thus the controller in this form is a very simple one, but now the complexity of the controller is shifted to the estimation problem. We need to estimate the slow acoustic waves propagating down the inlet. A detection scheme, for the slow acoustic waves, is shown in Figure 4.12.

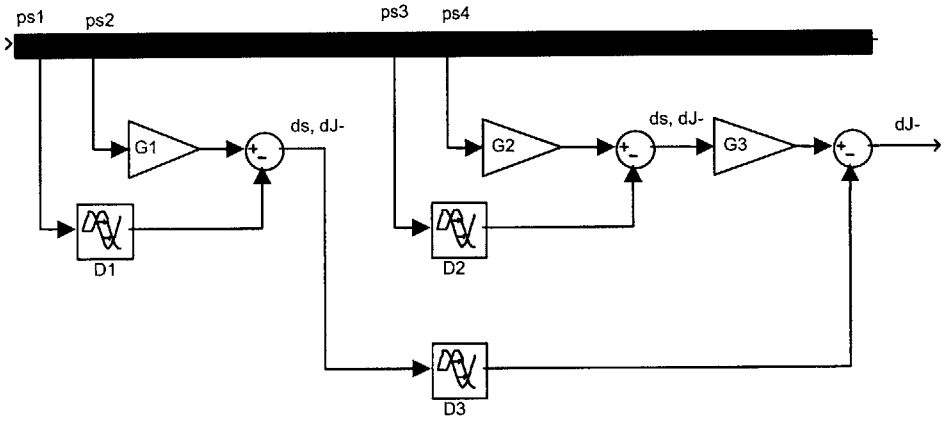

Figure 4.12: Detection of slow acoustic waves using four static pressure sensors.

Here ps1 to ps4 are static pressure sensors located along the inlet. They act in pairs such that ps1 and ps2 form one pair while ps3 and ps4 form the other pair. Gain G1 and delay D1 are selected such that the perturbations due to fast acoustic waves are cancelled at the output of the difference. Thus we get perturbations due to slow waves and entropy at the output. Similarly gain G2 and delay D2 are selected such that we get only perturbations due to entropy and slow waves at the output of the difference. Now treating each pair as a single pressure sensor that gives us only two perturbations, namely entropy and slow waves, we can select gain G3 and delay D3 such that the perturbations due to the entropy are cancelled at the output and we get only slow acoustic wave perturbations. The gains

and delays can be selected from the transfer function plots for each type of disturbance based on the location of pressure sensors along the inlet. Due to time constraints, this controller configuration was not implemented and tested to get the results for comparison. The implementation of this controller is recommended for future work.

4.2 Shock Motion Control

From the large signal frequency response of the shock motion due to various types of perturbations in the previous chapter, it can be seen that the shock motion magnitude is an inverse function of the amount of bleed located at the shock. Thus a simple form of control for preventing unstarts due to shock motion would be to use a linear proportional feedback controller based on the shock location [15]. Shock location can be estimated by using an array of static pressure sensors located close to each other as described in [22]. In this scheme location of the shock would be given by the discontinuity in the pressure across the pressure sensor array. Such a control scheme is shown in Figure 4.13.

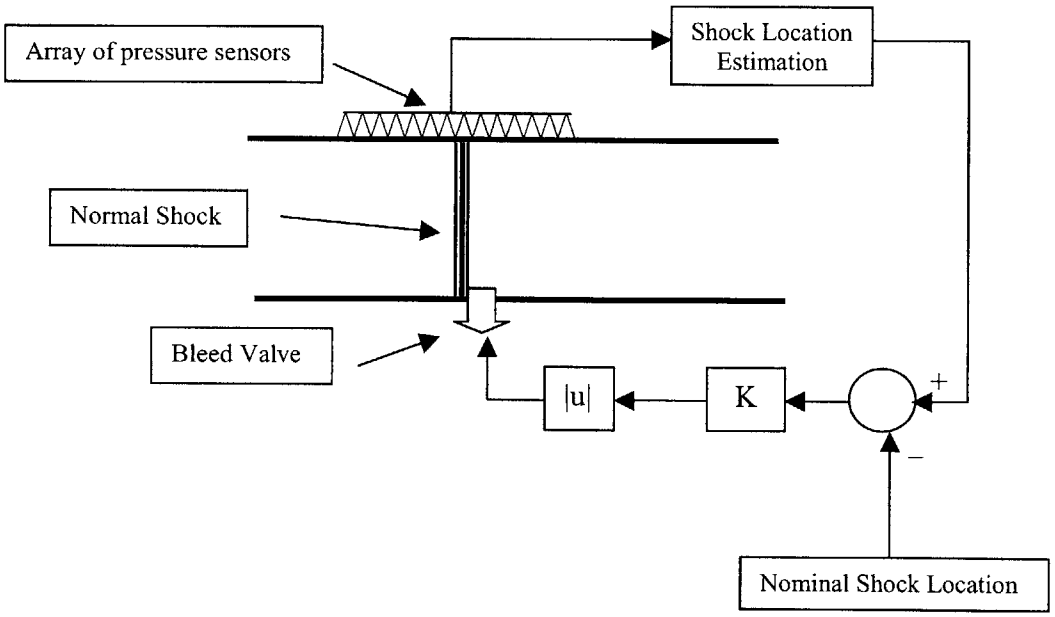

Figure 4.13: Shock position control using shock location feedback.

The gain K is selected such that the shock bleed valve is saturated for a given maximum allowable shock displacement. Under the nominal operating conditions the bleed valve typically bleeds around 1 to 2% of inlet mass flow. This steady bleed is required to prevent the growth of the boundary layer. It also serves to add a "dead band" around the nominal position of the shock as shown in Figure 3.21. As the shock tends to move upstream or downstream due to atmospheric or exit pressure perturbations the

proportional controller simply bleeds more air thus tending to prevent the shock from moving. This configuration was implemented along with the throat Mach number control and some test results are presented in the next chapter.

Chapter 5

Summary, Results and Conclusions

At supersonic speeds mixed compression inlets give high efficiency. High efficiency of the inlet is measured in terms of high total pressure recovery and low inlet drag. One can design a near isentropic supersonic inlet that requires bleed to prevent the growth of boundary layers. However, such a design has reduced stability, due to reduced unstart tolerance, and is prone to unstart in the face of atmospheric disturbances. Steady-state bleed for improving unstart robustness and boundary-layer control tends to increase the inlet drag, therefore, we need to use as low steady-state bleed as possible. We also need to use active control to increase the unstart tolerance of the inlet to acceptable levels during normal operation of the inlet.

In this thesis different issues that must be addressed for successful design of a controller for the active control of the inlet are investigated. First the atmospheric disturbances are characterized in terms of power spectral density and worst case atmospheric disturbance PSDs are transformed into the characteristic form for use in the control law design and analysis. CFD models, both quasi-1D and 2D, are used to obtain frequency response data, on the basis of which different feedforward controllers are designed to reject the incoming atmospheric disturbances. Shock position control is briefly discussed in terms of shock position feedback.

5.1 Some Time Domain Results

To see the effect of gusts in time domain on the throat Mach number and shock position in the presence of the controller, discussed in sections 4.1 and 4.2, a Gaussian bump (described in appendix B) is used as the worst-case atmospheric disturbance at the input of the inlet. Based on results of the quasi-1D simulation, different time histories of the input and controlled parameters are shown in Figure 5.1. One can clearly see the effect of the actuator saturation on the throat Mach number. It can also be seen that the upstream bleed is very effective in stabilizing the throat Mach number (if the actuator is not saturated), and that it does not affect the position of the shock significantly. Similarly Figure 5.2 shows the time histories, using the quasi-1D simulation, for a typical realization of worst-case atmospheric gust in the forward velocity and Figure 5.3 shows the response to the same input disturbance, using the 2D simulation. Figure 5.2 shows the effect of turning off the controller for the same disturbance.

From Figure 5.1, it is clear that 1% upstream bleed is barely enough to control the throat Mach number in the face of typical atmospheric disturbances. Therefore, to control the throat Mach number effectively for worst-case disturbances one must use a maximum

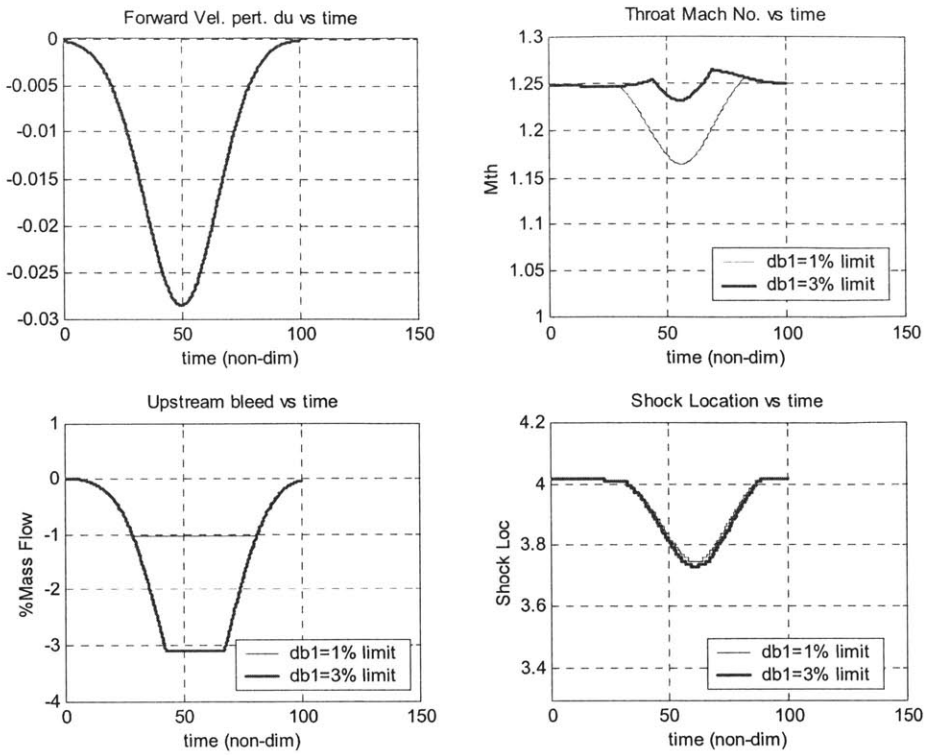

Figure 5.1: Time response, using quai-1D simulation, of the inlet to a Gaussian bump perturbation in the forward velocity.

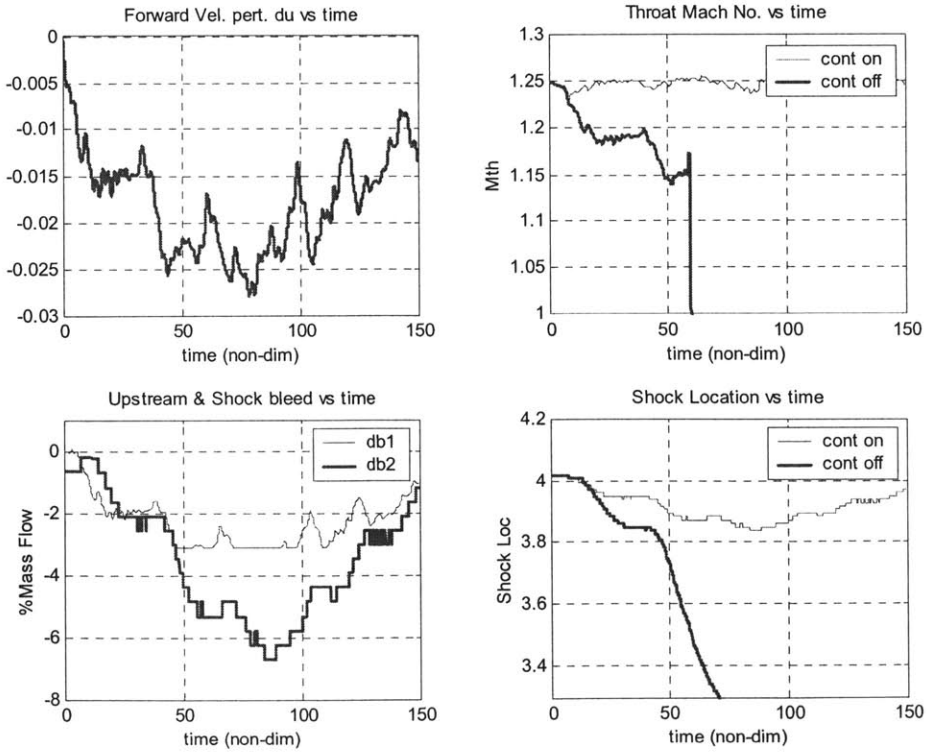

Figure 5.2 Time response, using 1D simulation, of the inlet to a typical atmospheric gust in forward velocity, with and without control.

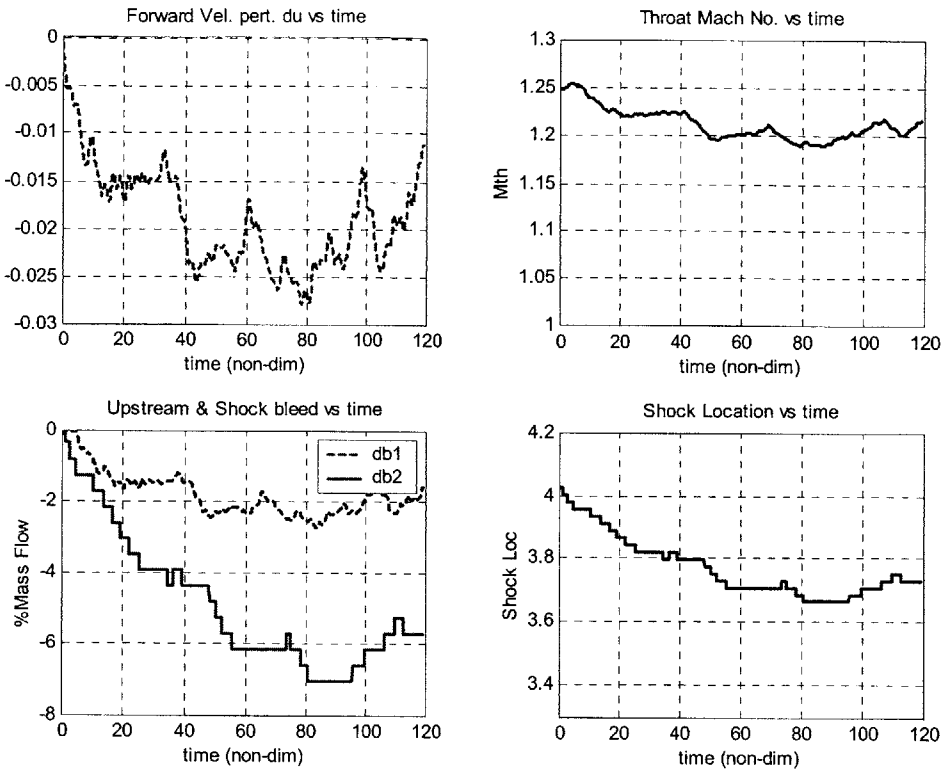

Figure 5.3 Time response, using 2D simulation, of the inlet to a typical atmospheric gust in forward velocity. Note that area-averaged values of the variables are shown.

value of the upstream bleed, db1, of 2 to 3% of the inlet mass flow. Figure 5.2 also shows the maximum shock bleed required in order to keep the shock from moving in the face of a typical realization of worst-case atmospheric perturbations in forward velocity.

For controlling this typical realization of the worst-case gust, the maximum transient shock-bleed required is around 5 to 6% of the inlet mass flow. Although these bleeds are large, they represent a transient and would go to the maximum only during the peak gust encountered during flight; this would happen over a very small time interval and overall efficiency of the system would not degrade significantly even for large bleed values. A comparison between the results of quasi-1D and 2D simulations shows that the controller controls the throat Mach number in quasi-1D simulation almost perfectly while in the 2D simulation there is a little drop in the throat Mach number. That is not surprising as the controller was specifically designed using the quasi-1D simulation results. Nevertheless, given this fact, the performance of the controller in 2D simulation is quite acceptable. These time-domain results also validate our initial conclusion, using the frequency response analysis, that over the range of frequencies of interest the quasi-1D Euler model is similar to the 2D Euler model of the inlet.

5.2 Conclusions

From the analysis and results presented in this thesis it is clear that a high recovery inlet can be designed that has low steady bleed requirements; if one relaxes the requirements for unstart tolerance to atmospheric disturbances. The unstart tolerance can then be enhanced using active control. During normal operation, when the inlet encounters the atmospheric gusts, the bleed valves bleed air as required and the robustness of the inlet increases. The net bleed required for this setup is much less as compared to a system that has to add robustness to unstart in the form of a static margin; which results in higher bleed requirements and lower recovery even when there are no atmospheric disturbances present. The low bleed requirements and enhanced recovery can have a significant impact on the propulsion system efficiency for long-range supersonic transport aircraft. It was shown that the quasi-1D model of the inlet is sufficient to design and implement the control law as the area-averaged 2D results are similar to the quasi-1D results if a symmetrical upstream bleed is used. A simple feedforward controller can significantly reduce the throat Mach number perturbations due to the atmospheric disturbances. Using a separate estimator for fast and slow waves, and designing the controller to cancel these waves specifically, can improve the performance of the presented throat Mach number controller. A (possibly reduced scale) experimental setup is necessary to verify the ideas presented in this thesis.

Appendix A:

Code Listing for Constant Delay Approximation of the Transfer Functions

In this appendix a sample code for the constant delay approximation fitting for the forward velocity to throat Mach number perturbations is listed. First of all the constPhaseFit() function is called that extracts the dominant mode in the transfer function. Then the function expFit() is used in the same manner as constPhaseFit() to find the remaining modes using a global search method. The amplitude of each mode is found by using a least square fit.

```
% main m file used for constant delay fitting:
% fit a tf from the Inlet U to throat Mach No. (MtDU):

clear all;
clc
global f mag phase;
load ..\ident\dutfs;

% used by expFit:
mag = abs(dutfs.MtDU);
phase = angle(dutfs.MtDU);
f = dutfs.f;

inv = 1;
T1 = constPhaseFit(2,10,0.001,inv,1);    % -1 for inversion (+ve sign of
the TF for MtDU)

pause;

% do a global search one by one:
n = 1;
dT2 = 1.0;
for num=2:2
    for y=0.002:0.01:1.5
        err(n) = expFit([dT2 y]*T1, 0,inv);
        delT(n) = y;
        n = n+1;
    end
    index = find(err == min(err));
    dT2(num) = delT(index)
    figure(2);
    clf;
    [minerr(num-1),A] = expFit(dT2*T1, 1,inv);
    pause;
    n = 1;
end

i = sqrt(-1);
fmtdu = linspace(0, max(f), 250);
```

```
tf = zeros(1,length(fmtdu));
delT = dT2*T1
for n=1:length(delT)
    cph = inv*A(n)*exp(-i*2*pi*fmtdu*delT(n));
    tf = tf + cph;
end

figure(2);

clf;
subplot(211);
lh1 = semilogx(f, mag);
set(lh1,'LineWidth',2);
hold on;
lh2= semilogx(fmtdu, abs(tf), 'r-.');
set(lh2,'LineWidth',2);
title('Transfer function from forward vel. to Mth');
xlabel('Reduced Frequency');
ylabel('Magnitude');

grid;
axis([10^-3 1 0 5]);
legend([lh1 lh2],'Numerical TF','Const. Delay App. TF');

subplot(212);
lh1= semilogx(f, phase*180.0/pi);
set(lh1,'LineWidth',2);
hold on;
lh2=semilogx(fmtdu, angle(tf)*180.0/pi,'r-.');
set(lh2,'LineWidth',2);
xlabel('Reduced Frequency');
ylabel('Phase');
grid;
axis([10^-3 1 -200 200]);

% save the model:
MtDUMod = tf;
save MtDuMod.mat MtDUMod fmtdu
```

```
function dT = constPhaseFit(lowlimit, highlimit, delta, inv, disp)
% fitting a constant phase to the inlet freq. resp. data:

global f mag phase;

Ph = phase*180/pi;

%figure(1);
%subplot(211);
%plot(f, Ph);grid;

% estimate the constant phase fit from the input phase:
n = 1;
v = [lowlimit:delta:highlimit];
wt = exp(-2.5*f);   % weightings
```

```
for delT=v
    i = sqrt(-1);
    constPh = angle(inv*exp(-i*2*pi*f*delT))*180.0/pi;
    %hold on;
    %subplot(211);
    %plot(f,constPh,'r');

    % subtract the constant phase:
    Phdiff = wt.*(Ph - constPh);
    %subplot(212);
    %plot(f,Phdiff);grid;
    err(n) = norm(Phdiff);
    n = n + 1;
end
delT = v;
%plot(delT,err);grid;
minerr = min(err);
ind = find(err == minerr);
dT = delT(ind);

if disp == 1
    figure(1);
    clf;
    subplot(211);
    % plot the error function:
    plot(delT, err);
    grid on;
    title('error function vs delays');
    xlabel('delay');

    % plot the given phase:
    subplot(212);
    plot(f,Ph);
    hold on;
    constPh = angle(inv*exp(-i*2*pi*f*dT))*180.0/pi;
    plot(f,constPh,'r-.');
    grid on;
    title('given phase (solid) and fitted constant phase (dotted)');
    xlabel('frequency');
    dT
end

return;
```

```
function [err,A] = expFit(delT,debug,invt);

global f mag phase;

i = sqrt(-1);
len = length(delT);

v = zeros(length(f)*2, len);

% weighting function:
```

```
W = [exp(-f) exp(-f)];

for n=1:len
    cPh = invt*exp(-i*2*pi*f*delT(n));   % inv for -ve tfs
    v(:,n) = [real(cPh)  imag(cPh)]'.*W';
end

M = v;

H = [mag.*cos(phase) mag.*sin(phase)].*W;     % [real part      imag part]

H = H(:);
A = M\H;         % least squares fit for the gains

Hhat = M*A;

% combine the real and img parts
len = length(f);
Hfit = complex(Hhat(1:len), Hhat(len+1:2*len));

if debug
    subplot(211);
    plot(f,mag);
    hold on;
    plot(f,abs(Hfit)./W(1:len)','r-.');
    grid;
    title('given mag (solid) and fitted mag (dotted)');

    subplot(212);
    cPhase = angle(invt*exp(-i*2*pi*f*delT(1)));
    ph1 = medfilt1(phase-cPhase,8);
    plot(f,ph1*180.0/pi);
    hold on;
    ph2 = medfilt1(angle(Hfit)'-cPhase,10);
    plot(f,ph2*180.0/pi,'r-.');
    grid;
    title('given phase (solid) and fitted phase (dotted)');
    A

end

Hgiven = complex(H(1:len), H(len+1:2*len));
if debug
    err = norm(abs(Hfit-Hgiven))
else
    err = norm(abs(Hfit-Hgiven));
end
```

Appendix B:

Gaussian Bump used as an Atmospheric Disturbance

Atmospheric disturbances having a Gaussian distribution in space can be used to model the typical gusts. Though these "Gaussian bumps" do not have the same spectral characteristics as those of typical atmospheric gusts but still they are useful as their spectral content can be adopted to lie within the atmospheric gust spectra by multiplying the Gaussian bumps with a sinusoidal waveform. Also these bumps do not have sharp edges as in a step thus representing the actual variations in the atmospheric variables to a good approximation.

A "Gaussian bump" is defined as:

$$h(t) = A_0 \exp\left[-g\left(t - t_p\right)^2\right] \cos\left(2\pi f_m t\right) \tag{B.1}$$

Where:

A_0 = Peak Amplitude of the disturbance.

t_p = Bump peak amplitude time (50 in figure 5.1).

g = Variable that sets the width of the bump (0.002 for figure 5.1). Smaller values of g make the bump wider and therefore reducing the higher frequency content.

f_m = Center frequency where we want to shift the spectral peak of the bump (0.001 for figure 5.1).

The spectrum of the "Gaussian bump" modulated by the cosine is given by:

$$H(f) = \frac{A_0}{2\sqrt{g/\pi}} \exp\left(j2\pi t_0 (f - f_m)\right) \exp\left(-\frac{\pi^2 (f - fm)^2}{g}\right) \tag{B.2}$$

References:

[1] David W. Mayer, Gerald C. Paynter, "Prediction of Supersonic Inlet Unstart Caused by Free stream Disturbances." AIAA Journal Vol. 33 No. 2 Feb 1995

[2] Jim Paduano, Ali Merchant, Mark Drela, Guillaume Lassaux, Brian Schuler, "Design and Tesing of a High-Recovery, Actively Controlled Supersonic Inlet." MIT GTL report.

[3] David Soreide, Rodney Bogue, Jonathan Seidel, L.J. Ehernberger "The use of a LIDAR Forward-Looking Turbulence Sensor for Mixed-Compression Inlet Unstart Avoidance and Gross Weight Reduction on a High Speed Civil Transport." AIAA Paper 1997

[4] John D. Anderson, "Modern Compressible flow with historical perspective." McGraw Hill Books 1982.

[5] W. Tank, J, Gillis, "Atmospheric Disturbance models for linear and nonlinear system response analysis." AIAA 34th Aerospace Sciences Meeting and Exhibit, Reno, NV Jan 1996

[6] William G. Tank, "Atmospheric Disturbance Environment Definition", NASA report CR-195315 Feb. 1994

[7] James A. Fay "Introduction to Fluid Mechanics". Book.

[8] C. W. Fairall, A. B. White, "A Stochastic Model of Gravity-Wave Induced Clear Air Turbulence." Journal of Atmospheric Sciences, 49, pages 1771-1790, 1991.

[9] J. Roskam, "Airplane Flight Dynamics and Automatic Flight Controls." Part 1.

[10] Brown & Hwang, "Stochastic Estimation and Control"

[11] Peter Giannola, Martin Haas, "Modeling the Dynamics of Supersonic Inlet/Gas-Turbine Engine Systems for Large-Amplitude High-Frequency Disturbances", 36th AIAA/ASME/SAE/ASEE Joint Propulsion Conference & Exhibit July 17-19, 2000 / Huntsvilie, AL

[12] Hurrell, H. G., "Analysis of Shock Motion in Ducts During Disturbances in Downstream Pressure." TN 4090, NACA, 1957.

[13] Culick, F. E. C. and Rogers, T., "The Response of Normal Shocks in Diffusers." AIAA Journal, Vol. 21, No. 10, pp. 1382-1390, 1983.

[14] Yang, V. and Culick, F. E. C., "Analysis of Unsteady Inviscid Diffuser Flow with a Shock Wave." AIAA Journal of Propulsion and Power, Vol. 1, No. 3, pp. 222-228, 1985.

[15] MacMartin, Douglas G., "Dynamics and Control of Shock Motion in a Near-Isentropic Inlet." AIAA 2002-2943.

[16] Numbers, Keith and Hamed, Awatef, "Development of a Coupled Inlet-Engine Dynamic Analysis Method." AIAA/ASME/SAE/ASEE Joint Propulsion Conference & Exhibit, 33rd, Seattle, WA, July 6-9, 1997.

[17] Freund, Donald and Sajben, Miklos, "Experimental Investigation of outflow boundary conditions used in unsteady inlet flow computation." AIAA Aerospace Sciences Meeting & Exhibit, 35th, Rno, NV, Jan. 6-9, 1997.

[18] Sajben, Miklos and Said, Hazem, "Acoustic-Wave/Balde-Row Interactions Establish Boundary Conditions for Unsteady Inlet Flows." Journal of Propulsion and Power, Vol. 17, No. 5, September-October 2001.

[19] E.L. Goldsmith, J. Seddon, "Practical Intake Aerodynamic Design." Blackwell Scientific Publications 1993.

[20] Umair Ahsun, Ali Merchant, James D. Paduano, Mark Drela, "Design of an Actively Stabilized, Near Isentropic Supersonic Inlet." AIAA Summer Conference, June 23-26th 2003, Orlando Florida.

[21] Martin Haas, United Technologies Research Center, East Hartford, CT. Personal communications.

[22] Miklos Sajben, John F. Donovan and Martin Morris, "Experimental Investigation of Terminal Shock Sensors for Mixed-Compression Inlets." Journal of Propulsion and Power, Volume 8 No. 1, 1992.